PRE-CONSTRUCTION GEOPHYSICAL INVESTIGATION OF THE PROPOSED THEATRE AND MEDIA ARTS COMPLEX WITHIN FEDERAL UNIVERSITY OYE – EKITI USING INTEGRATED GEOPHYSICAL METHODS

BY

FASANMI TEMITOPE TOSIN

(GPY/11/0294)

SUBMITTED TO THE DEPARTMENT OF GEOPHYSICS, FACULTY OF SCIENCE, FEDERAL UNIVERSITY OYE-EKITI, IN PARTIAL FULFILLMENT OF THE REQUIREMENT FOR THE AWARD OF BACHELOR OF SCIENCE (B.Sc.) DEGREE IN GEOPHYSICS

OCTOBER, 2015

CERTIFICATION

(a) (By the Student)

This is to certify that this work was carried out by Fasanmi Temitope Tosin (GPY/11/0294) in the Department of Geophysics, Federal University Oye-Ekiti and has not been presented elsewhere for the award of a degree, or any other purpose.

Candidate's Name: Fasanmi Temitope Tosin

Signature: ..... **Date:** 27/11/2015.....

(b) (By the Supervisor)

I certify that this research work was carried out by Fasanmi Temitope Tosin (GPY/11/0294) in the Department of Geophysics, Federal University Oye-Ekiti.

Supervisor's Name: Mr. O.E.Bamidele

Signature: ..... **Date:** 27/11/2015.....

DEDICATION

I dedicate the totality of this project work to God Almighty.

ACKNOWLEDGEMENTS

My profound gratitude goes to my creator and the father of light. He has counted me worthy to be a living soul from my first day in this institution till this present moment, all glory, honour and adoration is unto His holy name.

This dissertation would have not been possible without the guidance and the help of several individuals who in one way or another contributed and extended their valuable assistance in the preparation and completion of this study.

My profound gratitude to Mr. O.E. Bamidele, my project supervisor; who had kind concern and consideration regarding this research work, whose sincerity and encouragement I will never forget. He has been my inspiration in completing this research work.

My utmost gratitude also goes to those who effortlessly contributed to making me a Geophysicist of my choice: Dr O.J. Fatoba (Head of Department), Prof. A.O. Adelusi, thanks for your patience, kind supervision and monitoring to ensuring a glamorous project work, May God bless you richly. Also Mr. Fajana, Mrs. Olaseeni, Mr. Olabode, Mr. Chukwu, Mr. M. Bawallah, Mr. Tope and Mr.Julius. Your impact in making me who I am today is more than what words can express. God bless you richly, Amen.

To my special friends Adaramola Elizabeth, Olajide Olawale, Michael Oyinloluwa and Saliyuk Rebecca thanks for giving me a shoulder to lean on. I say a big thank you to all Executives, Workers and Members of Redeemed Christian Fellowship (RCF), FUOYE, Oye-Chapter.

Finally, to all my colleagues; Fashina Timilehin, Daramola Damilola, Eniola Adeyemi, to mention a few, I say a very big thank you for your wonderful positive contributions. I salute your tolerance, intelligence and struggle towards becoming professional Geophysicists.

TABLE OF CONTENTS

Chapter Four - Result and Discussion

LIST OF FIGURES

LIST OF TABLES

ABSTRACT

Integrated Geophysical investigation was carried out around the proposed Theatre and Media Arts Complex within the Federal University Oye-Ekiti, Ekiti State, Southwestern Nigeria.

Six (6) traverses were established in the area in the W-E and N-S directions along which the VLF-EM and Magnetic data were obtained in order to locate suitable VES stations. The dipole-dipole data were acquired along four traverses using the electrode separation of 5 m along traverse 2 and 4 (W-E) while 10 m was used along traverse 1 and 4 (N-S). Nineteen (19) Schlumberger vertical electrical soundings (VES) were carried out within the study area using a maximum current electrode separation (AB) of 130 m. The VES data was processed and interpreted by the method of partial curve matching and computer iteration technique to generate the subsurface model.

The VLF-EM results show a major conductive zone which is observed on traverse 2 between 62 and 80 m which is typical of a fracture/fault/lithological boundary. The Magnetic results show thick dykes beneath traverse 2 between 75 - 106 m and traverse 3 between distances 17 - 50 m. These thick dykes are interpreted as major conductive zones typical of fractures, faults, thick overburden or lithological boundary in the study area. The geoelectric sections generally reveal maximum of four geological layers which are: the topsoil, laterite, weathered layer and the partly weathered/fractured/fresh basement rock. The topsoil resistivity varies from 14 to 330 Ωm with thickness range of between 0.5 and 1.5 m. It is composed of clay, sandy clay, clayey sand and laterite. The Lateritic layer range in resistivity from 229 to 955 Ωm and its thickness varies between 0.6 and 12.1 m. The weathered layer ranges in resistivity from 7 to 264 Ωm and its thickness varies between 1.4 and 17.5 m. It is composed mainly of clay and sand. The bedrock which is partly weathered and fractured in some places varies in resistivity from 373Ωm to

infinity with depth to bedrock ranging between 1.9 and 26.4 m. The Dipole – Dipole 2-D resistivity structure on traverse 4 (close to traverse 2) show high resistivity above the weathered layer indicative of laterite, and basement beneath the weathered layer, generally undulating and depressed especially between distances 45 – 88 m. The topsoil is weak in some portions (NW and SE) and competent in some parts (central) of the study area (where it is lateritic and underlain by laterite) as revealed by the maps.

It is therefore concluded that the proposed site is good for construction but not all the entire part is good for construction purpose.

CHAPTER ONE

INTRODUCTION

1.1 Preamble

In recent time, the statistics of failures of engineering structures such as roads, buildings, and bridges throughout the nation has increased geometrically. Several probable reasons speculated to have been responsible for this ugly incidence have been highlighted (Oyedele and Okoh, 2011). These include inadequate supervision, poor construction materials, non-compliance to specifications, etc. Geophysical data provides vital information about the geology of subsurface strata, which is required for any engineering construction, drilling, production or mining activity. Therefore, scrupulous geophysical surveys and assessments of the earth are critical to reduce risk, failure and the cost of design of engineering foundations and structures.

Foundations are affected not only by design errors but also by foundation inadequacies such as sitting them on incompetent earth layers. When the foundation of a building is erected on less competent layers, it poses serious threat to the building which can also lead to its collapse (Adelusi *et al.*, 2013). Engineering geophysics therefore gives detail information on the degree of competence of the subsoil in foundation engineering (Ofomola *et al.*, 2009). Unfortunately, the search for adequate information on the nature of subsurface conditions prior to construction exercise has not been given serious attention in this part of the world. However, since every engineering structure is seated on geological earth materials, it is imperative to conduct pre-construction investigation of the subsurface of the proposed site in order to ascertain the strength and the fitness of the host earth materials as well as the timed post-construction monitoring of such structure to ensure its integrity.

The increase in the incessant failure of buildings has been attributed to subsurface problems which have not been taken into consideration by the owners and foundation engineers prior to foundation design and construction (Susan, 2004). Several lives have been lost and lots of properties have been wasted due to incessant collapse of buildings as a result of foundation problem, poor construction practice and the use of substandard building materials among other things (Bayode, *et al*., 2012).

In view of the above named factors , it is important to carry out pre-construction or post-construction geophysical investigation of a building site using appropriate geophysical field techniques (Akintorinwa and Adeusi, 2009; Ofomola, *et al*., 2009; Akintorinwa and Abiola, 2011; Bayode, *et al*., 2012 and Egwuonwu and Sule, 2012) to delineate the underlying geologic conditions. Foundation study of any site is necessary so as to provide subsurface and aerial information that normally assist Civil Engineers, Builders and Town Planners in the design and sitting of foundations for civil engineering structures (Omoyoloye, *et al*., 2008). For geophysical studies, electrical resistivity method is the most common technique used for such purpose (Gowd, 2004; Neil and Ahmed, 2006; Susan, 2004; Olorunfemi and Meshida, 1987; Dahlin, 1996), because the method is reliable, efficient and cost effective. Information such as thickness of the geological layers, depth to geological beds, depth to water table, depth to buried metals, and delineation of contaminant plumes, etc, can be determined using the method. Investigation involving foundation studies helps the civil engineers to know the depth at which the foundation could be placed and this will help in reducing the failure of the proposed civil structures and prevent enormous economic loss that always accompanies such failure.

1.2 Problem Definition

Foundations are affected not only by design errors but also by foundation inadequacies such as sitting them on incompetent layer which could lead to collapse of the building. It has been observed that inability to carry out pre-developmental geophysical studies have led to lots of structural problems, which result in dilapidation of building and loss of resources. In the light of the alarming rate of infrastructural failure despite geotechnical investigations, there is great need for geophysical engineering studies to be carried out in order to safeguard the infrastructures and buildings from any future distress that might arise. Hence, the need to carry out pre-construction engineering geophysical survey in the study area (Theatre and Media Arts Complex, FUOYE) as sitting engineering structures in this area without proper geophysical investigations may lead to failure and eventual collapse of buildings.

1.3 Description of the Study Area

1.3.1 Location and Accessibility

The study area is the site for the proposed Theatre and Media Arts Complex within the Federal University Oye-Ekiti, Ekiti State, Southwestern Nigeria. It is located beside the present Faculty of Science (Phase II), within the geographic grids of Eastings 755290 and 755698 mE and Northings 860074 and 860483 mN (Figure 1.1). It is accessible by road from Phase I of the campus.

1.3.2 Geomorphology

The study area is geographically located within the sub-equatorial climate belt of tropical rain-forest vegetation with evergreen and broad-leaved trees, luxuriant growth layer arrangement. During June through September, rainfall is critical and the amount is usually high, thus leading to high probability of soil erosion and flooding. July and September, are the first and second peak months. These two months are very significant because of sporadic,

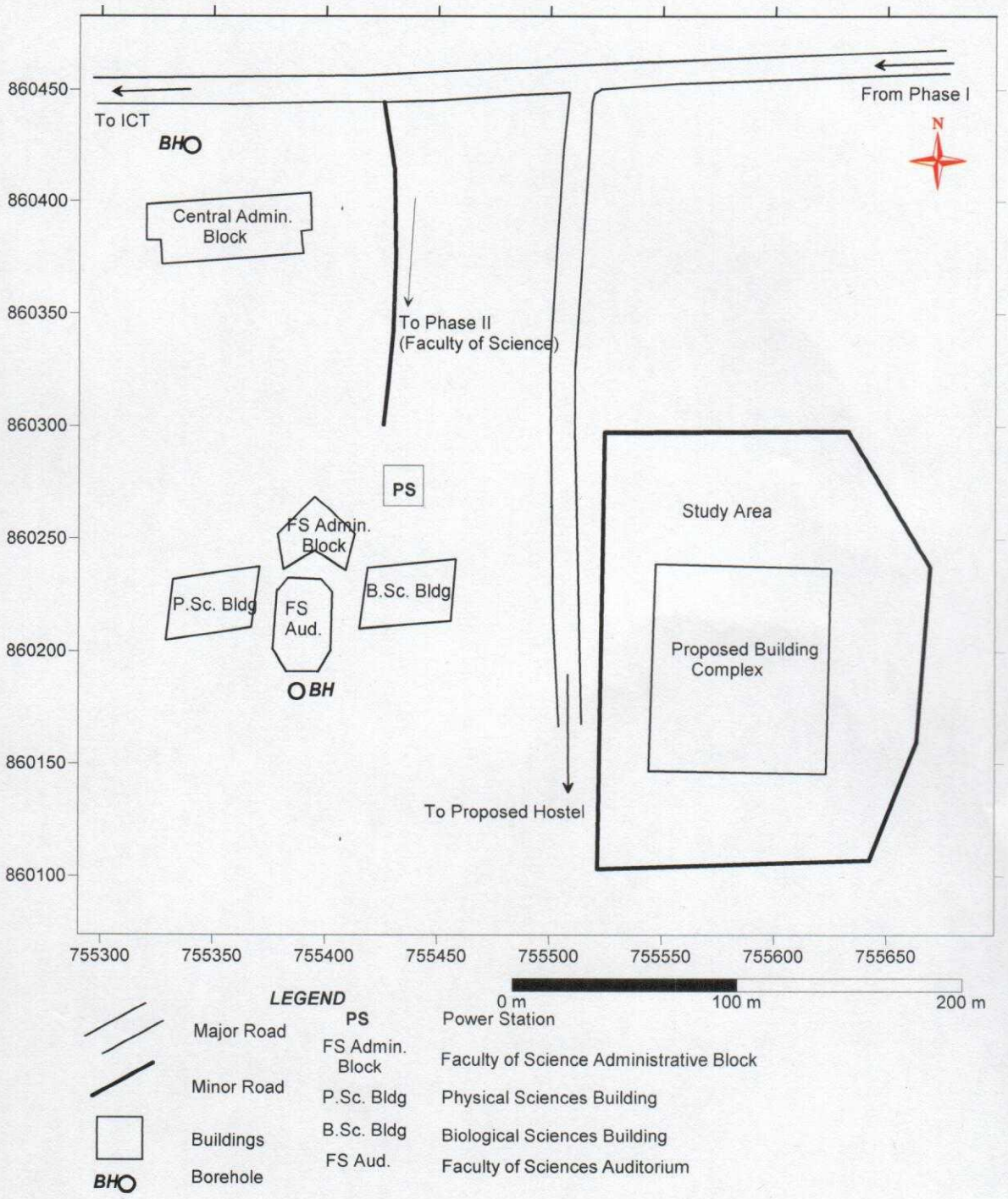

Figure 1.1: Base Map of the Study Area

heavy down pours. At times, rainfall in excess of 40 mm is recorded on a single day while the average annual rainfall is 1333.2 mm. The annual mean temperature is 33^0C while the mean minimum is 18^0C. Evaporation is usually low from June through September, ranging from 3.3 mm to 4 mm per day. Sunshine duration is short (4 to 6 hours per day) during the month or July to September, while the relative humidity ranges from 5.0 to 90% depending on the season (Owoyemi, 1996). The topography is generally undulating ranging between 510 and 535 m.

1.4 Aim and Objectives

The aim of this project is to conduct pre-construction geophysical investigation of the proposed Theatre and Media Arts Complex within Federal University Oye – Ekiti using integrated geophysical methods.

The objectives include to:

i. identify conductive/weak zones in the area
ii. map basement topography/bedrock structural deposition in the area
iii. delineate the subsurface sequence in the area
iv. determine the geoelectic parameters and the nature of the subsurface layers
v. identify any significant near-surface geologic structures such as cavity, sinkhole, fault, near-surface rock, and
vi. infer the level of competence of the near-surface layers to host the building foundation.

1.5 Previous Works

Among the several researchers that have worked on the subject matter are: Akintorinwa and Adeusi (2009), Adelusi *et al*. (2013) and Ogungbemi *et al*. (2013).

Akintorinwa and Adeusi (2009) carried out geophysical and geotechnical investigation for a newly proposed School of Earth and Mineral Sciences (SEMS) Lecture Complex, Federal

University of Technology, Akure using Electrical Resistivity Method. A total of 24 soundings were carried out using the Schlumberger configuration. It was deduced from the results that the topsoil Formation can be rated as relatively good as a foundation material, the foundation of the proposed civil structure can be hosted by this formation and the uneven nature of this layer has to be considered in the design of the foundation.

Adelusi *et al.* (2013) carried out geophysical investigation around School of Science, Obanla, Federal University of Technology, Akure, for post construction studies in assessing building foundation integrity. Three geophysical methods involving the magnetic, very low frequency electromagnetic (VLF-EM) and the electrical resistivity methods were adopted for this survey. Sixteen sounding stations were occupied along the two established traverses and the current electrode spacing (AB/2) was varied from 1 to 65 m. The VLF-EM result mapped three near surface conductive zones suspected to be fractures/faults which are inimical to foundation integrity. The magnetic results delineated series of bedrock ridges and depression. The VES result delineated four major geo-electric layers within the study area which are the topsoil, weathered layer, fractured bedrock and fresh bedrock. The dipole-dipole results also mapped linear features (fracture) at distance 60 to 100 m and 100 to 120 m respectively along the two traverses. It was concluded that the failure is due to lateral inhomogeneity of the subsurface layers, failure precipitated by differential settlement and failure initiated by geologic features such as fractures and faults.

Ogungbemi *et al.* (2013) combined geophysical investigation involving very low frequency electromagnetic (VLF-EM) and electrical resistivity methods at Ijapo Housing Estate, Akure, Southwestern Nigeria, to assess foundation integrity for future engineering construction in the area in a bid to stamp out the persisting incidence of collapse of buildings. The electrical resistivity method utilized the Vertical Electrical Sounding (VES) technique and delineated

about four major geoelectric layers namely: the topsoil, lateritic layer, weathered basement and the fresh basement and series of bedrock ridges and depressions. Therefore, subsequent construction are advised to be restricted to the competent zone, while building foundations within the incompetent zone should be anchored on the bedrock without exceeding the load bearing capacity.

1.6 Expected Contribution To Knowledge

The results of this integrated geophysical studies will provide the following contributions to knowledge:

i. provision of detailed information on the near-surface internal structure of the site,
ii. assist in construction planning programme for engineering designing of the proposed building that will safeguard the proposed infrastructure/building from any future distress.

CHAPTER TWO

LITERATURE REVIEW

2.1 Geologic Settings

2.1.1 Regional Geology

Geologically, Nigeria falls into two main geological terrain known as the Basement complex and Sedimentary basins/environment. The former consist of hard rocks like igneous and metamor- phic rocks, and the latter consists of soft rocks such as sandstone, clay, limestone, etc (Figure 2.1).

The crystalline basement rocks outc rops in the North Central, South East, North-East and Southwestern geologic regions of Nigeria. Four major groups of rocks have been recognised within the Precambrian basement complex rocks of Southwestern Nigeria (Rahaman, 1988) which are:

i. Migmatite-Gneiss-Quartzite complex, which comprises biotite, hornblende gneiss, quartzite and quartz schist and small lenses of calc-silicate rocks.

ii. Slightly migmatised to unmigmatised paraschists and meta-igneous rocks which consists of pelitic schists, quarzite, amphibolites, talcose rocks, metaconglomerates, marbles and calc-silicate rocks.

iii. Older granites, which comprises rocks varying in composition from granodiorite to true granites and potassic syenite, and Charnockitic rocks which have the coarse-grained variety, massive fine grained and the gneissic fine-grained types. All the Charnockitic rocks in the region are grey rocks with greenish quartz and bluish feldspars.

iv. Unmetamorphosed dolerite dykes believed to be the youngest, these rocks are mainly granites in composition and at different stages of metamorphism either as gneiss, migmatite, schist, phyllites and quartzite.

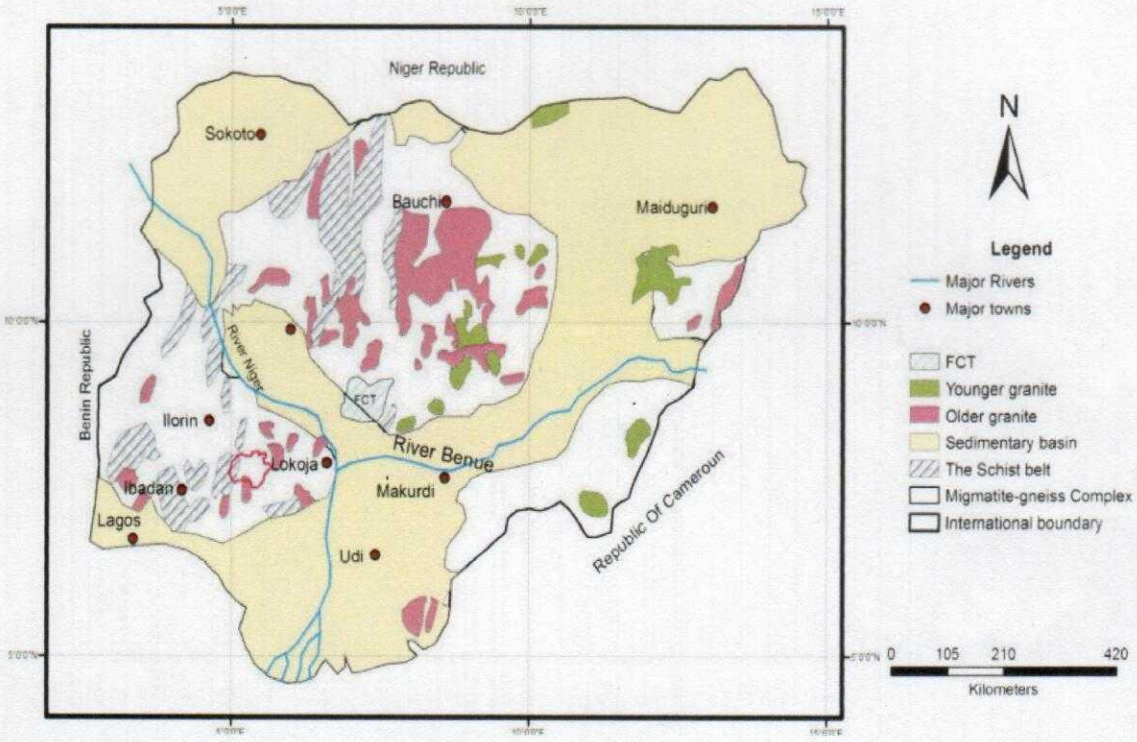

Figure 2.1: Geological Map of Nigeria showing the Basement Complex and Sedimentary Terrain (After Rahaman, 1988).

2.1.2 Local Geology

The geology of Federal University Oye-Ekiti is part of the basement complex rocks of Southwestern Nigeria. Major lithological rock unit present within the area is Migmatite (Figure 2.2). The rock is generally even textured and gneissic with mineral aggregates mainly of Quartz, biotite and feldspar. The superficial deposits are clay, laterite and fine sands (SiO_2) which are believed to have been formed from the weathering of the minerals present in the rock.

2.1.3 Hydrogeology

The hydrogeology of the study area (FUOYE) consists of streams and rivers that drain water away. The streams found within the school flows majorly from N-S. Underground water could also be found in the weathered layers and bedrock structures such as fault and fractured zones accumulated due to the process of infiltration of rain/meteoric water into the subsurface through interconnected pore spaces.

2.2 Basic Principles and Theory of Geophysical Methods Used

In the geophysical survey of Federal University Oye-Ekiti (FUOYE) three (3) geophysical methods were used

i. Electromagnetic method,
ii. Magnetic method, and
iii. Electrical Resistivity method.

2.2.1 Electromagnetic Method

Electromagnetic methods in general may be either natural or artificial. In principle, the VLF-EM method is a type of artificial electromagnetic method which makes use of the field of a vertical wire.

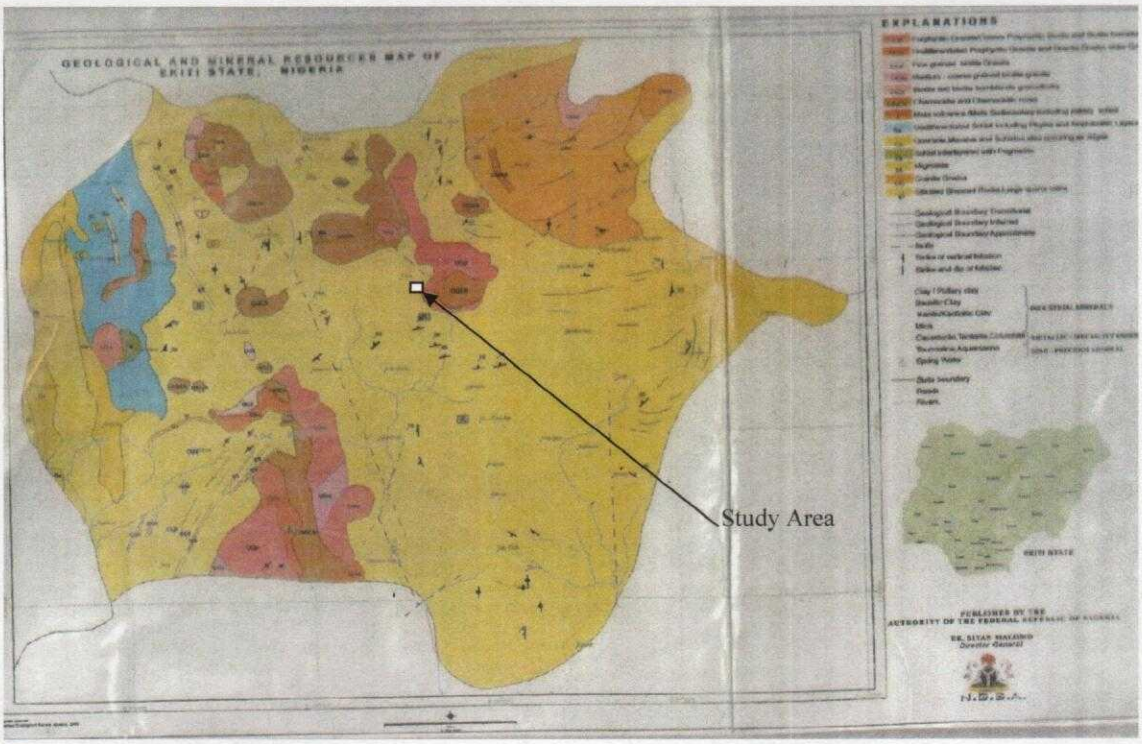

Figure 2.2: Geological Map of Ekiti showing the Study Area (after NGSA, 2006).

2.2.1.1 Electromagnetic Theory

The determination of both magnetic and electric fields generated in any region requires the use of some field vectors stated below:

E = Electric field intensity (V/M)
B = Magnetic flux density (Webers/m^2)
H = Magnetic field intensity (Ampere turns/m)
D = Electric displacement (Coulombs/m)
J = Current density (Ampere/m^2)
A = Vector magnetic potential

Maxwell's electromagnetic equation in equation 2.1 relates these vector fields

$$\nabla \times E = \frac{\partial B}{\partial t} \quad \text{.....2.1}$$

$$\nabla \times H = J + \frac{\partial D}{\partial t} \quad \text{.....2.2}$$

But $B = \mu H$ 2.3

Where μ = magnetic permeability

$$\nabla \times E = -\mu \frac{\partial H}{\partial t} \quad \text{.....2.4}$$

These equations and the Maxwell's law of induction are the basis on which electromagnetic theory is pivoted (Telford *et al.,* 1990).

The use of a potential to obtain field vectors is allowed in potential theory. Therefore, on differentiation, both electric and magnetic field vectors are obtainable from this magnetic induction B (Telford *et al.,* 1990) below:

$$\nabla \times E = B \quad \text{.....2.5}$$

Combining equation 2.1, 2.2 and 2.5, then:

$$E = \frac{-\partial A}{\partial t} \quad \text{.....2.6}$$

Taking the divergence of equation 2.1 and 2.2 using the vector identity

$$\nabla.\nabla\times A=0 \quad \text{.....2.7}$$

Time varying fields given below are obtained

$$\nabla.\nabla\times E=-\nabla\frac{\partial B}{\partial t}=-\frac{\partial}{\partial t}[\nabla.B] \quad \text{.....2.8}$$

Similarly,

$$\nabla.J+\nabla\frac{\partial D}{\partial t}=\nabla.J+\frac{\partial}{\partial t}\nabla[\nabla.D]=0 \quad \text{.....2.9}$$

Hence

$$\nabla.B=\nabla.E=0 \quad \text{.....2.10}$$

The following vectors identified below are useful when taking the curl of a vector.

$$\nabla\times\nabla\times A=\nabla(\nabla.A)-\nabla^2A=-\nabla^2A \quad \text{.....2.11}$$

Since $\nabla.A=0$ from equation (2.10) then taking the curl of equation (2.5) and using the identity in equation (2.11) results into:

$$\nabla\times\nabla\times A=-\nabla^2A=\nabla\times B \quad \text{.....2.12}$$

On substituting $B=\mu H$ into equation (2.12)

$$-\nabla^2A=\nabla\times\mu H=-\mu(\nabla\times H) \quad \text{.....2.13}$$

Since, $\nabla\times H=J+\frac{\partial D}{\partial t}$ from equation (2.2)

$$D=\in E \quad \text{.....2.14}$$

Where, $\in$= Electric permeability

Then equation (2.13) becomes

$$\nabla^2A=-\mu\left[J+\frac{\in\partial E}{\partial t}\right] \quad \text{.....2.15}$$

When $\in$ is very small, $\in\partial E$ becomes negligible such that equation (2.15) becomes

$$\nabla^2A=-\mu J \quad \text{.....2.16}$$

This relation stated in equation (2.16) resembles Poisson's equation in gravity and magnetic (Telford *et al.*, 1990).with the solution

$$A = \frac{\mu}{4\pi}\int \frac{J\partial v}{r} \quad \text{.....2.17}$$

Where $r = \left(x^2 + r^2 + z^2\right)^{1/2}$

Equation (2.17) is of great importance when determining various magnetic fields for different configurations of electromagnetic transmitters.

2.2.1.2 Biot-Savart Law

This law relates the magnetic field at a point in a space to a current flowing in a short straight element of a conductor some distance away (Figure. 2.3) (Telford *et al.*, 1990). This law can be derived using vector potential expression established in equation (2.17),

$$A = \frac{\mu}{4\pi}\int \frac{J\partial v}{r} \quad \text{.....2.17}$$

Equation (2.17) can be expressed in terms of a line integral as:

$$A = \frac{\mu}{4\pi}\oint \frac{I\partial s}{r} \quad \text{.....2.18}$$

Using equation 2.3, 2.5 in equation 2.18 and carrying out the line integral over a closed path surrounding the wire element, gives:

$$dH = \frac{\partial B}{\mu} = \frac{\nabla \times \partial A}{\mu} \quad \text{..... 2.19}a$$

$$dH = \nabla \times \frac{\partial\left[\frac{\mu}{4\pi}\oint \frac{I\partial s}{r}\right]}{\mu} \quad \text{..... 2.19}b$$

$$dH = \frac{I\partial s}{4\pi}\left[\hat{r} \times \nabla\left[\frac{I}{r}\right]\right] \quad \text{..... 2.19}c$$

$$dH = \frac{I\partial s \times \hat{r}}{4\pi r} \quad \text{..... 2.19}d$$

This on further simplification yields

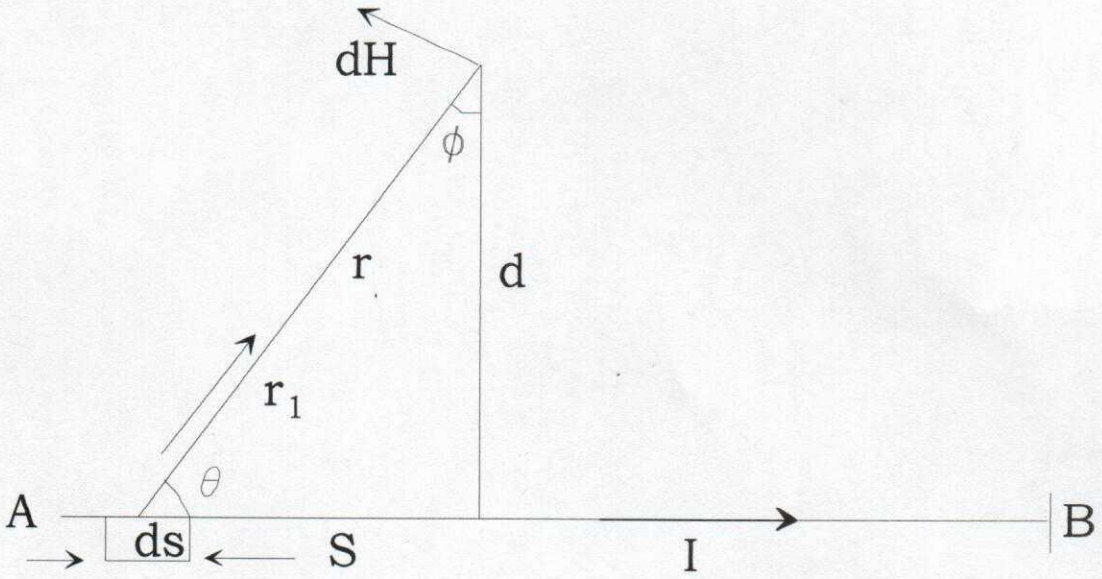

Figure 2.3: Illustration of Biot – Savart Law (Telford *et al.*, 1990).

$$dH = \frac{I\partial Sin\theta}{4\pi r} \quad \text{.....2.20}$$

Equation (2.20) is referred to as the Biot-Savart equation. It describes the magnetic field dH at a point P a distance r away to current I flowing through an element *ds* of a wire (Telford *et al.,* 1990).

2.2.1.3 The Field of a Vertical Wire

It is applicable in VLF-EM method. In theory, there are two electric field components E_θ and E_r and one magnetic field component H_θ (Figure 2.4), (Telford *et al.,* 1990).

$$H_\theta = \frac{I\delta l}{4\pi} \ell^{j\omega\left[t-\frac{r}{c}\right]}\left[\frac{j\omega}{rc}+\frac{1}{r^2}\right]Sin\,\theta \quad \text{..... ....2.21}$$

$$E_\theta = \frac{I\delta l}{4\pi} \ell^{j\omega\left[t-\frac{r}{c}\right]}\left[\frac{j\omega}{rc^2\varepsilon}+\frac{1}{r^2 c\varepsilon}-\frac{j}{r^3\omega\varepsilon}\right]Sin\theta \quad \text{.....2.22}$$

$$E_r = \frac{I\delta l}{2\pi} \ell^{j\omega\left[t-\frac{r}{c}\right]}\left[\frac{1}{r^2 c\varepsilon}-\frac{j}{r^3\omega\varepsilon}\right]Cos\,\theta \quad \text{.....2.23}$$

Where,

$$C = \frac{1}{\sqrt{\mu\varepsilon}}$$

$$\omega = 2\pi f$$

At a large distance from the source (transmitter) $\frac{1}{r^2}$ *and* $\frac{1}{r^3}$ becomes negligible. Thus equation 2.21, 2.22 and 2.23 becomes;

$$H_\theta = \frac{j\omega I\delta l}{4\pi cr} \ell^{j\omega\left[t-\frac{r}{c}\right]}Sin\theta \quad \text{.....2.24}$$

$$E_\theta = \frac{j\omega\ I\delta l}{4\pi c^2\varepsilon r} \ell^{j\omega\left[t-\frac{r}{c}\right]}Sin\,\theta \quad \text{..... ....2.25}$$

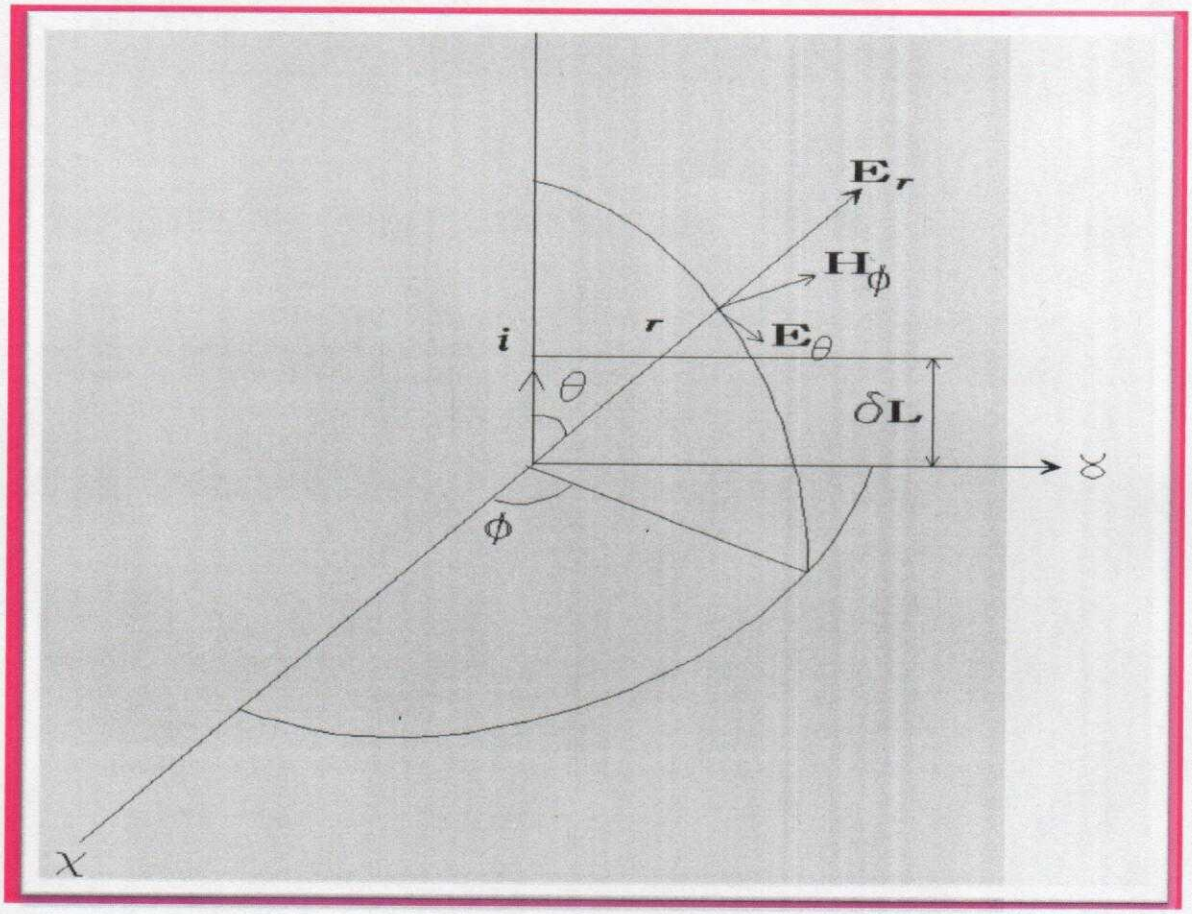

Figure 2.4: Field of a Current Flowing in a Short Straight Element of a Conductor (Telford *et al.*, 1990).

$E_r = 0$.....2.26

Where,

C = Speed of light in free space

j = Current Density

ω = Angular Velocity

r = Radius

I = Current

l= Length of the vertical wire

t = Time

ℓ = Electric Resistivity

E = Electric Field Intensity (volt/m)

ε = Permittivity of a medium

H = Magnetic Field Intensity (Teslas)

2.2.1.4 Principle of VLF-EM Method

An alternating current usually with a frequency of between 15 to 30 kilohertz is passed through a transmitting vertical coil into the ground which generates an electromagnetic field around the coil. When the field emitted by the transmitter strikes an anomaly having low electrical resistivity, it generates secondary current or eddy current, which in turn creates a magnetic (secondary) field that opposes the original field that is emitted from the transmitter (Telford *et al.,* 1990) (Figure 2.5). The magnetic field received and measured by the receiver at the surface is the resultant of the secondary field created by this induced current and that of the primary field due to the transmitter. Usually, there is difference in direction and phase between the primary and the secondary field, and the current induced in resultant field and its magnitude. The signal from the receiver is usually divided into two components; one that is in-phase with the signal generated in the receiving coil by the transmitter in the presence of a

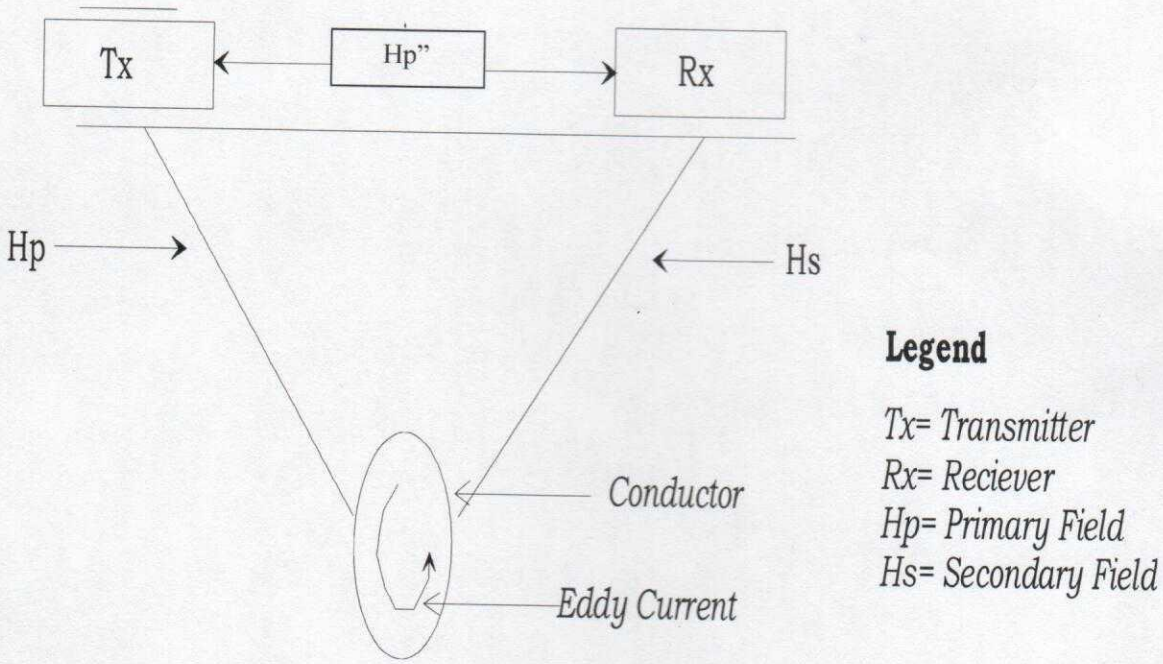

Figure 2.5: Typical Tx-Rx Electromagnetic Layout. (Sharma)

secondary field and the other is out of phase (or quadrature part) by a difference of 90^0 with it. The in-phase represents the real part of the signal while the quadrature part represents the imaginary part (Telford *et al.,* 1990). A body must have a minimum size and sufficient low resistivity for any secondary field to be created. More so, the strike length of the body must exceed about 5 m, and the depth extent must exceed about 10 m for induction to occur. The thickness of the body in any case needs only to be about 0.5 – 1 m. Nevertheless, the field from the VLF transmitter must pass perpendicularly through the body, i.e. the direction to the transmitter is in the strike direction of the body.

2.2.1.5 Depth of Penetration of Electromagnetic Field

The depth of penetration of an electromagnetic field depends on its frequency and electrical conductivity of the medium through which it is propagated. The passage of electromagnetic field through the ground causes their attenuation and thus results in the decrease in their amplitude exponentially with depth. The depth of penetration of electromagnetic wave 'd' is defined as the depth at which the amplitude of the field A_d is decreased by a factor e^{-1} compared with its surface amplitude A_0 (Telford *et al.,* 1990).

Therefore,

$$A_d = A_0 e^{-1} \quad \text{.....2.27}$$

Thus,

$$D = 503.8\,(\sigma f)^{-½} \quad \text{.....2.28}$$

Where D (skin depth) is in metres, the conductivity of the ground (σ) is in Sm^{-1} and the frequency (f) of the field is in Hertz. The depth of penetration is therefore inversely proportional to both the frequency of the electromagnetic field and the conductivity of the ground.

Equation (2.28) above only analyses a theoretical path of penetration, hence Z_c is used and this represents the maximum depth at which a conductor may be and still produces a recognizable electromagnetic anomaly.

Thus,

$$Z_c = 100(\sigma f)^{-\frac{1}{2}} \quad \text{.....2.29}$$

Equation (2.29) is approximate because the penetration of electromagnetic waves depends upon such factors as the nature and magnitude of the effects of near surface variations in conductivity, the geometry of the subsurface conductor and instrumental noise.

2.2.1.6 Applications of VLF-EM Method

(i) To delineate fracture zones for groundwater development.

(ii) To locate buried pipes, electrical cables and tanks.

(iii) To map metallic ores particularly sulphides.

(iv) To delineate steeply dipping structures such as faults and fractures.

2.2.1.7 Limitations of VLF-EM

The limitations of VLF-EM method is that the depth of penetration is somewhat less than that attainable by tilt-angle method using a local transmitter. Moreso, for a particular survey area, there may be no suitable transmitter providing a magnetic vector across the geological strike.

2.2.2 Principle of Magnetic Method

Magnetic survey investigates subsurface geology using the earth's magnetic field. Magnetic properties of the underlying rock forming minerals are measured with certain rock types containing sufficient magnetic anomalies. Also man-made ferrous object generate magnetic anomalies. The study of the earth's magnetic is the oldest method of geological investigation exploration works used to explore for oil, minerals and locating features and faults zones. It is an undisputable fact that the earth behaves as a large and somewhat irregular magnet (Sharma

1997). This method in applied geophysics depends on measuring accurately the anomalies of local magnetic field produced by the variations in the intensity of magnetization in rock formation. The magnetization of rock is partly due to the induction of magnetizing forces associated with the earth fields and partly by their permanent (remanent) magnetization. The induced intensity depends primarily on the magnetic susceptibility as well as magnetizing force and the permanent (remanent), intensity depends on the geological history of the rock.

The method is the measurement of direction of gradient or intensity of the earth's magnetic field and interpretation of variation in quantities over the area of investigation. The magnetic method is of great relevance in areas of contrasting magnetic contents bringing out variations due to change in magnetic properties of subsurface rock. The anomaly caused by these changes in physical properties is termed the magnetic anomalies which are often diagnostic of minerals, structures as well as regional structures.

The horizontal and the vertical variations in magnetic susceptibilities of underlying rock units causing these departures are the origin of the magnetic anomaly. The conventional unit of magnetic intensity is the oersted though most geological literature often uses the numerically equivalent gamma. This is due to the fact that, the practical use is prospecting. The gamma defined as 10^{-5} Oe is more convenient and has become most common unit of field intensity for geophysical works. The most significant magnetic property of rocks is their susceptibility K which is defined as a measure of the magnetic mineral content in a rock (Folami, 1980). It is the fundamental parameter in magnetic prospecting. Another property of rocks is natural magnetization.

For a vacuum and for entirely non-magnetic substances, K is equal to zero (K = 0). Magnetic mineral having positive susceptibility are known as para-magnetic grains as such material tends to line up with their long dimension in the direction of the external field. A para-

magnetic material of very high susceptibility may be referred as ferromagnetic. There are few cases of negative susceptibility as rock salt and anhydrites which are designated as diamagnetic. Grains of such material tend to line up with their long dimension across the external field. In case of homogenous external field H, for a field normal to the surface of a material, capable of being magnetized, the induced pole strength per unit area is:

$$J = KH \quad \ldots\ldots 2.30$$

$$J = KH \cos \theta \quad \ldots\ldots 2.31$$

Where, J = Magnetization

K = Susceptibility (proportional constant)

H = External Magnetic field making angle Θ with the normal to the surface of material.

For low magnetic concentration, there is an approximately linear relationship between the percentage of magnetic and susceptibility, K, which is expressed as K = 0.3P, where P is the percentage (by volume) of magnetic dissemination (Owoeye, 2000). Generally, the darker basic rocks are more magnetic than the light coloured acidic rocks.

2.2.2.1 Fundamental Definition and the Physical Concepts of Magnetics

2.2.2.1.1 Magnetic Force

A magnetic force is the mechanical force which a magnet experiences in the area of an electric current and the converse; mechanical force exerts on the current (Parasnis 1979). This may be attractive or repulsive depending on the nature of its poles. Magnetic poles are region where lines of force leaves and enter a magnetic body following a curve path from one end of the magnetic body designated as the North pole to a corresponding South pole near the other end (Figure 2.6).

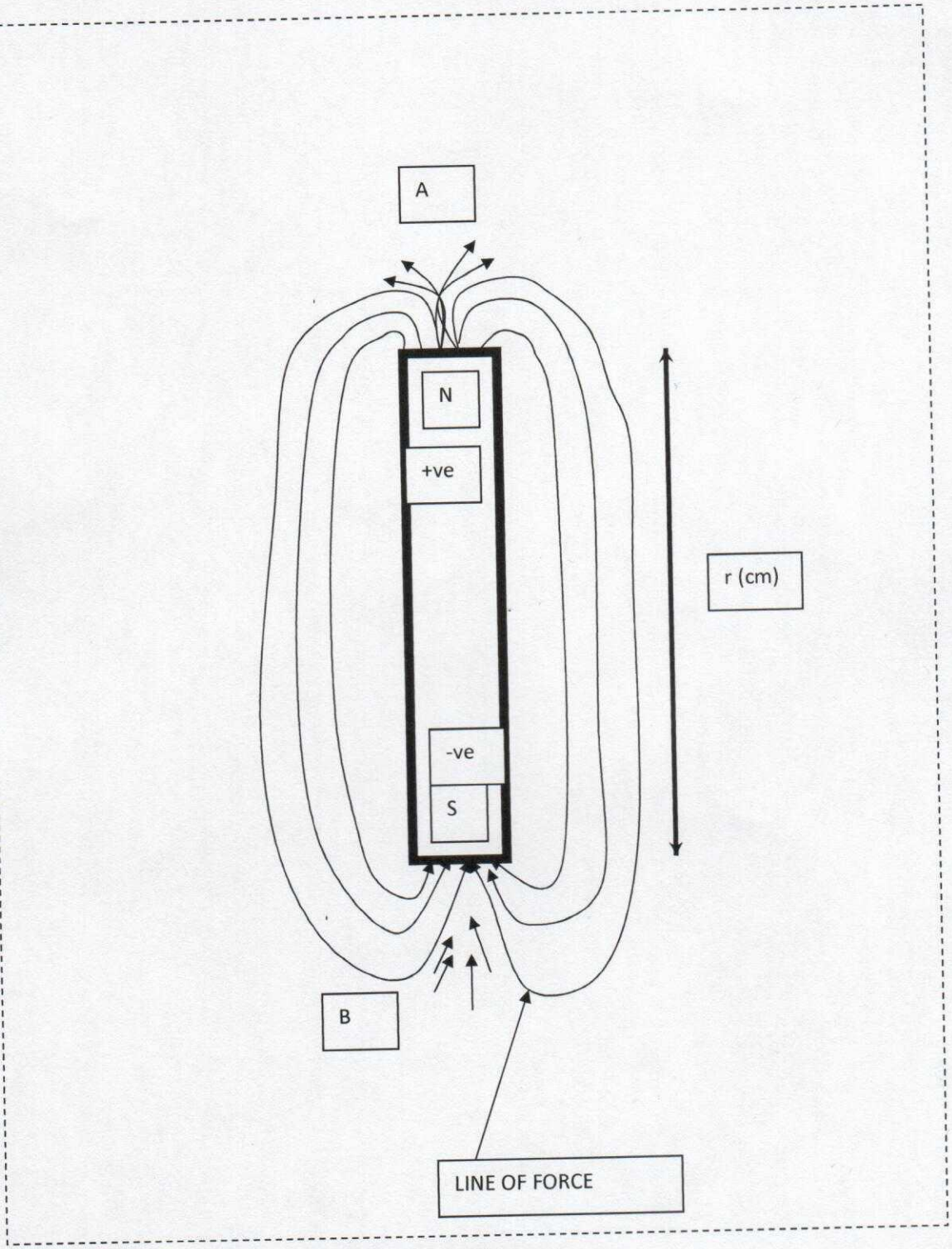

Figure 2.6: Line of Force around a Bar Magnet.

The Magnetic force for the poles of strength M_1 and M_2 at a distance r apart is thus:

$$F(r) = \frac{M_1 M_2}{r^2} \quad \text{..... 2.32}$$

This is obtained from the Coulomb's law for magnetic poles. This force is one of repulsion between like pole and attraction between unlike poles for dipole interpretation, if M, is a limit pole straight at the point P, the force per unit pole strength H(r) is given by

$$\overrightarrow{H(r)} = \frac{F(r)}{m_1} = \frac{m_2}{r^2} \quad \text{..... 2.33}$$

The field is conservative and is therefore desirable for a sector potential $\overrightarrow{A(r)}$, such that

$$\overrightarrow{H(r)} = \frac{F(r)}{m_1} = \overrightarrow{A(r)} \quad \text{..... 2.34}$$

Where,

$$\overrightarrow{A(r)} = \frac{m_2 \cos\theta}{r^2} \quad \text{..... 2.35}$$

Where,

θ is the angle measured from m to r

r and θ are unit vectors

H(r) is the force per unit pole strength of magnetic field intensity at P.

Putting equation (2.34) into (2.35) and expressing it in the form of equation (2.36), we obtain

$$T = \frac{M}{r^3} \quad \text{.....2.36}$$

M is the magnetic moment and r is the distance to the pole Where, H(r) is equivalent to T, the total magnetic intensity along the axis $\theta = 0^0$,

T = 2m end along the line of right angle to the dipole where

$\theta = 90^0$,

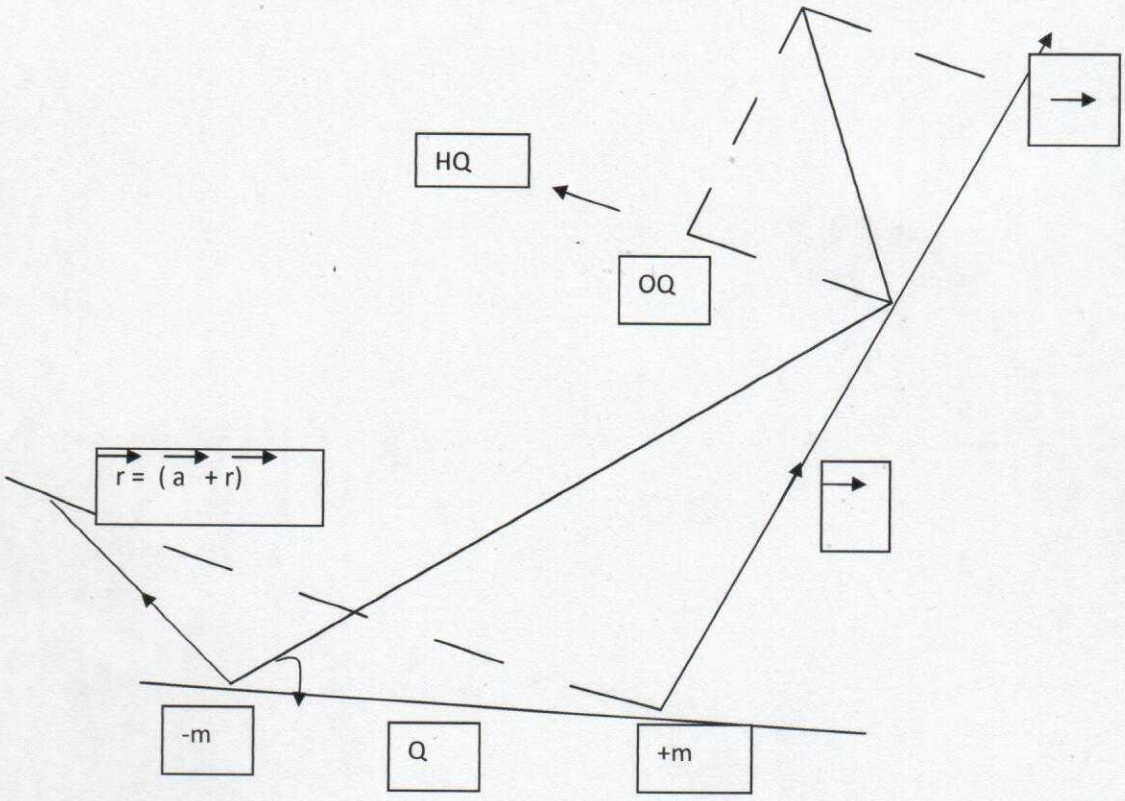

Figure 2.7: Intensity at a Point Due to A Bar Magnet

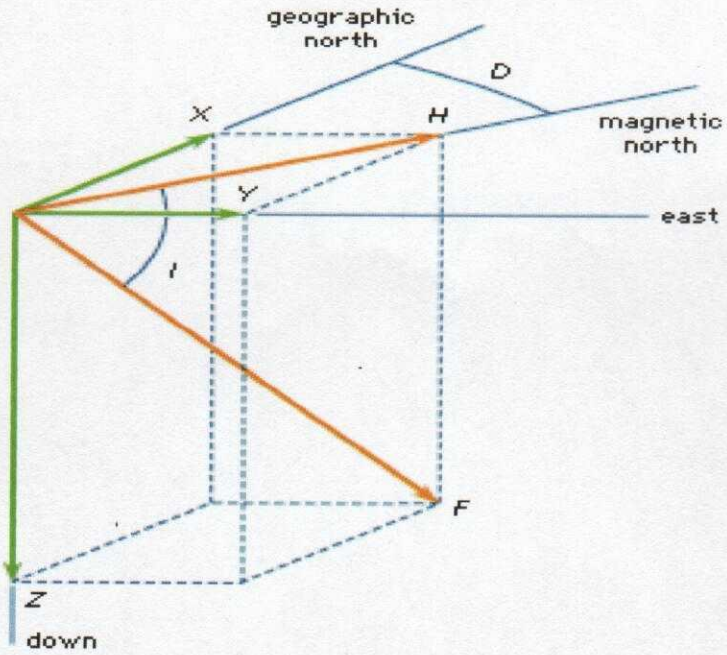

Figure 2.8: Element of the Earth Magnetic Field (Sharma, 1997).

The angle which T makes with its horizontal component H is the inclination I and the angle between H and X (which by convention points North) is the declination D (Sharma, 1997). The quantities X, Y, Z, D, I. H and T, known as magnetic elements are related as follows:

$H = \text{Cos } i$ 2.38

$Z = T \text{ Sin } i \text{ or } H \text{ Sin } i$ 2.39

$X = H \text{ Cos } D$ 2.40

$Y = H \text{ Sin } D$ 2.41

$H^2 = X^2 + Y^2$ 2.42

$T^2 = H^2 + Z^2$ 2.43

$T^2 = H^2 + Y^2 + Z^2$ 2.44

The two points (in principle) on the earth's surface where the dip is equal to 90^0 are known as the dipoles. However, because of local anomalies there may be several points in the general polar region where the dip is vertical ($+90^0$). The earth's magnetic field resembles the field of a large bar magnet near its centre. But unlike the field of a bar magnet, it does not vary in intensity with distance from the poles on the surface of the earth according to the inverse square law.

2.2.2.3 Magnetic Properties

Magnetic mineral content in a rock are of varying properties such as the magnetic susceptibility and remanent magnetization. The magnetic susceptibility is the measure of magnetic mineral content in a rock (Folami, 1980) given by:

$$K = \frac{J}{N \times 10^{-5}} \quad \text{.....2.45}$$

Where,

J = Induced magnetization

N = Field strength

K = Susceptibility (Constant of proportionality depending on the material of the body).

This is called magnetic susceptibility per unit volume.

For an anisotropy crystal, the susceptibility along the three principal magnetic axis are different and the measurement on their power samples given the average of the three values. However, for isotropic crystals, the susceptibility is the same in all direction. Magnetic anomalies are by induced and remanent (permanent) magnetization. The induced magnetization refers to the action of the field on the materials where in the ambient field is enhanced while the remanent magnetization is preserved in the rock and is dependent on the direction and the intensity on the earth's field at the time the rock last cooled. Though, the curie temperature of the magnetic mineral present in the rock, the remanent magnetization is of great importance in mapping and interpretation which often dominates the induced ore and should not be omitted so as to avoid errors in calculating the dip, breadth, and volume. In practice, residual magnetism often contributes to the total magnetization in rocks both in amplitude and direction. The effect is quite complicated because of dependence on magnetic history of the rocks.

2.2.2.4 Types of Magnetization

The residual magnetism is called **Natural Remanent Magnetization** (NRM) which may be due to ore of several causes.

Chemical Remanent Magnetization (CRM) takes place where magnetic grains increases in size as a result of chemical action at moderate temperature. This process is particularly significant in sedimentary and metamorphic rocks.

Detrital Remanent Magnetization (DRM) occurs during the slow selling of fine grained particles in the presence of an external field.

Isothermal Remanent Magnetization (IRM) is the residual magnetism left following the removal of an external field. Lightening strokes produce IRM over very small irregular areas.

Thermo-Remanent Magnetization (TRM) results from magnetic material being cooled from the Curie point in the presence of an external field e.g cooling of magma on the earth's surface. The remanent magnetism acquired in this fashion is stable.

Viscous Remanent Magnetization (VRM) is produced by a long exposure to an external field. The building up for remanence being a logarithm functions of time. The remanence is quite stable.

Of all the above discussed, the IRM is the most important cause of NRM. Hence, NRM is of considerable importance in interpreting magnetic survey over areas of igneous rocks (Reedman, 1979).

2.2.2.5 The Geomagnetic Field

The earth magnetic field is a vector quantity with variable magnitude and direction defined over an almost spherical polarized sphere. Physically, the origin of the field seems to be a system of electric currents within the earth (Parasnis, 1979). The earth's field is not constant at any point on its surface but undergoes variation of different periods.

It is established that the geomagnetic field is composed of two parts:

The Main Field: This is the field of internal origin not constant in time. It varies relatively slowly.

The External Field: This is a small fraction of the main field which varies rather rapidly, partly cyclically, partly randomly and originates outside the earth.

2.2.2.6 Limitations of Magnetic Survey

i. **Secular Variation**: Changes in the earth magnetic field which occur over many years are called secular variation. From continuous observation at many stations one can

conclude that secular are not regular and varies depending on the position and epoch. The cause may be attributed mostly to the internal phenomenon of the earth.

ii. **Diurnal Variation**: In addition to secular variation magnetic element changes within a period of 24hrs. The variations are not all that regular for each day but depend on the position of the observation and the day of observation. This effect is also called Solar Diurnal Variation. The Diurnal variation is usually corrected for from the observed magnetic values.

iii. **Magnetic Storm:** Sudden and violent variation in geomagnetic field which affect the magnetic reading. There is no satisfactory method of correcting it. The safest method is to discontinue the field and resume when the storm is over.

2.2.3 Theory of Electrical Resistivity Method

2.2.3.1 Basic Principles and Theory of Electrical Resistivity Method

Electrical resistivity prospecting method involves the passage of electric current (usually direct current or low frequency alternating current) into the subsurface, through two electrodes (the current electrodes). The potential difference is measured between another pair of electrodes, which may or may not be within the current electrodes depending on the electrode array in use.

Consider a current flowing in a cylindrical conductor of length, L, with cross-sectional area A, and current I, flowing through it (Figure 2.9).

The resistance R is expressed as:

$$R \propto \frac{L}{A} \quad \text{.......... 2.46}$$

$$R = \rho \frac{L}{A} \quad \text{.......... 2.47}$$

Where ρ is the constant of proportionality called resistivity.

However, from ohms law:

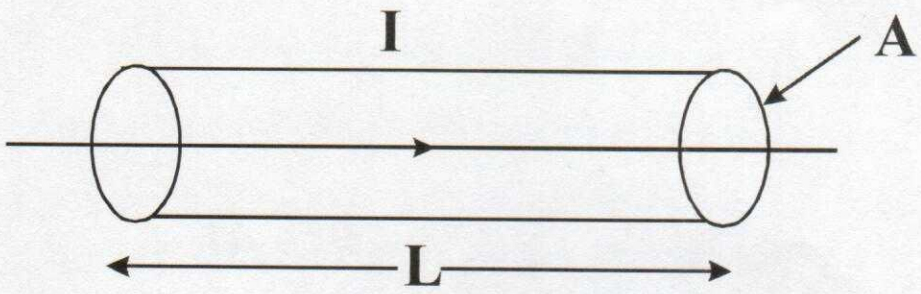

Figure 2.9: Schematic Diagram of the Flow of Current through a Cylindrical Model (Conductor).

$$R = \frac{\Delta V}{I} \quad \text{..... 2.48}$$

By substituting for 'R' in equation (2.47)

$$\frac{\Delta V}{I} = \rho \, L/A$$

$$\frac{\Delta VA}{I} = \rho L$$

$$\therefore \rho = \frac{\Delta VA}{IL} \quad \text{---------- 2.49}$$

Where, ΔV = Potential difference between any two points measured in volts.

Equation (2.49) can be used to determine the resistivity of a homogeneous and isotropic medium provided the geometry is simple e.g cylinder, cuboid, parallelopipe.

$$\rho = \frac{\lim_{L \to 0} \frac{\Delta V}{L}}{\lim_{A \to 0} \frac{I}{A}} = \frac{E}{J} \quad \text{..... 2.50}$$

Where, E is the electric field and J is the current density.

From Equation (2.50);

$$E = J\rho \quad \text{.....2.51}$$

Imagine that the current source is located at the centre of a spherical body (earth) of radius 'r' (Figure 2.10), then the current density at the spherical surface is:

$$J = \frac{I}{A} \quad \text{.....2.52}$$

Where A = area of the spherical surface,

Given; $A = 4\pi r^2$;

$$J = \frac{I}{A} = \frac{I}{4\pi r^2} \quad \text{..... 2.53}$$

Substitute equation (2.51) into (2.53);

$$E = \frac{I\rho}{4\pi r^2} \quad \text{.....2.54}$$

Since, E is the gradient of scalar potential;

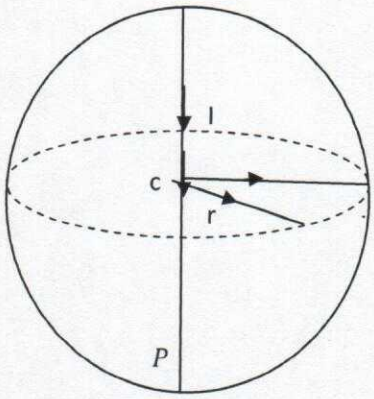

Figure 2.10: Current Source on a Spherical Surface

$$E = -\Delta V = \frac{-\delta V}{\delta r} \quad \text{.....2.55}$$

Equating equations (2.54) and (2.55);

$$\delta V = \frac{-I\rho\delta r}{4\pi r^2} \quad \text{.....2.56}$$

Taking the integral of both sides:

$$V = \frac{I\rho}{4\pi r} \quad \text{.....2.57}$$

In practice the earth surface structure is taken as an approximate hemisphere (Figure 2.11).

The current density (J) is defined as:

$$J = \frac{I}{A} \quad \text{.....2.58}$$

The area of a hemisphere is $2\pi r^2$, thus

$$J = \frac{I}{2\pi r^2} \quad \text{.....2.59}$$

$$\therefore E = \frac{I\rho}{2\pi r^2} \quad \text{.....2.60}$$

But, $E = -\Delta V = \frac{-\delta V}{\delta r}$ 2.61

$$\delta V = \frac{-I\rho}{2\pi r^2}\partial r \quad \text{.....2.62}$$

Taking the integral of both sides, equation (2.62) becomes:

$$\int \delta V = \int \frac{-I\rho}{2\pi r^2}\delta r \quad \text{.....2.63}$$

i.e. $V = \frac{I\rho}{2\pi r}$ 2.64

2.2.3.2 Generalized Apparent Resistivity Equation

Consider the diagram in Figure 2.12; it illustrates a simple current source at the surface of the earth. The potential 'V' is at a distance 'r' from the current source. The potential at point P_1

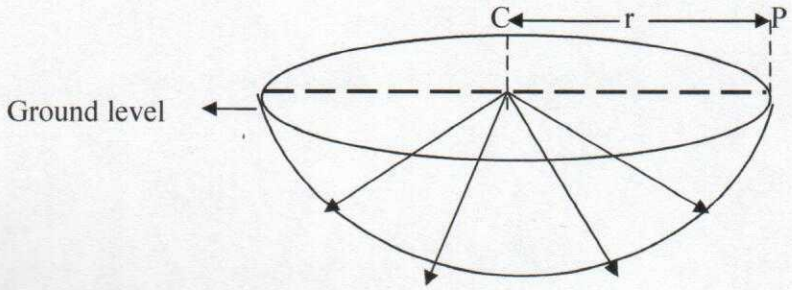

Figure 2.11: Current Source at the Hemispherical Surface

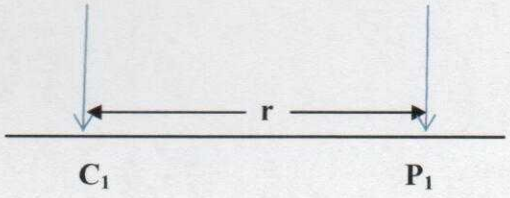

Figure 2.12: A Simple Current Source

due to current at point C_1 at the earth's surface is given as:

$$V = \frac{I\rho}{2\pi r} \quad \text{..... 2.65}$$

But in practice, four electrodes are usually used in resistivity survey as shown in Figure 2.13.

The potential at P_1 due to current at C_1 is;

$$V_{11} = \frac{I\rho}{2\pi r_1} \quad \text{..... 2.66}$$

The potential at P_1 due to current at C_2 is;

$$V_{12} = -\frac{I\rho}{2\pi r_2} \quad \text{..... 2.67}$$

The sum total of potential at P_1 due to current at C_1 and C_2 is;

$$V_{11,12} = \frac{I\rho}{2\pi r_1} + \frac{(-I\rho)}{2\pi r_2} \quad \text{..... 2.68}$$

$$V_{11,12} = \frac{I\rho}{2\pi r_1} - \frac{I\rho}{2\pi r_2} \quad \text{.....2.69}$$

$$V_{11,12} = \frac{I\rho}{2\pi}\left[\frac{1}{r_1} - \frac{1}{r_2}\right] \quad \text{.....2.70}$$

Similarly,

Potential at P_2 due to current at C_1 is;

$$V_{21} = \frac{\rho I}{2\pi r_3} \quad \text{.....2.71}$$

The potential at P_2 due to current at C_2 is;

$$V_{22} = \frac{-\rho I}{2\pi r_4} \quad \text{.....2.72}$$

The sum total Potential of P_2 due to current at C_1 and C_2 is;

$$V_{21,22} = \frac{I\rho}{2\pi r_3} - \frac{I\rho}{2\pi r_4} \quad \text{..... 2.73}$$

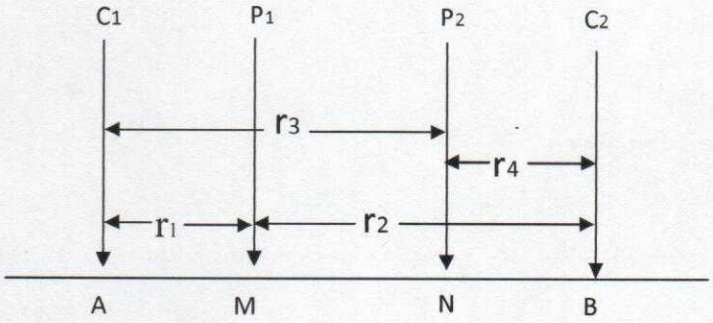

Figure 2.13: Array Configuration for Generalized Apparent Resistivity Equation

$$V_{21,22} = \frac{I\rho}{2\pi}\left[\frac{1}{r_3} - \frac{1}{r_4}\right] \quad \text{.....2.74}$$

But the potential difference ΔV between P_1 and P_2 can be obtained by subtracting equation (2.70) and (2.74)

$$\Delta V = V_{1,12} - V_{21,22}$$

$$= \left[\frac{\rho I}{2\pi r_1} - \frac{\rho I}{2\pi r_2}\right] - \left[\frac{\rho I}{2\pi r_3} - \frac{\rho I}{2\pi r_4}\right] \quad \text{.....2.75}$$

Therefore, $$\rho = \frac{2\pi\Delta V}{I}\left[\frac{1}{r_1} - \frac{1}{r_2} - \frac{1}{r_3} + \frac{1}{r_4}\right]^{-1} \quad \text{.....2.76}$$

This is the generalized apparent resistivity equation for any electrode array system. Equation (2.76) could also be written as

$\rho = KR$

Where, K is the Geometric Factor

2.2.3.3 Electrode Configurations

There are several types of electrode configurations used in electrical resistivity method. Generally four electrodes are used in resistivity survey and the common electrode arrays are:

i. Wenner Array
ii. Schlumberger Array
iii. Dipole-dipole Array
iv. Pole-dipole Array
v. Pole-pole Array.
vi. Square Array.
vii. Gradient Array.
viii. Lee Partition Array

2.2.3.3.1Wenner Electrode Array

Wenner array utilizes four electrodes system that are collinearly arranged with uniform spacing between them as shown in Figure 2.14. The potential electrodes are fixed in between the current electrodes, that is, the current electrodes are at both ends. The apparent resistivity equation for wenner array is derived from:

$$\rho_a = 2\pi R \left[\frac{1}{AM} - \frac{1}{MB} - \frac{1}{AN} + \frac{1}{NB}\right]^{-1} \quad \text{..... 2.77}$$

If AM = a, MB = 2a, AN = 2a and NB = a:

Hence, substituting them into Equation (2.77)

$$\rho_a = 2\pi R \left[\frac{1}{a} - \frac{1}{2a} - \frac{1}{2a} + \frac{1}{a}\right]^{-1} \quad \text{.....2.78}$$

$$\rho_a = 2\pi R \left[\frac{2 - 1 - 1 + 2}{2a}\right]^{-1} \quad \text{.....2.79}$$

Thus, $\rho a = 2\pi R a$ 2.80

Where, ρa = Apparent resistivity in (Ωm)

$2\pi a$ = Geometric Factor

R = Resistance in(Ω)

a = Electrode separation in (m)

2.2.3.3.2 Schlumberger Electrode Array

Schlumberger electrode array also utilizes four electrodes system like Wenner array but they are arranged linearly with different inter-electrode spacing as shown in Figure 2.15. The electrodes are arranged such that the distance AB between the current electrodes is greater or equal to five times the distance MN, between the potential electrodes. The potential electrodes are fixed about the data station in which the current electrodes are spread until the required maximum separation is attained.

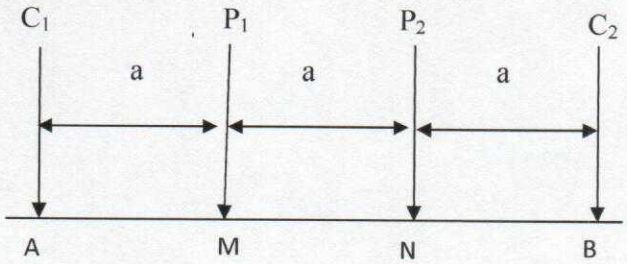

Where, AB = Current Electrode Separation

MN = Potential Electrode Separation

AB = MN = a

Figure 2.14: Typical Wenner Configuration

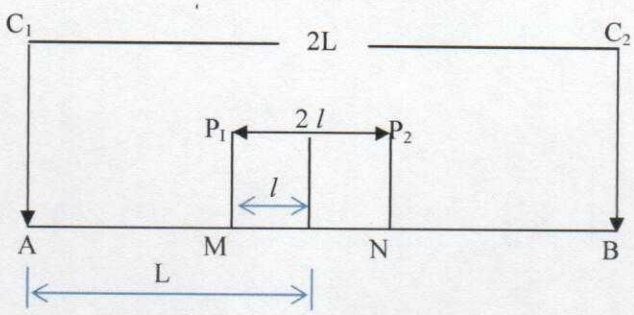

Where: AB = Current Electrode Separation

MN = Potential Electrode Separation

AB = 2L

MN = 2*l*

AB ≥ 5MN

Figure 2.15: Typical Schlumberger Configuration

The apparent resistivity equation for Schlumberger array is derived from:

$$\rho_a = 2\pi R \left[\frac{1}{AM} - \frac{1}{MB} - \frac{1}{AN} + \frac{1}{NB}\right]^{-1} \quad \text{..... 2.77}$$

If, AM = $L - l$

MB = $L + l$

AN = $L + l$

NB = $L - l$

By substituting into equation (2.77)

$$\rho a = 2\pi R\left[\frac{1}{L+l} - \frac{1}{L+l} - \frac{1}{L+l} + \frac{1}{L-l}\right]^{-1}$$

$$\rho a = 2\pi R\left[\frac{L+l-L+l-L+l+L-l}{L^2-l^2}\right]^{-1}$$

$$\rho a = 2\pi R\left[\frac{4L}{L^2-l^2}\right]^{-1}$$

$$\rho a = 2\pi R\left[\frac{L^2-l^2}{4l}\right]^{-1} \quad \text{.....2.81}$$

But, l^2 is negligible when comparing with L^2, therefore, equation (2.81) becomes

$$\rho a = \frac{\pi RL}{2l} \quad \text{..... 2.82}$$

Equation (2.82) is the apparent resistivity for Schlumberger electrode array.

2.2.3.3.3 Dipole-Dipole Electrode Array

Dipole-Dipole Electrode Array also makes use of four electrodes with two potential electrodes outside the current electrodes (Figure 2.16). The potential electrodes would move "n" times before the current electrodes were moved. The potential difference of the current passed into the earth sub-surface is measured from the response of the two potential electrodes.

Using the generalized apparent resistivity equation (equation 2.77)

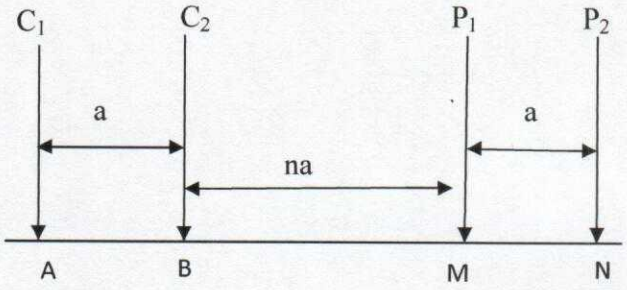

Figure 2.16: Dipole-Dipole Configuration.

$$\rho_a = 2\pi R \left[\frac{1}{AM} - \frac{1}{MB} - \frac{1}{AN} + \frac{1}{NB}\right]^{-1}$$

Where,

$r_1 = na + a = a(n+1)$

$r_2 = na$

$r_3 = na + 2a = a(n+2)$

$r_4 = na + a = a(n+1)$

$$\rho dda = 2\pi R \left(\frac{1}{\frac{1}{a(a+1)} - \frac{1}{na} - \frac{1}{a(n+2)} - \frac{1}{a(n+1)}}\right)$$

$$\rho dda = 2\pi R \left|\frac{1}{\frac{-2}{a(n+1)(n+2)n}}\right|$$

$$\rho dda = 2\pi R \left|\frac{a(n+1)(n+2)n}{-2}\right|$$

$$\rho dda = -\pi Rna(n+1)(n+2) \quad \text{.......} \quad 2.83$$

2.2.3.4 Field Procedure

There are three main field techniques used in electrical resistivity survey. These are;

i. Horizontal Resistivity Profiling (HRP),

ii. Vertical Electrical Sounding (VES),

iii. Combined Horizontal Profiling and Vertical Electrical Sounding (VES).

i. **Horizontal Resistivity Profiling (HRP):** This involves the use of fixed electrode spacing between the four electrodes, which is moved across area of interest to determine the resistivity of each station. It is mostly used to determine lateral variation in resistivity with respect to a fixed depth. Array type usually used is Wenner Array and results are presented as profiles. It is used to map 2D bodies.

ii. **Vertical Electrical Sounding (VES):** It is used to map vertical variation in electrical properties beneath the earth surface with respect to a fixed centre of the array. The

survey is carried out by gradually increasing the electrode spacing about a central position whose vertical resistivity variation is sought. Resistance measurements are made at each expansion and multiplied by the respective geometric factor (K) to give the resistivity. The depth of investigation is dependent on the electrode spacing (expansion). It can be used to map the depth to bedrock and delineate aquifers. Array types used include: Wenner, Schlumberger and Dipole-dipole array. Results are presented as depth sounding curves.

iii. **Combined Horizontal Profiling and Vertical Electrical Sounding (VES):** Measurement is done in two dimensions but in a vertical sense or section. Electrode spacing are increased on the field in such a way that measurements are taken both laterally and vertically. The data can be inverted (modeled). Array types usually used include: Dipole-Dipole and Pole-Dipole. Results are presented as pseudosections.

2.2.3.5 Field Operational Problems

i. **Lateral In-homogeneity**: This usually degrades the quality of resistivity data. The problem could be reduced by using multiple electrodes or mechanical smoothening.

ii. **Poor Electrical Contact**: This could lead to acquisition of erroneous data especially if the poor contact is at current electrodes position. It may be due to a very dry ground surface. The problem could be solved by creating saline water medium around the electrodes or watering the electrode positions.

iii. **Dip Effect:** In a situation where the interface is dipping, the quality of data is seriously affected likewise the interpretation. However, if the dip angle is less than 45^0, the effect is negligible.

iv. Cable Leakages.

v. Cultural and Geological Noise such as fences, topography, etc.

2.3 Basic Theory of Foundation Studies

Foundation is the part of a superstructure, which serves exclusively to transmit loads, be it dead or alive, from the structure such as bridges, towers, etc, on the subsoil. If the structure of soil lying close to the ground surface possesses adequate strength to take on the loads from the superstructure, the foundation of such structure may lie at shallow depth. However, if the topsoil is so weak to transmit the load, the loads have to be transmitted to deeper depth by means of piles, piers, etc. Hence, foundation can be detailed under two main categories.

i. Shallow foundation

ii. Deep foundation

2.3.1 Shallow Foundation

Shallow foundations are those founded near to the finished ground surface; generally where the founding depth (D_f) is less than the width of the footing and less than 3 m. These are not strict rules, but merely guidelines: basically, if surface loading or other surface conditions will affect the bearing capacity of a foundation it is 'shallow'. Shallow foundations (sometimes called 'spread footings') include pads (isolated footings), strip footings and rafts. Shallow foundations are used when surface soils are sufficiently strong and stiff to support the imposed loads; they are generally unsuitable in weak or highly compressible soils, such as poorly-compacted fill, peat, recent lacustrine and alluvial deposits, etc.

Shallow foundation can be classified into three types;

i. Pad footing

ii. Strip footing, and

iii. Raft foundation

2.3.1.1 Pad Foundations

Pad foundations are used to support an individual point load such as that due to a structural column. They may be circular, square or rectangular. They usually consist of a block or slab of uniform thickness, but they may be stepped or haunches if they are required to spread the load from a heavy column. Pad foundations are usually shallow, but deep pad foundations can also be used.

2.3.1.2 Strip Foundations

Strip foundations are used to support a line of loads, either due to a load-bearing wall, or if a line of columns need supporting where column positions are so close that individual pad foundations would be inappropriate.

2.3.1.3 Raft Foundations

Raft foundations are used to spread the load from a structure over a large area, normally the entire area of the structure. They are used when column loads or other structural loads are close together and individual pad foundations would interact. A raft foundation normally consists of a concrete slab which extends over the entire loaded area. It may be stiffened by ribs or beams incorporated into the foundation. Its foundations have the advantage of reducing differential settlements as the concrete slab resists differential movements between loading positions. They are often needed on soft or loose soils with low bearing capacity as they can spread the load over a larger area.

2.3.2 Deep Foundations

Deep foundations are those founded too deeply below the finished ground surface in order for their base bearing capacity not to be affected by surface conditions, this is usually at depth >3 m below finished ground level (Figure 2.17). They include piles, piers and caissons or compensated foundations using deep basements and also deep pad or strip foundations. Deep foundations can be used to transfer the loading to deeper, more competent strata at depth if

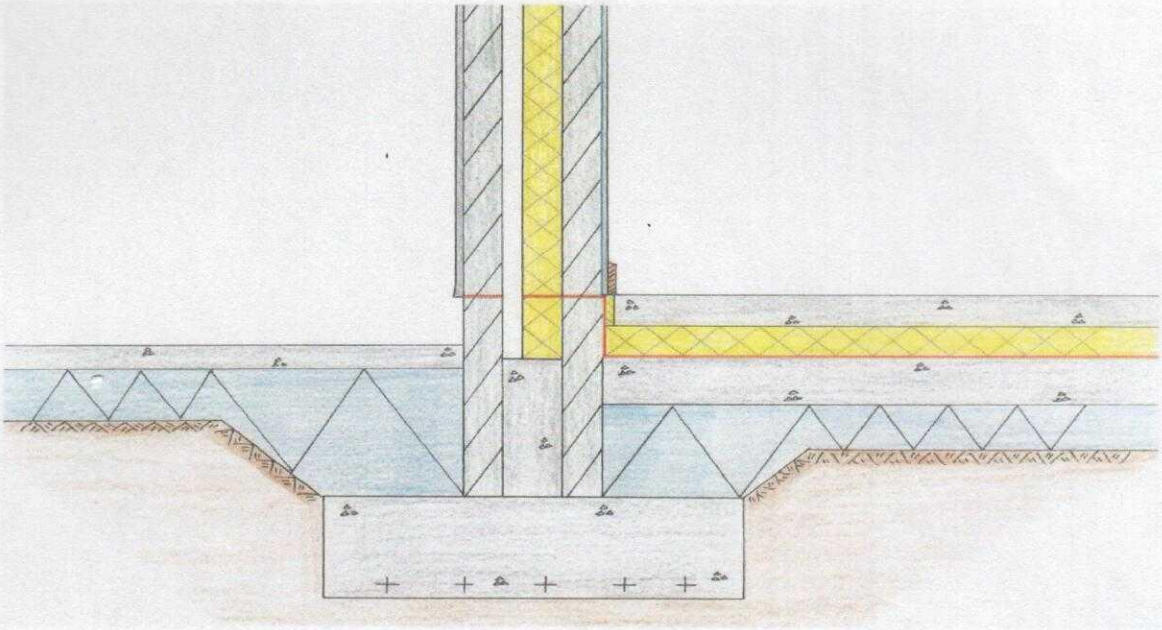

Figure 2.17: Deep Foundation

incompetent soils are present near the surface. Deep foundations are normally defined as those that have depth-width (D/B) ratio greater than two. Very deep foundations have (D/B) ratio greater than four. They are used mainly to transmit loads to deeper layers of soil; piles and drilled piers for supporting many engineering structures whereas caissons piers are normally used for bridges and sometimes for multi-storied buildings.

Deep foundations may be classified as:

i. Pile foundations
ii. Pier foundations
iii. Caisson foundations
iv. Compensated foundations

2.3.2.1 Pile Foundations

Piles are relatively long, slender members that transmit foundation loads through soil strata of low bearing capacity to deeper soil or rock strata having a high bearing capacity. They are used when for economic, constructional or soil condition considerations, it is desirable to transmit loads to strata beyond the practical reach of shallow foundations. In addition to supporting structures, piles are also used to anchor structures against uplift forces and to assist structures in resisting lateral and overturning forces.

2.3.2.2 Pier Foundations

Piers are foundations for carrying a heavy structural load which is constructed *in situ* in a deep excavation.

2.3.2.3 Caisson Foundations

Caissons are a form of deep foundation which are constructed above ground level, then sunk to the required level by excavating or dredging material from within the caisson.

2.3.2.4 Compensated Foundations

Compensated foundations are deep foundations in which the relief of stress due to excavation is approximately balanced by the applied stress due to the foundation. The net stress applied is therefore very small. A compensated foundation normally comprises a deep basement.

2.3.3 Factors Affecting Choice of Foundation

There are many factors that can affect the choice of a foundation. All factors need to be considered and their relative importance taken into account before reaching a final decision.

i. Type of construction
ii. Durability
iii. Type of building e.g. residential or industrial
iv. Soil type i.e. compressibility, porosity, plasticity, soil cohesion.
v. Magnitude of the load/intensity
vi. Site condition
vii. Location and type of structure
viii. Physiological factor
ix. Economic condition i.e. financial implication

CHAPTER THREE

MATERIALS AND METHODS OF STUDY

3.1.1 Materials

The equipments used during the geophysical field measurements in this study are:

i. ABEM WADI VLF-EM Equipment.

ii. Proton-Precession Magnetometer.

iii. Resistivity Meter

iv. Cutlass

v. Hammer

vi. Tape Rule

vii. Connecting Cables

viii. Electrodes

ix. Global Positioning System (GPS)

x. Compass Clinometer

ABEM WADI VLF-EM Equipment: The instrument is an EM signal receiver with the transmitter located far away. It incorporates data storage and processing/interpretation functions. It measures the distortion in the VLF signal and presents the results directly on the display screen. The WADI instrument is hand held and operated on dry cell batteries usually 12-15 volts. It is single person survey equipment (Figure 3.1)

Resistivity Meter: This is the instrument for measuring the earth resistivity. The resistivity meter used is the Ohmega Resistivity Meter (Figure 3.2) which has a power source which may be DC (battery) or low frequency AC (battery powered Oscillator). It sends current into the ground through two current electrodes, and measures the potential difference across them through two other potential electrodes. These electrodes are connected to the resistivity meter.

Figure 3.1: ABEM-WADI VLF-EM Equipment

Figure 3.2: Ohmega Resistivity Meter

Hammer: This is used in driving down the electrodes into the ground at the respective electrode positions during investigations.

Tape, Threads, Pegs and Cutlass: Tapes are used to measure the electrode separation which may be marked on a thread. The thread is used in lining or making sure that the electrodes are in a straight line, cutlass is used for clearing bush or trees that may serve as hindrances.

Reels of Connecting Cables: These are light weight, high strength and very conductive cables. They are used to connect the electrodes to the meter.

Electrodes: These are steel metal rods which are about half a meter in length so that it can be driven into the ground firmly for good electrical contact. Four were employed in the survey; two electrodes are used for sending the currents into the ground and the other two for potential difference measurements.

Global Positioning System (GPS): The type used is the GARMIN 72H Global Positioning Systems. This is used to measure the geographical co-ordinates of stations and as well as prominent structures or buildings for their proper placement on the base map.

Compass Clinometer: This is used to determine the orientation of the traverse and roads as a guide for its proper location on the base map

3.2.1 Methodology

3.2.2 Preliminary Studies

The preliminary studies involved the review of journals that are related to the study, this was followed by reconnaissance study which includes site visitation and the use of Global Positioning System (GPS) to acquire geographical data for the generation of relevant maps such as the base map.

3.2.2 Data Acquisition and Processing

Geophysical data were acquired at the study area in Federal University Oye-Ekiti using three geophysical methods which are the VLF-EM, Magnetics and Electrical Resistivity methods. Six (6) traverses were established in the area in the W-E and N-S directions with maximum length of 185 m along which the VLF-EM and Magnetics data were obtained (Figure 3.3). The dipole-dipole data were acquired along four traverses using the electrode separation of 5 m along traverse 2 and 4 (W-E) while 10 m was used along traverse 1 and 4 (N-S). Nineteen (19) Schlumberger Vertical Electrical Soundings (VES) were acquired within the study area using a maximum current electrode separation (AB) of 130 m (Figure 3.3). The obtained geophysical data were processed using the appropriate filter equations for each method. The VES data was interpreted by the method of partial curve matching and computer iteration technique to generate the subsurface model.

3.2.3 Data Interpretation

The interpretation techniques employed for the interpretation of the data obtained involves:

i. Qualitative Interpretation

ii. Quantitative Interpretation

Qualitative Interpretation: involves the visual inspection of profiles, maps and pseudosections for anomaly signatures that are diagnostic of a particular target. VLF-EM profiles and pseudosections, 2D Dipole-Dipole resistivity pseudosections, generated geoelectric sections and maps were interpreted qualitatively.

Quantitative Interpretation: involves modeling of data. Two types of models can be employed:

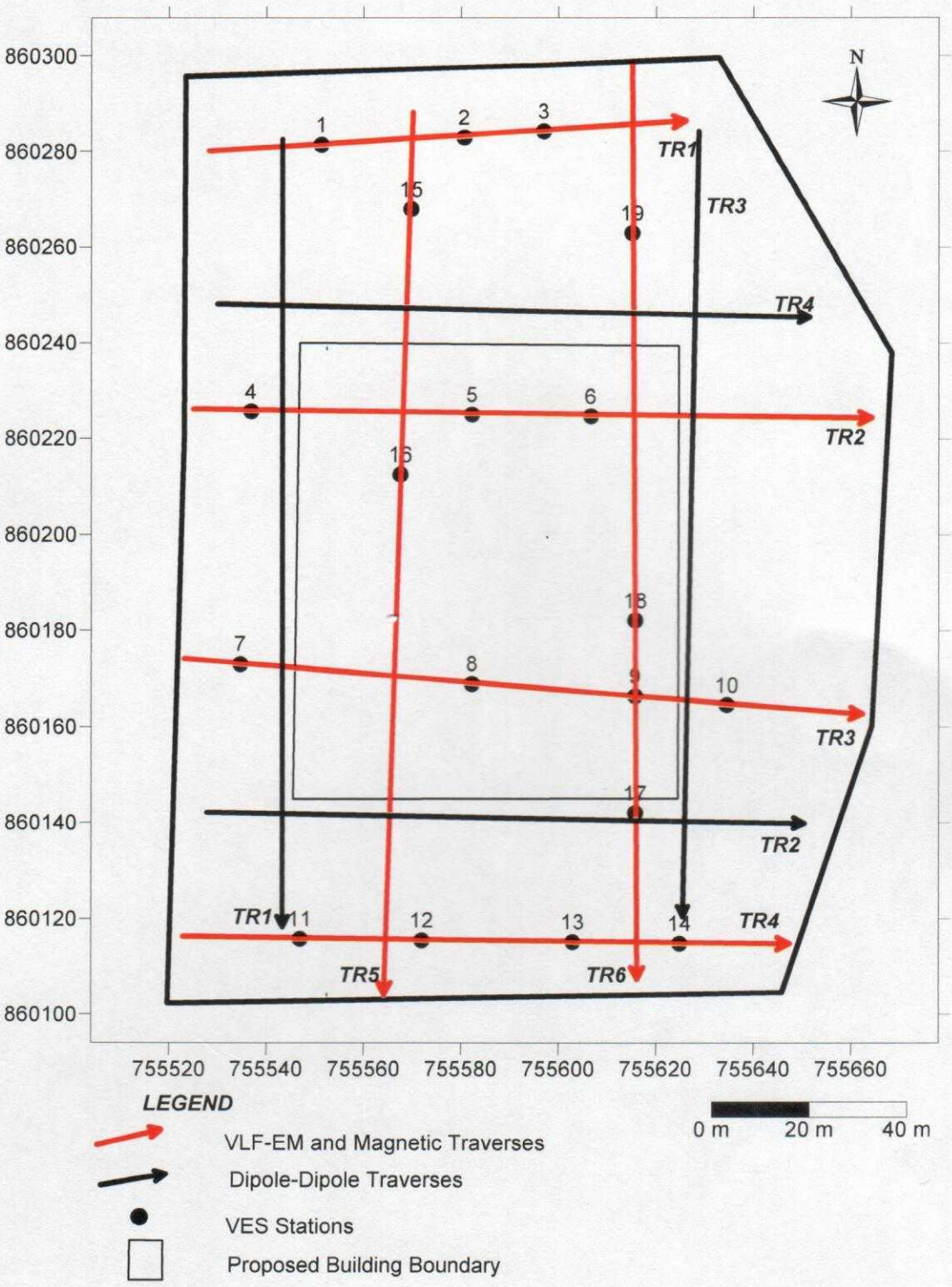

Figure 3.3: Data Acquisition Map of the Study Area

i. **Forward Modeling:** which entails comparison of field processed data with that of a theoretically generated model.

ii. **Inverse modeling** which involves direct interpretation by inputting data into software for interpretation.

VES curves are usually interpreted qualitatively by partial curve matching technique (Keller and Frishknecht, 1966).

3.2.3.1 Partial Curve Matching Technique

It involves segment by segment matching of a field curve starting from small electrode spacing to large spacing with theoretical two layer model and auxiliary curves (K, H, Q and A type). This technique adopts the Principle of Superposition of layers or Replacement of Resistivity and Thickness.

The procedure of partial curve matching involves the plotting of field data on a transparent double logarithmic paper that has the same modulus as that used for the 2-layer model curve and the field curve is superimposed on the master (model) curve while keeping the axes parallel, it is moved around until a match is obtained over as many point as possible on the field curve at small electrode spacings. The point of intersection of the origin of the two layer master curve is marked on the transparent paper as $+_1$. The coordinates of $+_1$ on the field curve gives ρ_1 and h_1 which are the resistivity and thickness of the first layer respectively. ρ_2 is calculated as the product of ρ_1 and K_1. Where, K_1, is the resistivity ratio of the matched 2-layer curve (Awoniyi, 2013).

The field curve is then superimposed on the appropriate auxiliary curve, while keeping the axes parallel and $+_1$ at the origin of the auxiliary curve, the auxiliary curve with resistivity ratio K_1 is traced on the field curve. The field curve is again superimposed on the 2-layer master curve and the field curve is then moved around until a fit is obtained over as many

points as possible on the field curve at large electrode spacings. The origin of the 2-layer master curve is marked on the transparent paper as $+_2$. The resistivity ratio K_2 of the matched 2-layer curve is noted which is then traced on the appropriate auxiliary curve type. This process is repeated until the complete curve has been matched (Awoniyi, 2013).

The field curve is later placed on the appropriate auxiliary curve and with the axes parallel and cross ($+_1$) at the origin, the thickness ratio $(Dn/Dr)_1$ is read at the second cross ($+_2$). The value of $(Dn/Dr)_1$ is multiplied with h_1 to give the thickness of the second layer h_2. $Dn/Dr)_2$ is also multiplied with h_{2r} to give the thickness of the third layer h_3 and so on (Awoniyi, 2013).

The equations for the calculation of the different layer resistivity and thicknesses are:

$$\rho_2 = \rho_1 \times K_1 \quad \text{.....3.0}$$

$$\rho_3 = \rho_{2r} \times K_2 \quad \text{.....3.1}$$

$$\rho_4 = \rho_{3r} \times K_3 \quad \text{.....3.2}$$

$$\rho_n = \rho_{(n-1)r} \times K_{(n-1)} \quad \text{.....3.3}$$

Where,

$K_1, K_2, K_3, \ldots, K_{(n-1)}$ = Layer resistivity ratios

ρ_1, ρ_2, ρ_3 = resistivity of the 1st, 2nd and 3rd layer respectively

ρ_n= resistivity of the nth layer

ρ_{2r}, $\rho_{(n-1)r}$= replacement apparent resistivity of the second layer and the layer above the nth layer.

Similarly,

$$h_2 = h_1 \left(\frac{Dn}{Dr}\right)_1 \quad \text{..... 3.4}$$

$$h_3 = h_2 r \left(\frac{Dn}{Dr}\right)_2 \quad \text{.....3.5}$$

$$h_4 = h_3 r \left(\frac{Dn}{Dr}\right)_3 \quad \text{.....3.6}$$

$h_n = h_{(n-1)r} \left(\frac{Dn}{Dr}\right)_{(n-1)}$ 3.7

Where,

$h_1, h_2, h_3, \ldots, h_{(n-1)}$ = thickness of the 1st, 2nd, 3rd and nth layer respectively

$h_{(n-1)r}$ = replacement thickness of the layer above the nth layer.

$\left(\frac{Dn}{Dr}\right)_{(n-1)}$ = depth ratio

3.2.3.2 Computer Iteration Technique

The result of the layer resistivity parameters (resistivities and thicknesses) derived from the partial curve matching are used as initial interpretation of the field curves for the computer iteration. These parameters are supplied into the WinRESIST version 1.0 software (Vander Velpen, 2004) for a particular input data which then display the corresponding theoretical curves. The theoretically generated parameters were subsequently varied until a best possible fit between the field and the model curves are obtained. The final theoretically generated parameters are the later resistivities and thickness for each VES Station.

The KHFfilt (Karous-Hjelt) software was used for the modeling of the Electromagnetic data and the DIPROfWIN version 4.0 (Kigam, 2001) was used for the modeling and iteration of the 2-D dipole-dipole resistivity data.

CHAPTER FOUR

RESULTS AND DISCUSSION

4.1 Presentation of Results

The results of the data obtained from the field are presented in the form of Tables, Profiles, Depth Sounding Curves, Pseudosections and Geo-electric Sections. Typical examples of these are shown in the tables and figures presented in this chapter. The remaining tables and figures of the results are presented in the Appendix.

4.2 Discussion of Results

4.2.1 VLF-EM Method

The VLF-EM profiles (Figures 4.1a-f) shows the plot of the Real and the filtered Real (Q-factor) data against distance within the study area. The 2-D inversion models of the data were also shown beneath them using the Karous-Hjelt Filter software. The Raw Real plot indicates anomalous zones and linear features as indicated by the 2-D models.

Prominent VLF-EM anomaly suspected to be conductive zones were identified along traverse 1 around 22.5 m, 53 m and 67 m (Figure 4.1a); traverse 2 around 13 m, 58 m and 82 m (Figure 4.1b) ; traverse 3 around 12.5 m, 59 m, 93 m and 112 m (Figure 4.1c); traverse 4 around 23 m, 48 m, 80 m and 102 m (Figure 4.1d); traverse 5 around 20 m, 75 m, 100 m and 130 m (Figure 4.1e); traverse 6 around 35 m, 115 m, 135m and 155 m (Figure 4.1f); which are marked along the profiles. Moderate conductive zones were observed on all the traverses which appear as green to yellow colour on the 2-D models (Figures 4.1 a-f). Intermediate between them are the minor resistive zones which appears as blue colour. A major conductive zone is observed on traverse 2 between 60 and 90 m reaching a depth of 20 m which is typical of thick overburden, a fault/fracture or lithological boundary in the area.

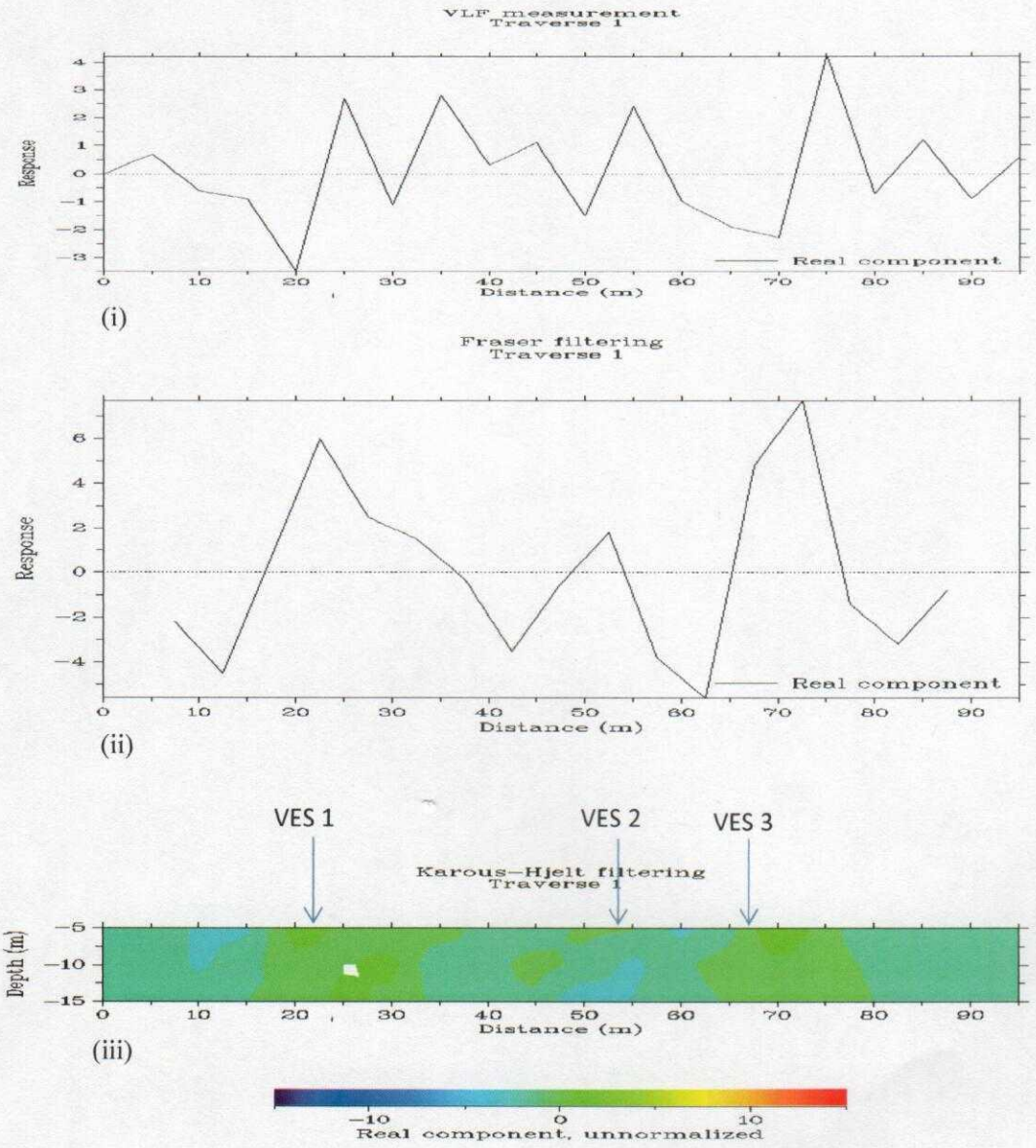

Figure 4.1a: VLF-EM Plot of (i) Raw Real (ii) filtered Real (iii) 2-D Model along Traverse 1

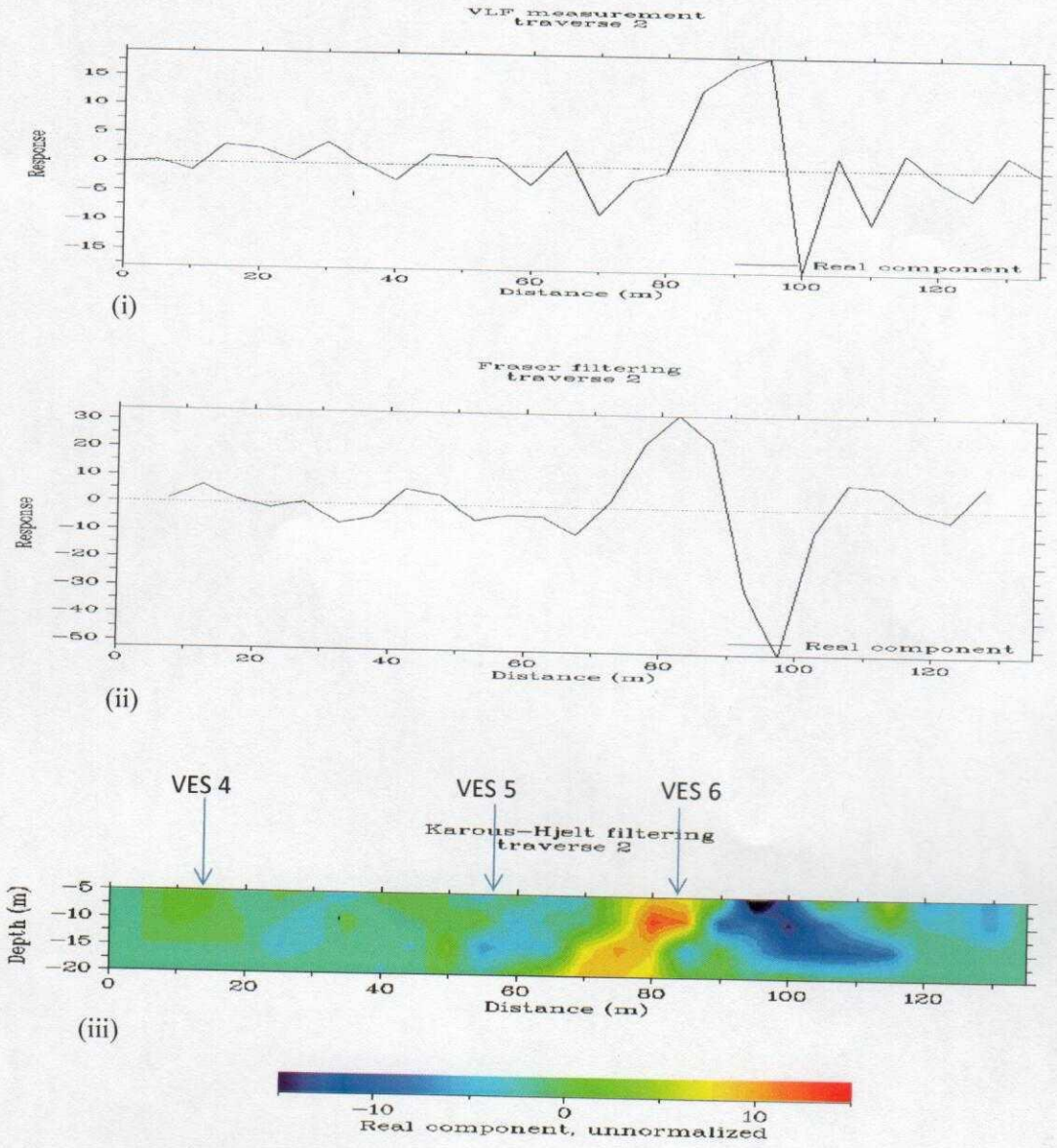

Figure 4.1b: VLF-EM Plot of (i) Raw Real (ii) filtered Real (iii) 2-D Model along Traverse 2

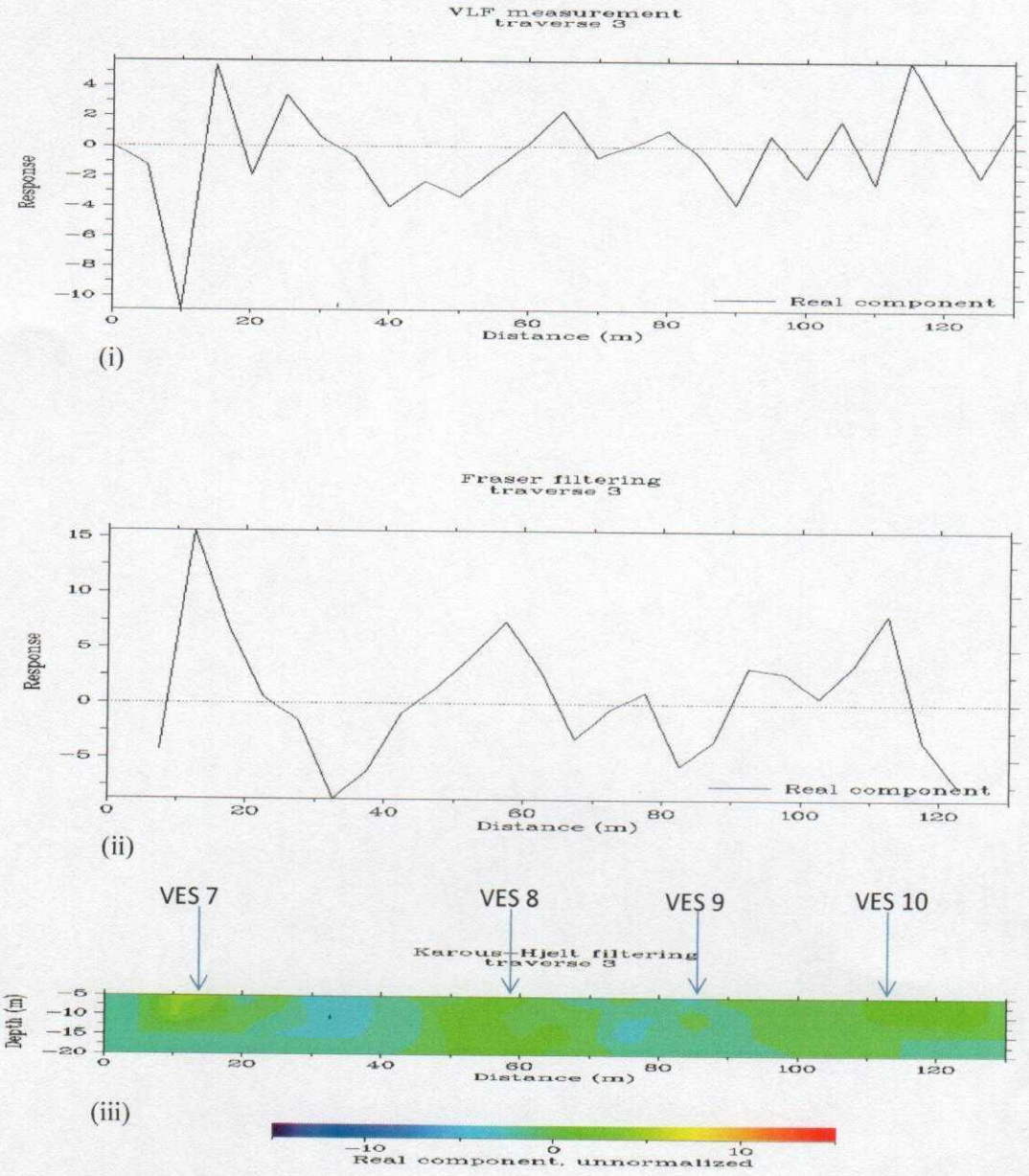

Figure 4.1c: VLF-EM Plot of (i) Raw Real (ii) filtered Real (iii) 2-D Model along Traverse 3

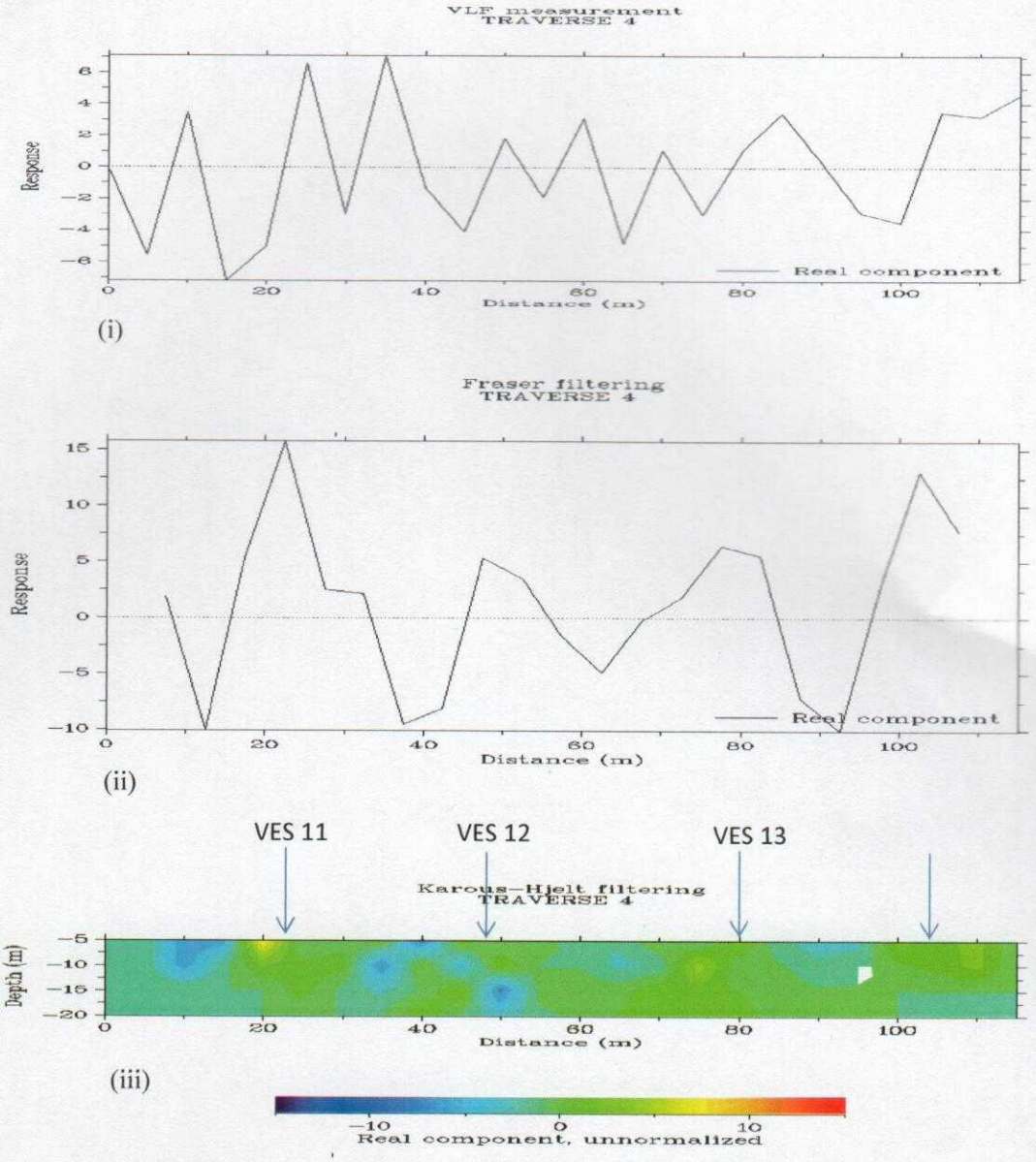

Figure 4.1d: VLF-EM Plot of (i) Raw Real (ii) filtered Real (iii) 2-D Model along Traverse 4

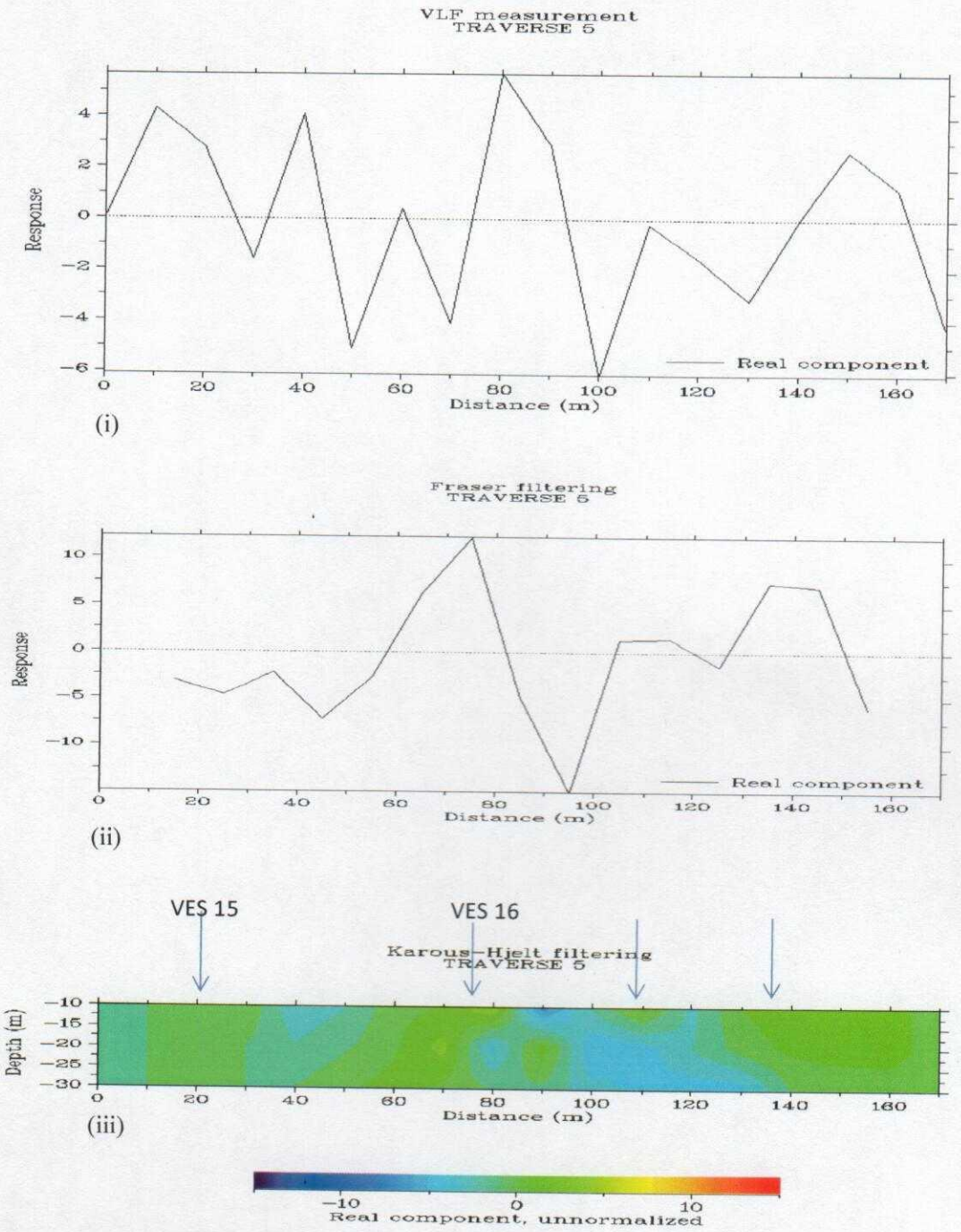

Figure 4.1e: VLF-EM Plot of (i) Raw Real (ii) filtered Real (iii) 2-D Model along Traverse 5

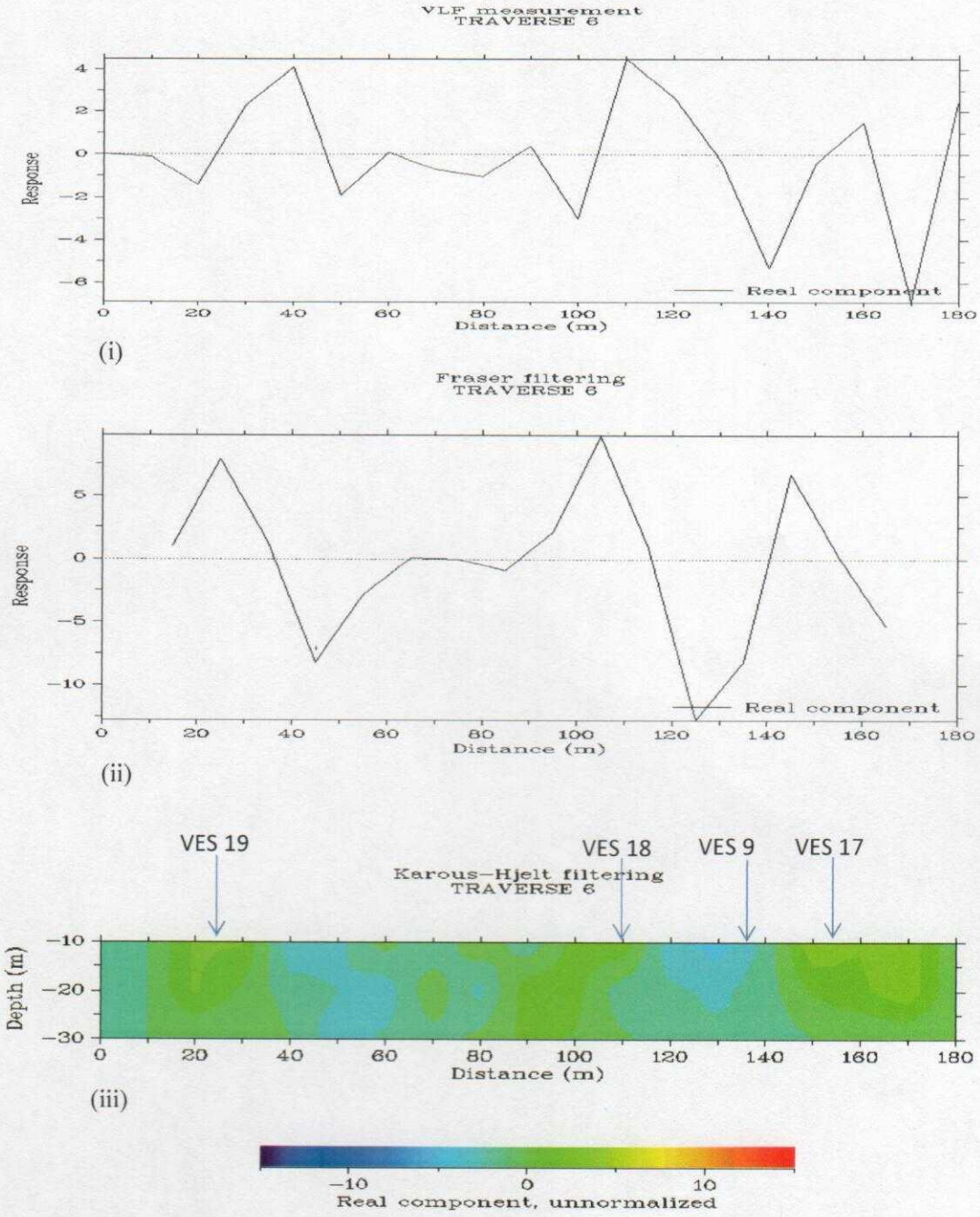

Figure 4.1f: VLF-EM Plot of (i) Raw Real (ii) filtered Real (iii) 2-D Model along Traverse 6

4.2.2 Magnetic Method

The magnetic data were interpreted qualitatively using the three point moving average. Prominent magnetic anomalies suspected to be thin and thick dykes which are indicative of weak zones, faults, fractures or lithological discontinuities were identified within the study area (Figures 4.2a-f).

The magnetic anomaly observed beneath traverse 1 between distances of 10 and 35 m is that of a thin dyke (Figure 4.2a); such anomalous zones of a thin dyke were observed at traverse 2 between distances 15 and 28 m (Figure 4.2b); traverse 3 between distances 80 and 107 m (Figure 4.c); traverse 4 between distances 10 and 50 m (Figure 4.2d); traverse 5 between distances 10 and 40 m and 100 and 150 m (Figure 4.2e) and traverse 6 between distances 50 and 110 m (broad magnetic anomaly) (Figure 4.2f). These thin dykes are interpreted as minor conductive zones typical of clayey overburden in the area and/or deep seated fracture (where the magnetic anomaly is broad). Major thick dykes were observed beneath traverse 2 between distances 75 and 106 m (Figure 4.2b) and traverse 3 between distances 17 and 50 m (Figure 4.2c). These thick dykes are interpreted as major conductive zones typical of fractures, faults, thick overburden or lithological boundary in the study area.

4.2.3 Electrical Resistivity Method

4.2.3.1 Vertical Electrical Sounding (VES) Curves

The VES data were presented as depth sounding curves. The field curves obtained within the study area are the H, A and KH curve types with the KH-types being dominant. The H curve is about 21%, A curve is about 32% and KH has about 47% of the total curve type within the study area (Table 4.1). Typical curve types obtained within the study area are shown in Figures 4.3a – c while the summary of the VES results are presented in Table 4.2.

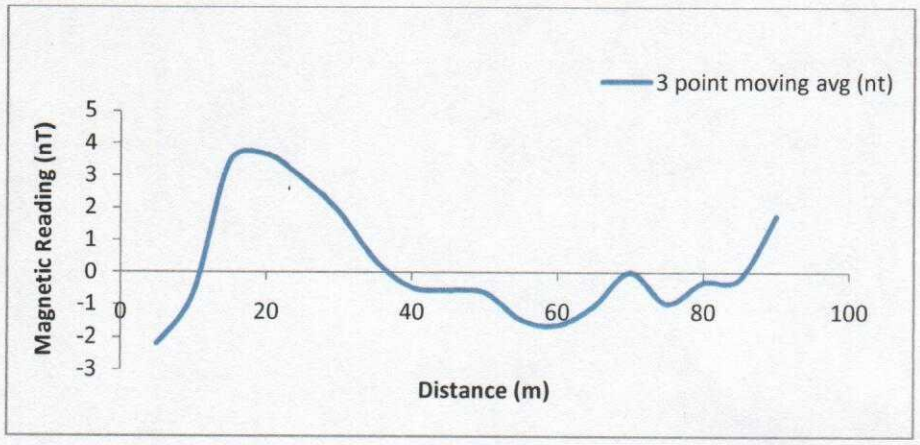

Figure 4.2a: Magnetic Profile beneath Traverse 1

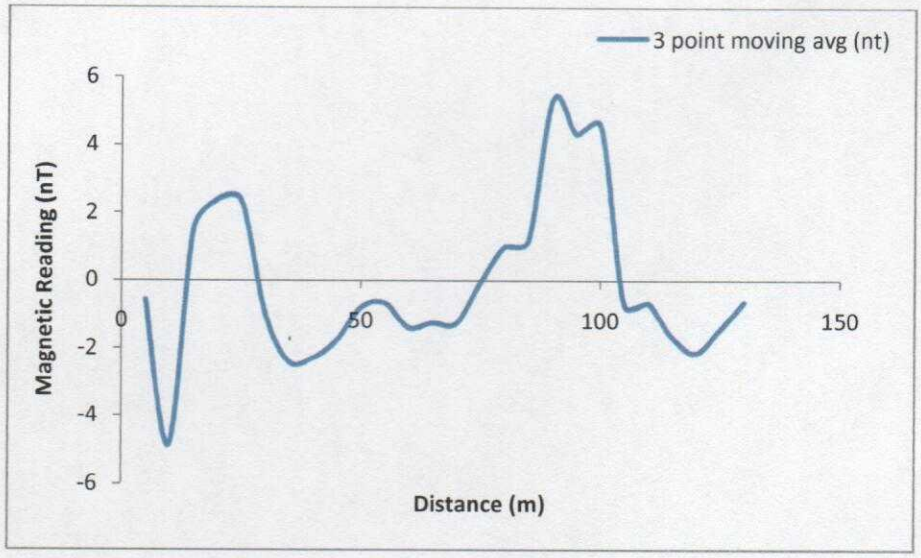

Figure 4.2b: Magnetic Profile beneath Traverse 2

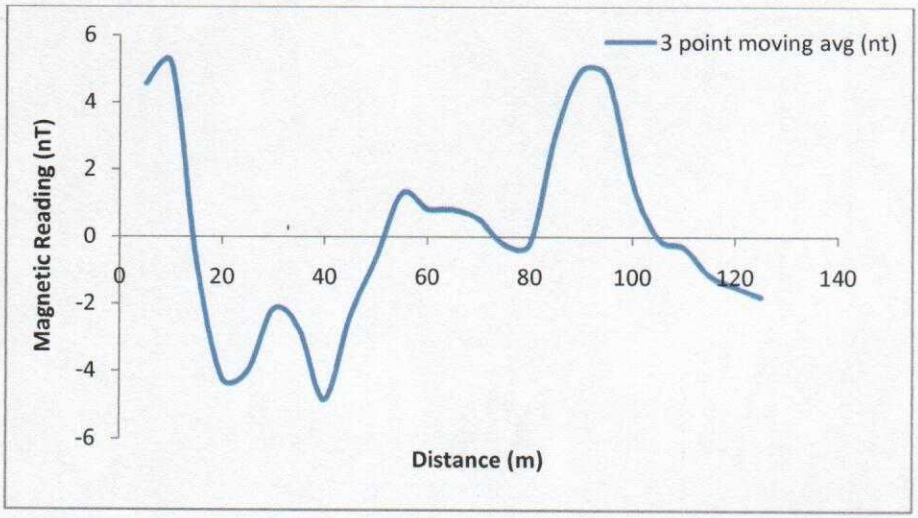

Figure 4.2c: Magnetic Profile beneath Traverse 3

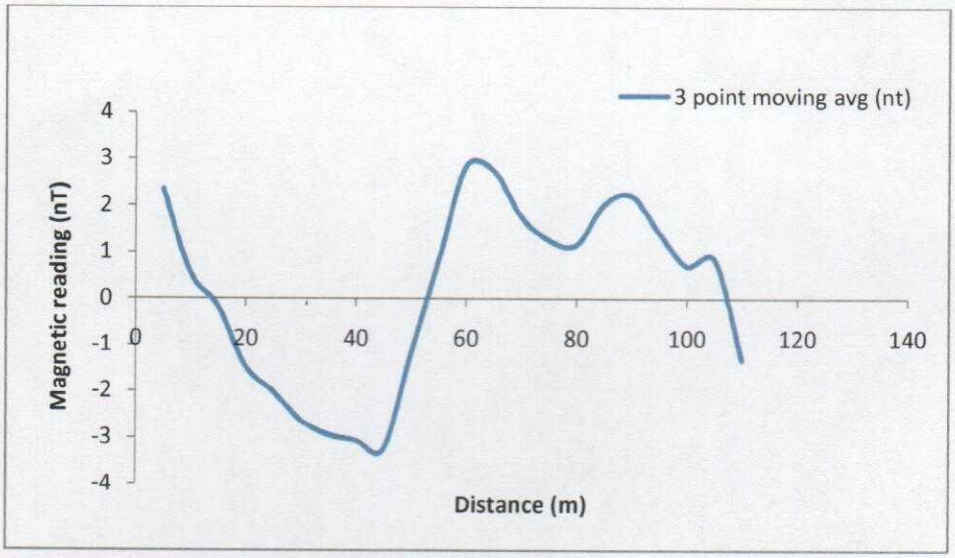

Figure 4.2d: Magnetic Profile beneath Traverse 4

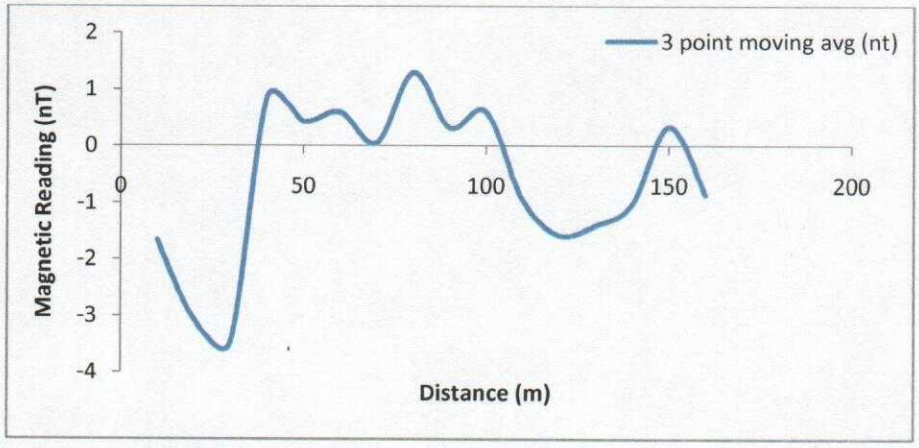

Figure 4.2e: Magnetic Profile beneath Traverse 5

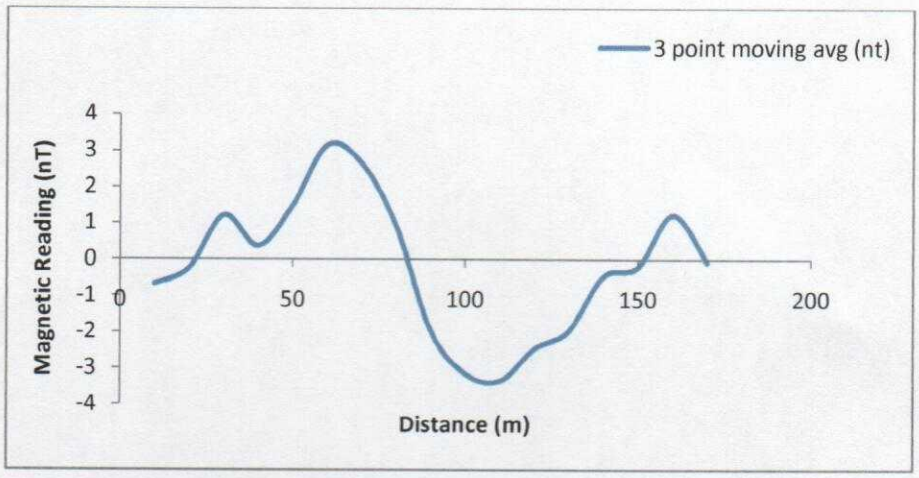

Figure 4.2f: Magnetic Profile beneath Traverse 6

Table 4.1: Percentage Curve Types obtained within the Study Area

Curve Type	**No. obtained within the Study Area**	**Percentage**
H	4	21%
A	6	32%
KH	9	47%
Total	**19**	**100%**

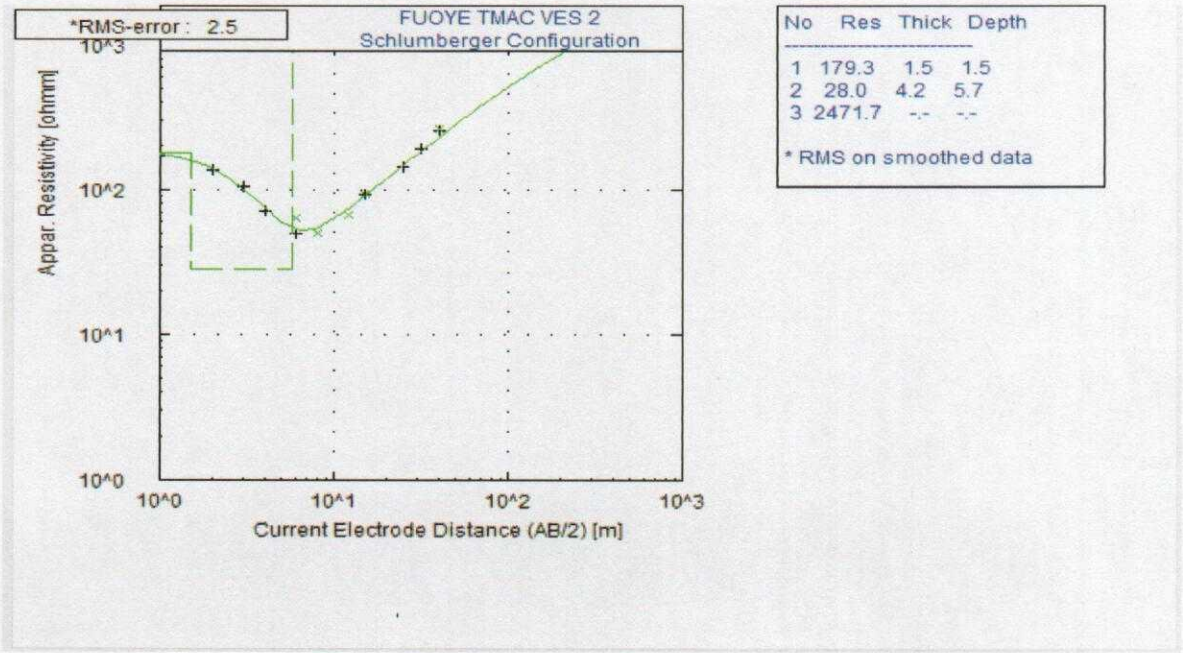

Figure 4.3a: Typical H Curve Type

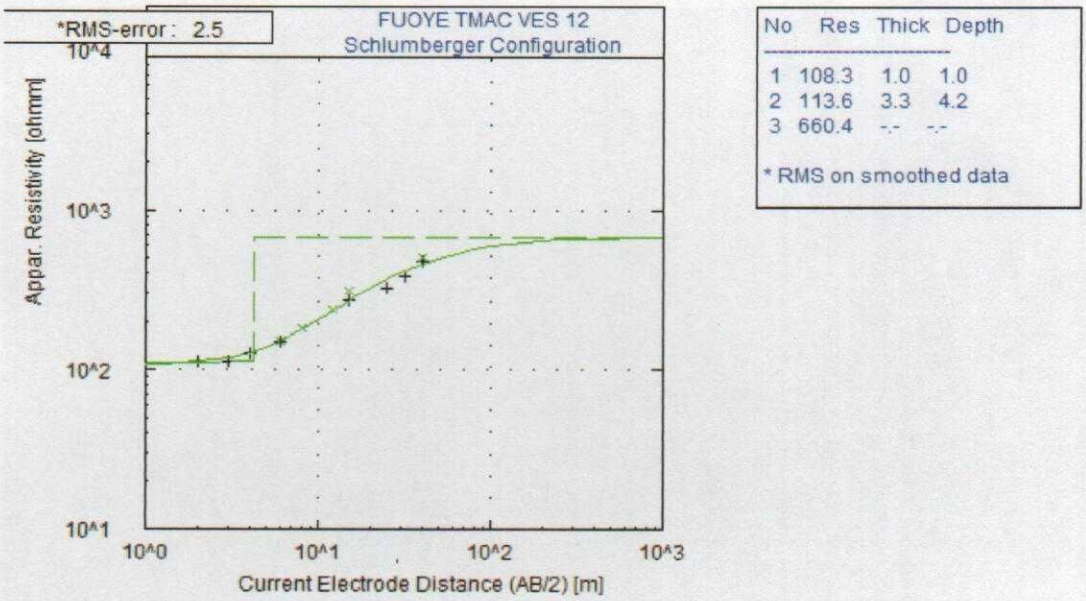

Figure 4.3b: Typical A Curve Type

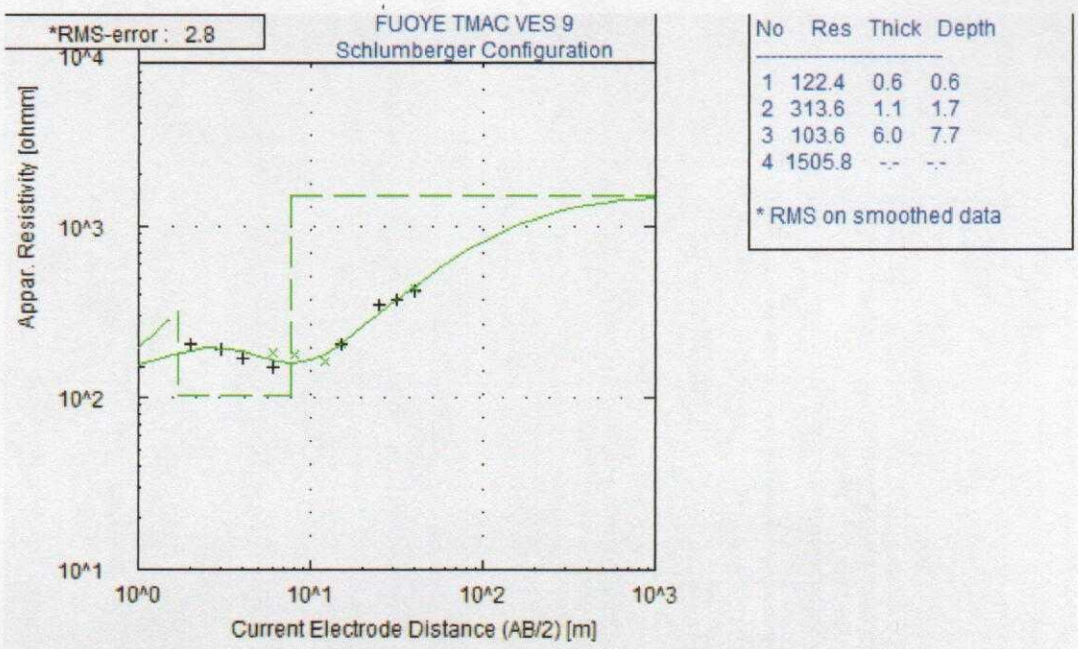

Figure 4.3c: Typical KH Curve Type

Table 4.2: Summary of VES Interpretation

VES Station	Curve Type	Layers	Resistivity (Ohm-m)	Thickness (m)	Depth (m)	Lithological Equivalence
1	A	1	14	1.3	1.3	Topsoil
		2	19	2.0	3.3	Weathered Layer
		3	373	-	-	Partly weathered/Fractured Basement
2	H	1	180	1.5	1.5	Topsoil
		2	28	4.2	5.7	Weathered Layer
		3	2472	-	-	Fresh Basement
3	H	1	104	0.5	0.5	Topsoil
		2	7	1.4	1.9	Weathered Layer
		3	10658	-	-	Fresh Basement
4	KH	1	172	1.0	1.0	Topsoil
		2	288	2.7	3.8	Laterite
		3	77	3.8	7.5	Weathered Layer
		4	1247	-	-	Fresh Basement
5	KH	1	122	0.6	0.6	Topsoil
		2	331	1.6	2.2	Laterite
		3	130	14.5	16.6	Weathered Layer
		4	3202	-	-	Fresh Basement
6	KH	1	217	0.7	0.7	Topsoil
		2	955	12.1	12.8	Laterite (Hard-pan)
		3	191	13.6	26.4	Weathered Layer
		4	19140	-	-	Fresh Basement
7	KH	1	255	0.8	0.8	Topsoil
		2	319	2.5	3.3	Laterite
		3	130	17.5	20.8	Weathered Layer
		4	6400	-	-	Fresh Basement
8	KH	1	330	0.7	0.7	Topsoil
		2	653	1.5	2.2	Laterite
		3	261	12.4	14.7	Weathered Layer
		4	10243	-	-	Fresh Basement
9	KH	1	122	0.6	0.6	Topsoil
		2	314	1.1	1.7	Laterite
		3	104	6.0	7.7	Weathered Layer
		4	1506	-	-	Fresh Basement
10	KH	1	174	0.5	0.5	Topsoil
		2	543	0.6	1.1	Laterite
		3	82	2.5	3.3	Weathered Layer
		4	602	-	-	Partly weathered/Fractured

						Basement
11	A	1	95	1.5	1.5	Topsoil
		2	178	7.7	9.2	Weathered Layer
		3	705	-	-	Partly weathered/Fractured Basement
12	A	1	108	1.0	1.0	Topsoil
		2	113	3.3	4.2	Weathered Layer
		3	660	-	-	Partly weathered/Fractured Basement
13	A	1	42	1.5	1.5	Topsoil
		2	78	2.2	3.7	Weathered Layer
		3	2182	-	-	Fresh Basement
14	A	1	72	1.4	1.5	Topsoil
		2	186	6.5	8.0	Weathered Layer
		3	2238	-	-	Fresh Basement
15	H	1	164	1.2	1.2	Topsoil
		2	28	3.4	4.6	Weathered Layer
		3	761	-	-	Partly weathered/Fractured Basement
16	KH	1	127	0.8	0.8	Topsoil
		2	229	0.6	1.5	Laterite
		3	89	9.1	10.6	Weathered Layer
		4	980	-	-	Fresh Basement
17	A	1	97	1.3	1.3	Topsoil
		2	264	3.8	5.1	Weathered Layer
		3	937	-	-	Fresh Basement
18	KH	1	257	0.5	0.5	Topsoil
		2	297	1.1	1.7	Laterite
		3	180	7.9	9.5	Weathered Layer
		4	1402	-	-	Fresh Basement
19	H	1	148	0.7	0.7	Topsoil
		2	66	1.6	2.3	Weathered Layer
		3	428	-	-	Partly weathered/Fractured Basement

4.2.3.2 Geo-electric Sections

Figures 4.4a-f shows the geoelectric sections drawn in the W-E and N-S directions within the study area. The sections generally reveal three to four geoelectric layers within the study area which are: the topsoil, laterite, weathered layer and the partly weathered/fractured/fresh basement bedrock.

The topsoil resistivity varies from 14 to 330 Ωm with thickness range of between 0.5 and 1.5 m. It is composed of clay, sandy clay, clayey sand and laterite. The Lateritic layer range in resistivity from 229 to 955 Ωm and its thickness varies between 0.6 and 12.1 m. The weathered layer ranges in resistivity from 7 to 264 Ωm and its thickness varies between 1.4 and 17.5 m. It is composed mainly of clay and sand. The bedrock which is partly weathered and fractured in some places varies in resistivity from 373 Ωm to infinity (∞) with depth to bedrock ranging between 1.9 and 26.4 m.

The high resistivity variation of the topsoil show high degree of in homogeneity in the topsoil. The topsoil is generally thin (not greater than 1.5 m), the lateritic layer is very thick beneath VES 6 to a depth of 12.1 m, and the bedrock shows depression beneath VES 2, 5, 6, 7, 8, 9, 11, 14, 16 and 18. Some portions of the basement are partly weathered/fractured. The high resistivity portions of the topsoil, indicative of laterite are competent portions of the area which may be able to withstand the bearing load of the building coupled with the lateritic layer present beneath it.

4.2.3.3 Dipole-Dipole Pseudosections

The dipole-dipole pseudosections and the 2-D resistivity structure shown in Figures 4.5a-d were obtained within the study area. The 2-D resistivity structures show the subsurface images inverted from the field data and its calculated theoretical data pseudosection revealing both lateral and horizontal variation in ground apparent resistivity values of the subsurface.

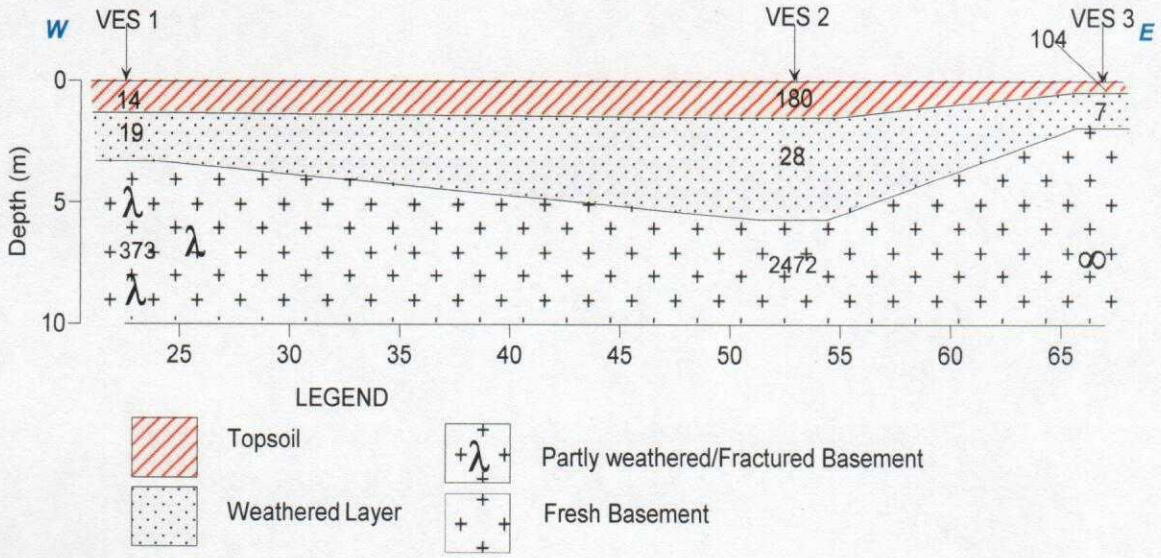

Figure 4.4a: Geoelectric section Beneath Traverse One (1)

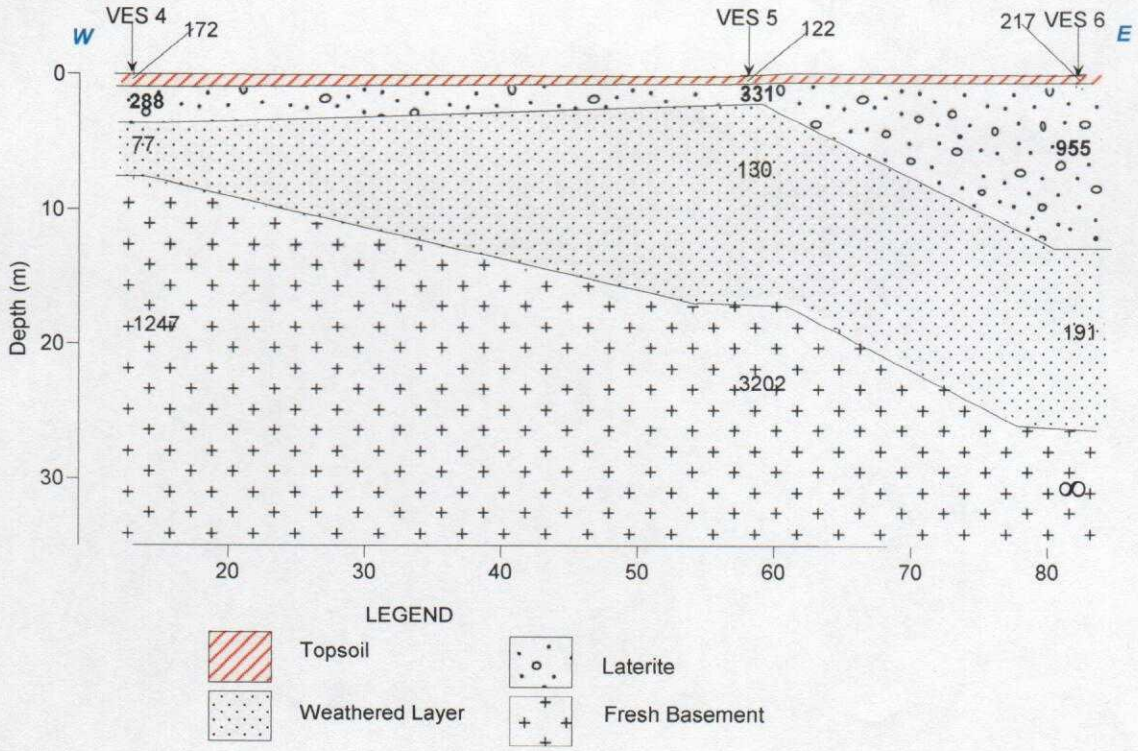

Figure 4.4b: Geoelectric section Beneath Traverse Two (2)

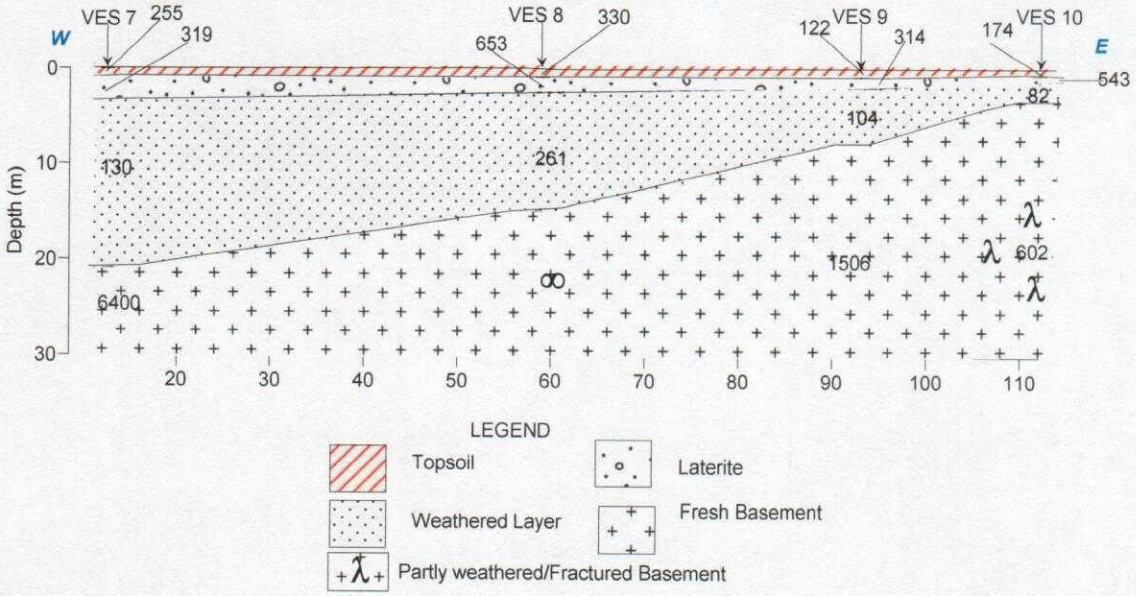

Figure 4.4c: Geoelectric section Beneath Traverse Three (3)

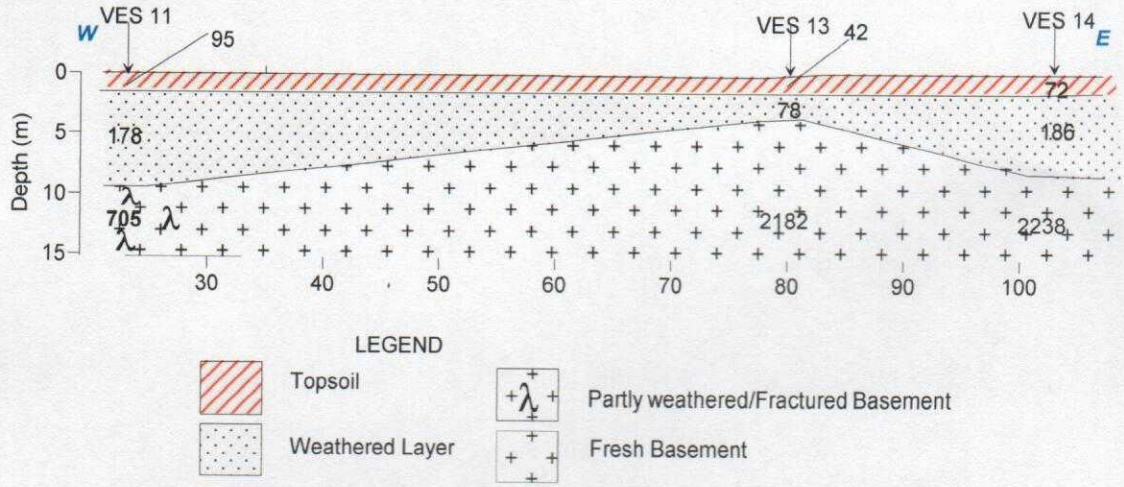

Figure 4.4d: Geoelectric section Beneath Traverse Four (4)

N S

Traverse 1 (Field Data Pseudosection)

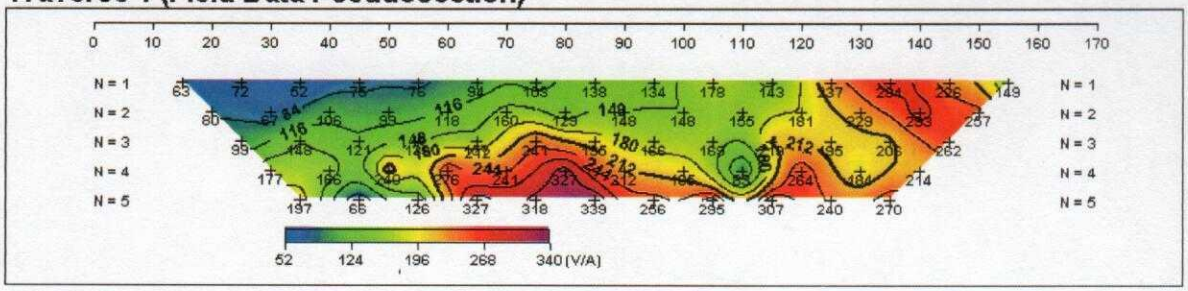

Traverse 1 (Theoretical Data Pseudosection)

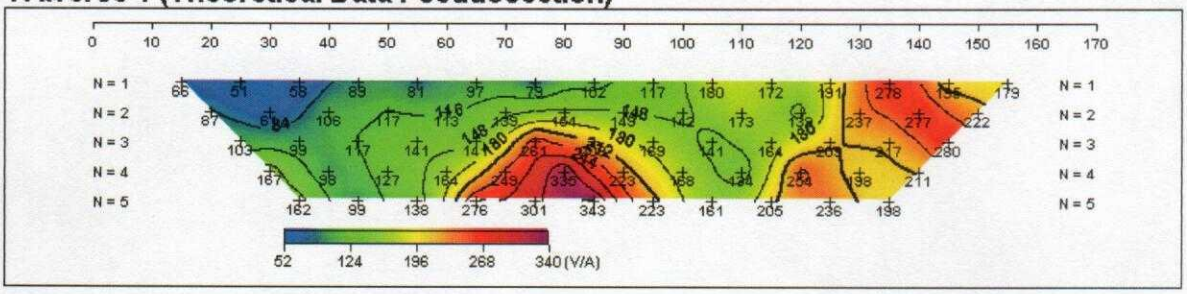

Traverse 1 (2-D Resistivity Structure)

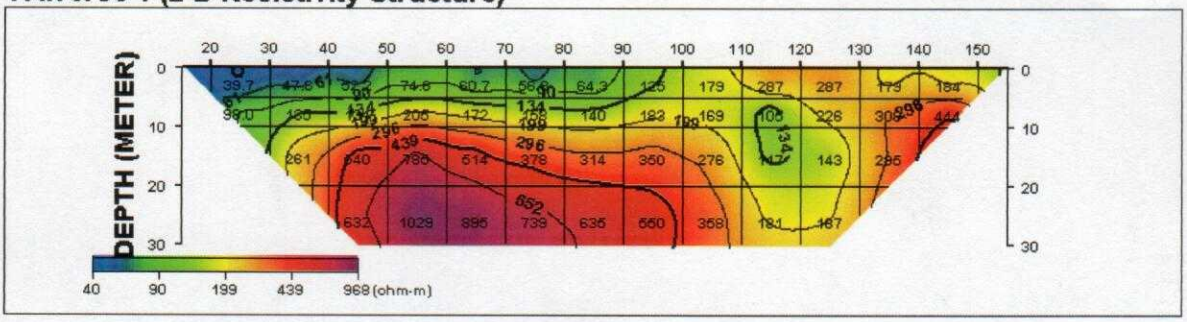

Figure 4.5a: 2-D Modeling of Dipole-Dipole Data obtained beneath Traverse 1

W E

Traverse 2 (Field Data Pseudosection)

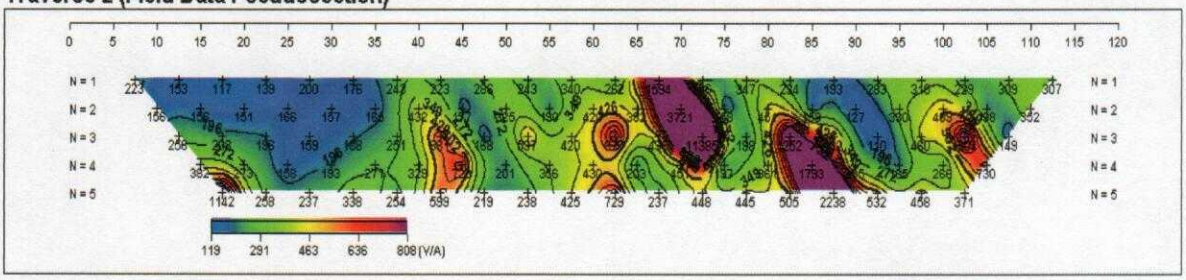

Traverse 2 (Theoretical Data Pseudosection)

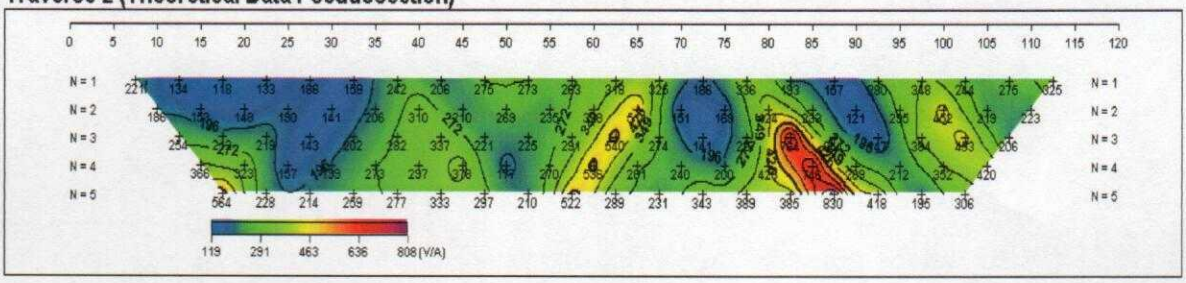

Traverse 2 (2-D Resistivity Structure)

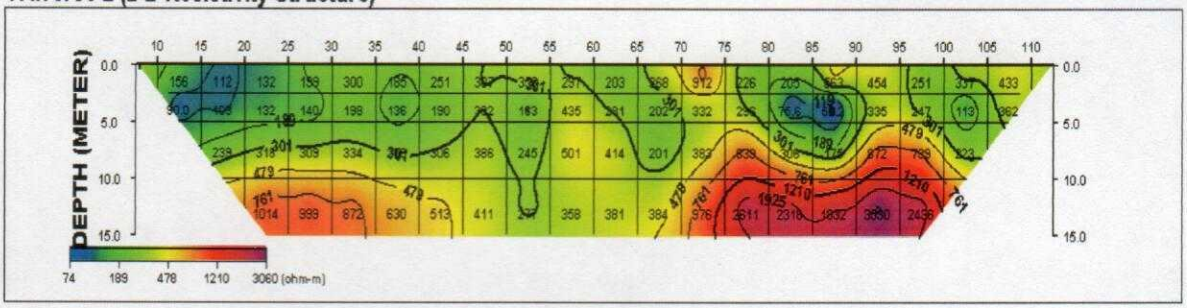

Figure 4.5b: 2-D Modeling of Dipole-Dipole Data obtained beneath Traverse 2

N S

Traverse 3 (Field Data Pseudosection)

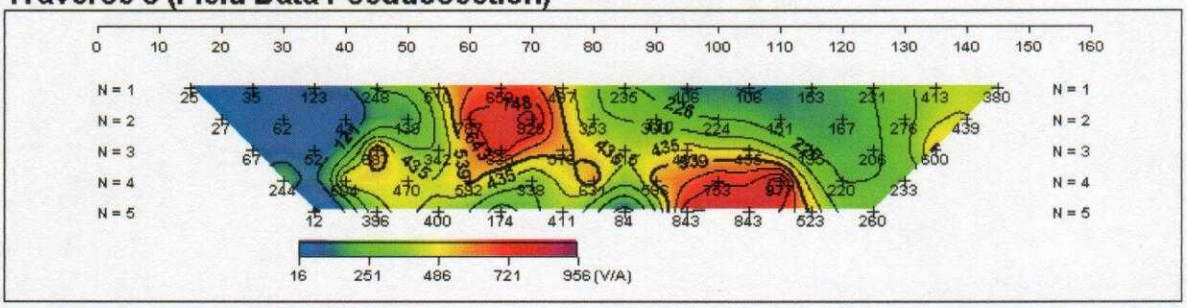

Traverse 3 (Theoretical Data Pseudosection)

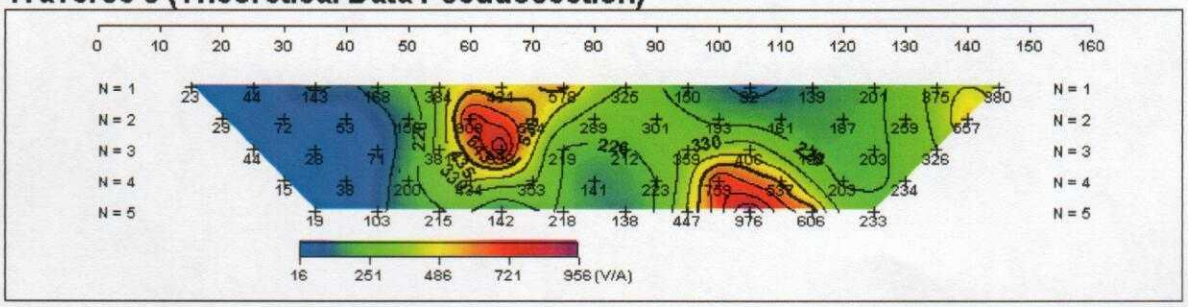

Traverse 3 (2-D Resistivity Structure)

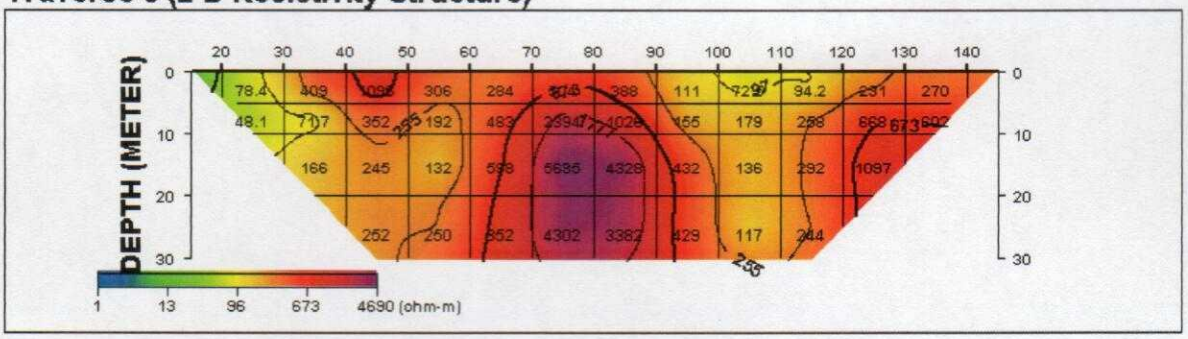

Figure 4.5c: 2-D Modeling of Dipole-Dipole Data obtained beneath Traverse 3

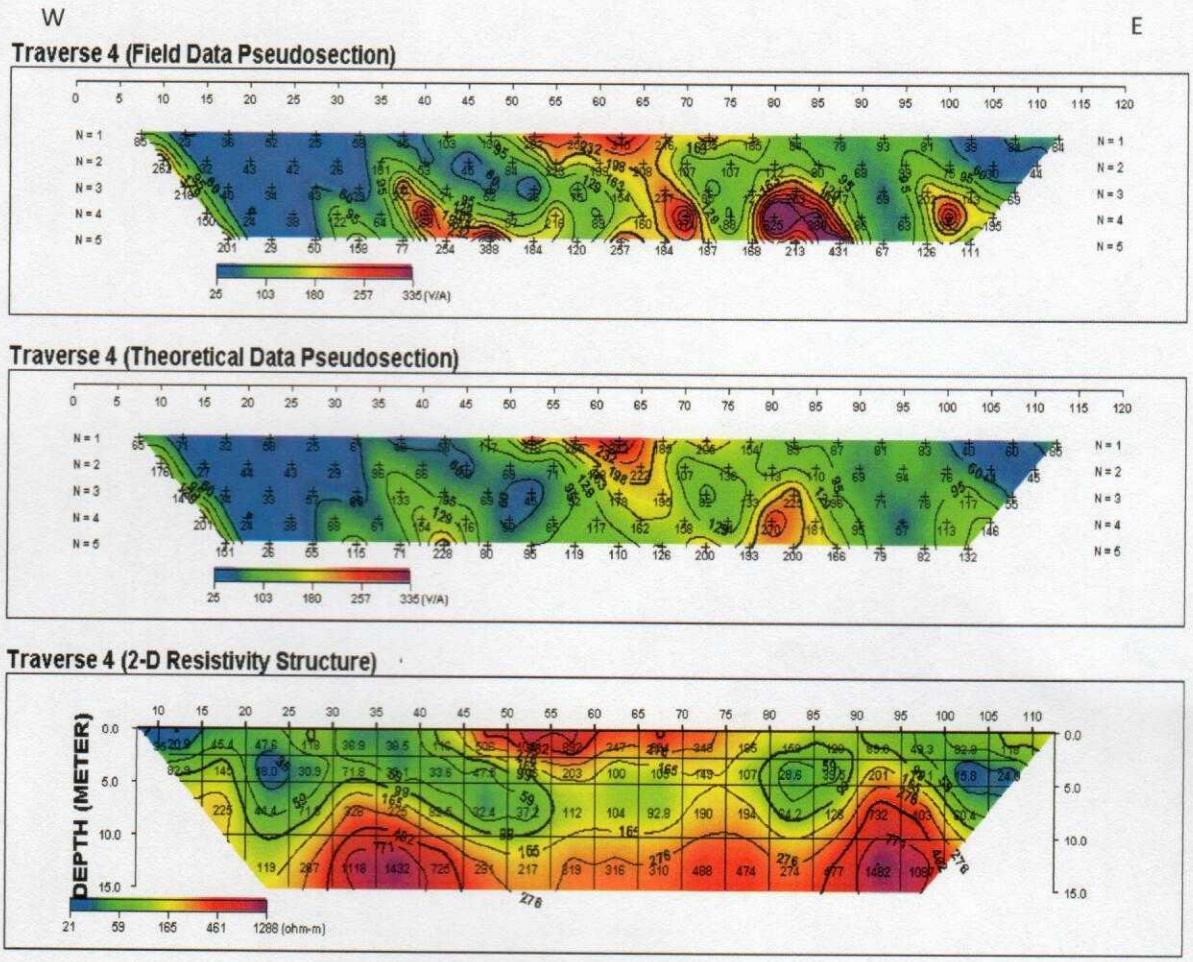

Figure 4.5d: 2-D Modeling of Dipole-Dipole Data obtained beneath Traverse 4

The 2-D resistivity structures delineated three major subsurface layers: the topsoil/laterite, the weathered layer and the fractured/fresh basement bedrock.

The 2-D resistivity structure beneath traverse 1 (Figure 4.5a) shows inhomogeneity of the subsurface. It reveals low resistivity topsoil between 0 - 95 m, reaching a depth of about 5 - 10 m beneath the sub-surface and moderately resistive topsoil extends from about 95 – 150 m. Underneath this conductive zone is the very high resistive layer at about 10 - 12 m extending from about 35 – 110 m. This high resistivity layer indicates the presence of the fresh basement. A basement depression was observed beneath the traverse between distances 110-130 m which could be typical of fractured zone within the basement. This could be inimical to the engineering structure to be constructed in the study area.

The 2-D resistivity structure beneath traverse 2 (Figure 4.5b) show pockets of conductive zones between distances 10 and 30 m and 76 - 90 m, the other parts are moderately resistive but the topsoil is resistive (lateritic) between 70 and 75 m and 85 – 95 m. Generally, the overburden is to a depth of about 10 m on this traverse. A basement depression was observed beneath the traverse between distances 40 and 70 m which could be typical of fractured zone within the basement. This could also be inimical to the engineering structure to be constructed in the study area.

The 2-D resistivity structure beneath traverse 3 (Figure 4.5c) shows moderately high resistivity of the subsurface and a boulder/basement structure was identified between distances 60 - 95 m. It is close to the surface at a depth of about 5 m. This area could be good for engineering structure to be constructed on because of its resistive nature. Nevertheless, a low resistivity zone is observed between distances 100 and 112 m (indicative of a fracture/lithological boundary) which could endanger the engineering structure to be constructed in the study area.

The 2-D resistivity structure beneath traverse 4 (Figure 4.5d) shows inhomogeneity within the topsoil. It reveals very low resistivity portion between distances 0 and 40 m indicative of clay while between 45 and 80 m show high resistivity layer which could be indicative of laterite and reaches a depth of about 10 m beneath the sub-surface. Beneath the topsoil is the weathered layer with low to moderate resistivity values. The basement shows high resistivity beneath the weathered layer, generally undulating and depressed especially between distances 45 – 88 m. The depth to the basement is about 7 – 10 m along this traverse.

4.2.3.4 Correlation of Geophysical Results

Figures 4.6a-b shows the combined correlation of the geophysical results obtained within the study area beneath Traverses Two (2) and Six (6). Traverse 2 is in the W-E direction while Traverse 6 is in the N-S direction. The Magnetic profile along traverse 2 (Figure 4.6a) shows high magnetic intensity between distances 15 and 28 m and 75 – 106 m. This could be indicative of the presence of geologic feature within the subsurface. The VLF-EM Model obtained show conductive zones between 8 and 18 m and 60 - 90 m which also correspond to that seen on the magnetic profile. The conductive zones identified on the VLF-EM and Magnetics at about 70 – 90 m corresponds to the thick overburden seen on the geoelectric section beneath VES 6. The conductive zones on VLF-EM, Magnetic and thick overburden from the geoelectric section correlates with that observed on the 2-D Dipole-Dipole pseudosection (Figure 4.6a).

The Magnetic profile obtained along traverse 6 (Figure 4.6b) shows high magnetic intensity (at 50 - 72 m) which corresponds to the resistive zone observed by the VLF-EM result. The low magnetic intensity zone (between 72 and 120 m) corresponds to the conductive zone observed by the VLF-EM result within this area beneath VES 18 identified as thick overburden as seen on the geoelectric section (Figure 4.6b). The 2-D Dipole–Dipole

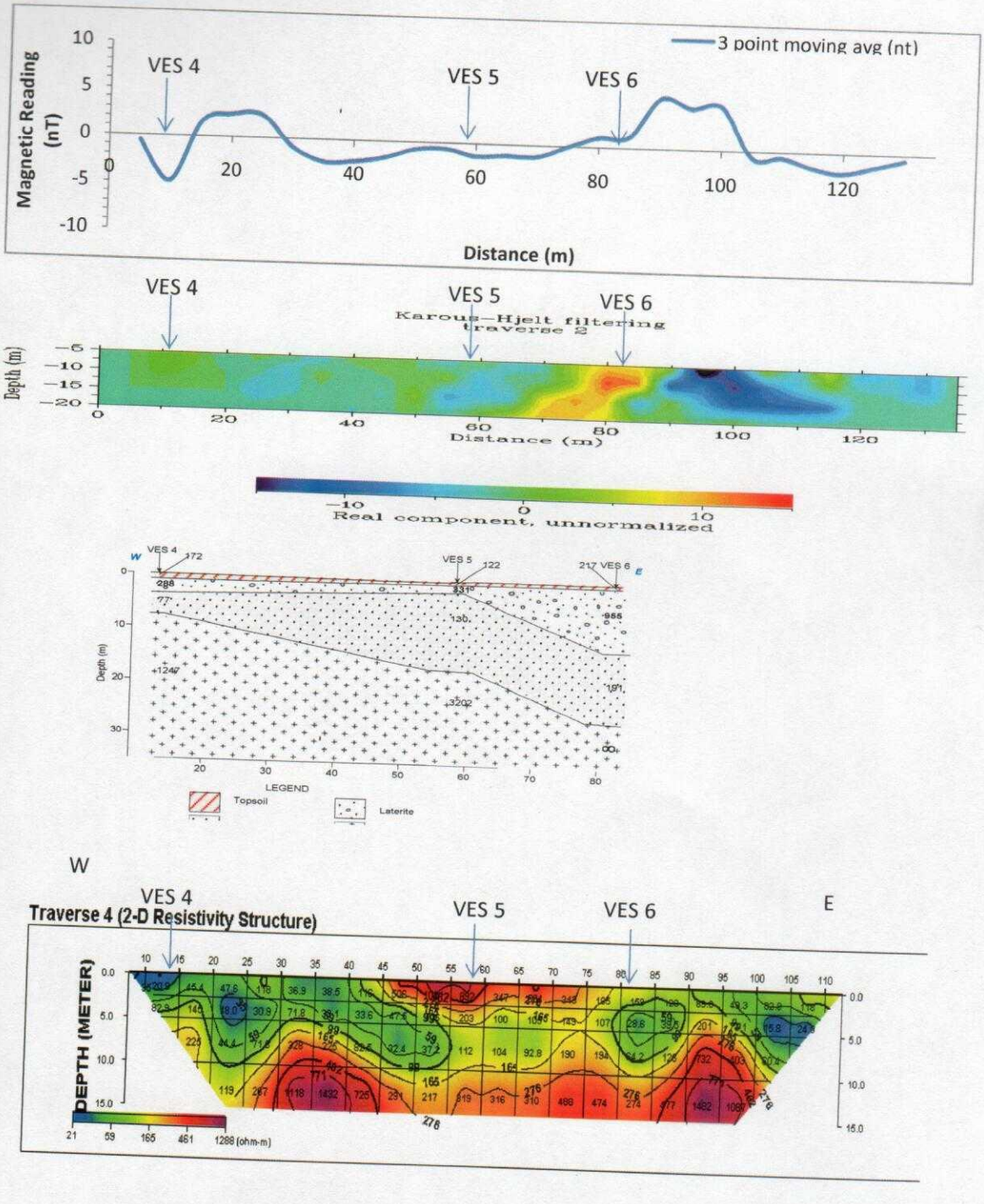

Figure 4.6a: Correlation of Geophysical Results beneath Traverse 2

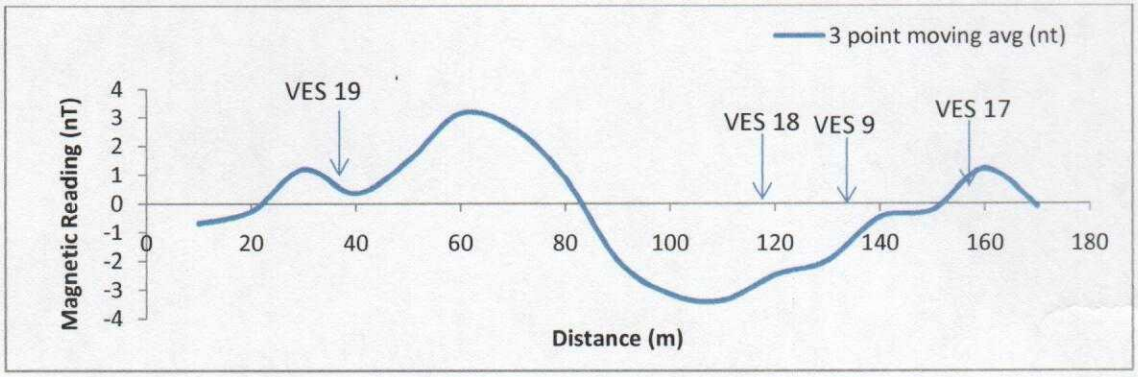

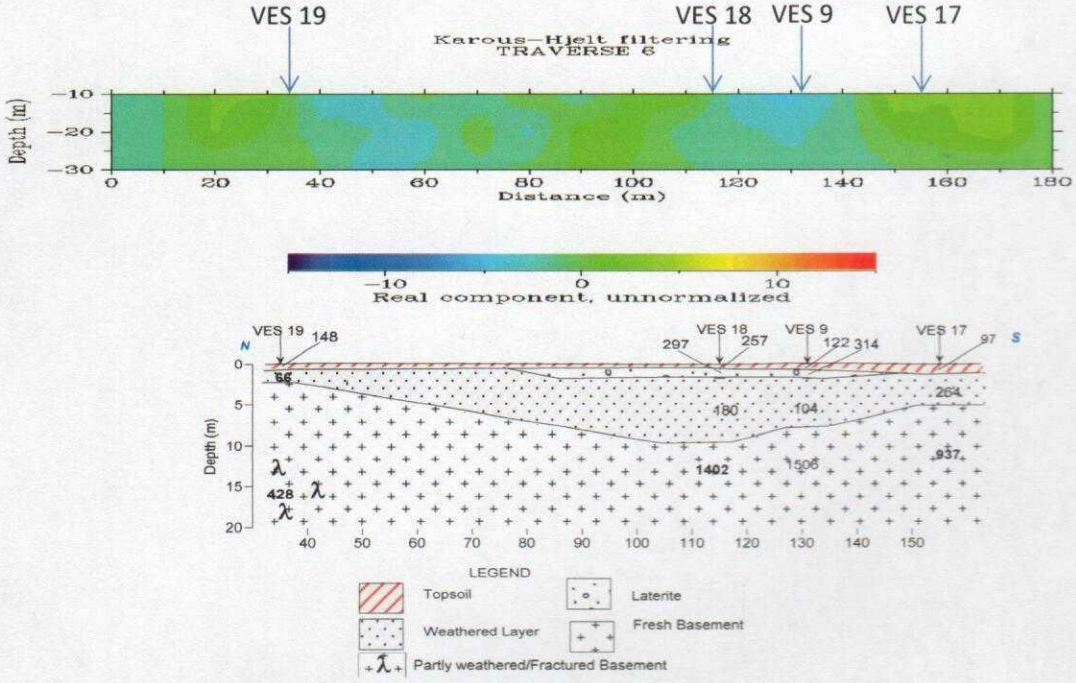

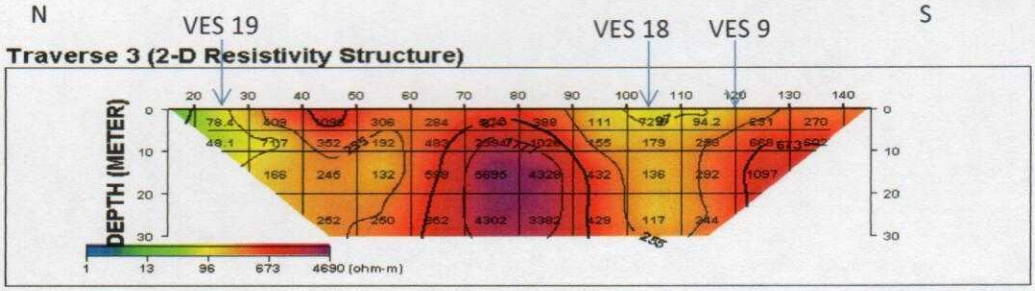

Figure 4.6b: Correlation of Geophysical Results beneath Traverse 6

Resistivity Structure obtained along traverse 3 close to traverse 6 also showed it as a low resistivity zone. This area could be good for engineering structure as it shows much competence except for the northern part of it where there is no presence of laterite and revealing a fractured basement as delineated by the geoelectric section (Figure 4.6b).

4.2.4 Geo-electrical Maps

4.2.4.1 Iso-resistivity Map of the Topsoil

Figure 4.7a shows the iso-resistivity map of the topsoil. The topsoil resistivity varies from 14-330 Ωm. The resistivity is higher (160 - 320 Ωm) in the central portion of the study area extending eastward and westward and lower (40 – 120 Ωm) in the south and northern part. The high resistivity zone of the topsoil is lateritic and indicative of competent topsoil. The low resistivity portions are clayey and depicts incompetency of the topsoil in that area.

4.2.4.2 Isopach Map of the Topsoil

Figure 4.7b shows the thickness map of the topsoil. The topsoil thickness varies between 0.5 and 1.5 m. The isopach map of the topsoil shows that the thickness is higher (0.85 - 1.5 m) in the northwestern part and in the southern part and thin (0.5 -0.85 m) in the northeastern part and in the centre. Areas with high topsoil thickness and high resistivity may be able to carry the load of the building. Nevertheless, areas with high topsoil resistivity in the study area shows thin topsoil (Figures 4.7a and b).

4.2.4.3 Depth to Weathered Layer Map

Figure 4.7c shows the depth/thickness of all materials on the weathered layer. The thickness of materials above the weathered layer varies between 0.5 and 12.8 m. The depth to weathered layer map shows that the northeastern part of the proposed building has thick overburden (6 – 12.8 m) especially beneath VES 6. Generally, most part of the area has this upper layer thickness within the range of 2 - 4 m. Therefore, the materials above the

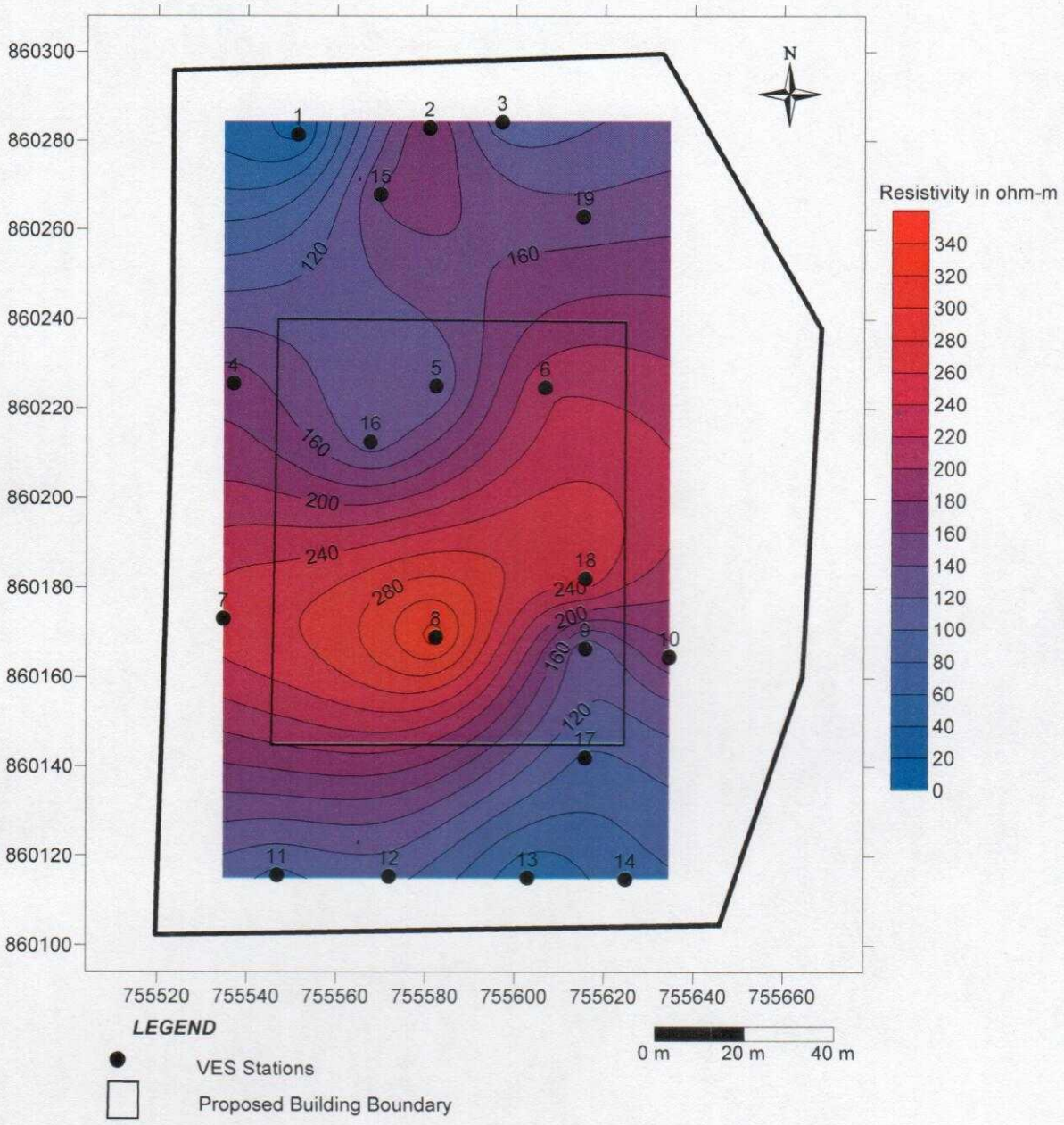

Figure 4.7a: Iso resistivity Map of the Topsoil in the Study Area (TMAC, FUOYE)

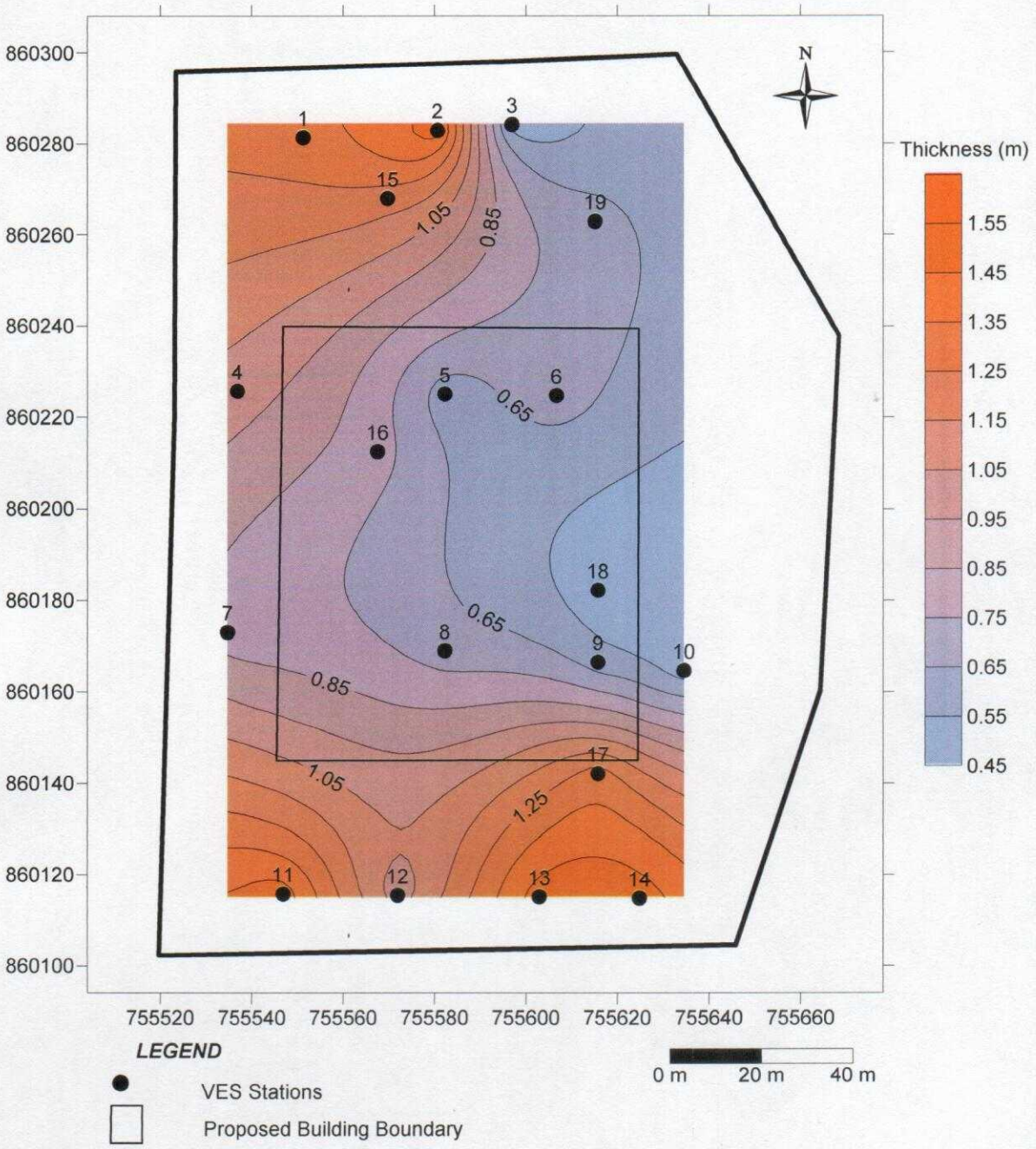

Figure 4.7b: Isopach Map of the Topsoil in the Study Area (TMAC, FUOYE)

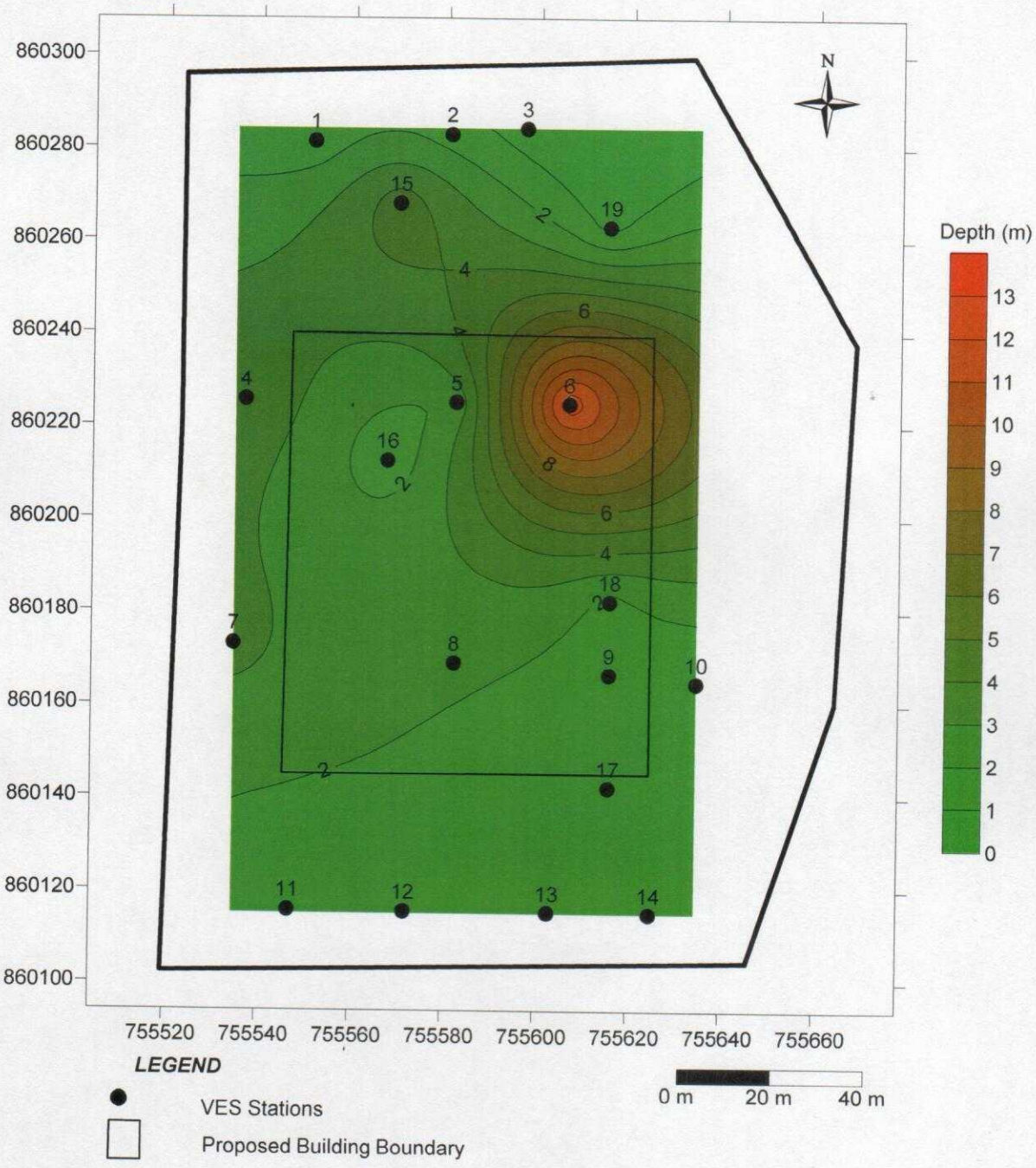

Figure 4.7c: Depth to Weathered Layer Map of the Study Area (TMAC, FUOYE)

weathered layer may be able to bear the load of the building as a result of the lateritic nature of some of the areas either at the topsoil or beneath it but may not be due to thickness.

CHAPTER FIVE

CONCLUSIONS AND RECOMMENDATIONS

5.1 Conclusions

Integrated Geophysical investigation was carried out around the proposed Theatre and Media Arts Complex within the Federal University Oye-Ekiti, Ekiti State, Southwestern Nigeria.

The results reveal the presence of conductive zones on the VLF-EM and Magnetic profile results obtained along the traverses within the study area. The conductive zones correspond to low resistivity zones or thick overburden above the basement or fractures as revealed by the geoelectric sections. They also appear as basement depression, fracture, faults and/or lithological boundary on the Dipole-Dipole 2-D resistivity structures. The topsoil is weak in some portions (NW and SE) and competent in some parts (central) of the study area (where it is lateritic and underlain by laterite) as revealed by the maps.

Therefore, based on the results obtained from this research work, it could be concluded that the proposed site for the construction of Theatre and Media Arts complex in Federal University Oye-Ekiti is good for construction but not all the entire part of the study area is suitable for construction purpose.

5.2 Recommendations

It could therefore be recommended that:

i. geophysical investigations should be carried out in mapping construction sites before any construction,

ii. the use of VLF-EM, Magnetics and Electrical Resistivity Geophysical Methods are suitable for geophysical engineering site investigation,

iii. heavy structure should not be constructed in the study area to avoid future collapse, or

iv. the weak portion is either piled, competent materials should be introduced to replace them or a raft foundation could be used for the building.

REFERENCES

Adelusi, A.O. Akinlalu, A.A. and Nwachukwu, A.I. (2013). Integrated Geophysical Investigation for Post-construction studies of Buildings around School of Science Area, Federal University of Technology, Akure, Southwestern, Nigeria. *International Journal of Physical Sciences. Vol. 8(15), pp. 657-669.*

Akintorinwa, O.J. and Abiola, O. (2011). Subsoil Evaluation for Pre-foundation Study using Geophysical and Geotechnical Approach. *Journal of Emerging Trends in Engineering and Applied Sciences (JETEAS) 2 (5): 858-863*

Akintorinwa, O.J. and Adeusi F.A. (2009). Integration of Geophysical and Geotechnical Investigations for a Proposed Lecture Room Complex at the Federal University of Technology, Akure, SW, Nigeria. *Ozean Journal of Applied Sciences 2(3), pp 241-254.*

Awoniyi, O.O. (2013). Application of Geophysical Investigation to Evaluate the Impact of a Dumpsite on Groundwater: Case Study of Awotan-Apete, Ibadan. *Unpublished. M.Tech. Thesis, Federal University of Technology: Akure, Nigeria, pp. 59-61.*

Bayode, S., Omosuyi, G.O. and Abdullah, H.I. (2012). Post-Foundation Engineering Geophysical Investigation in Part of the Federal University of Technology, Akure, Southwestern Nigeria, *Journal of Emerging Trends in Engineering and Applied Sciences (JETEAS), 3(1):203-210.*

Dahlin, T. (1996). 2-D Resistivity Surveying for Environmental and Engineering Applications. *First Break, Vol 14, No 7. pp 275-283.*

Egwuonwu, G.N. and Sule, P.O. (2012). Geophysical Investigation of Foundation Failure of A Learning Superstructure in Zaria Area, Northern Nigeria. *Research Journal in Engineering and Applied Sciences, 1(2) 110-116.*

Folami, S.L. (1980). Interpretation of Aeromagnetic data over Mahin area, Southwestern Nigeria. *Journal of Mineral Geology. 28(2):391-396.*

Gowd, S.S. (2004). Electrical resistivity surveys to delineate groundwater potential aquifers in Peddavanka water shed, Ananater pur District, Andhra prodesh India. *Environ. Geol. 46, 118–131.*

Keller, G.V. and Frischknecht, F.C. (1966). Electrical Methods in Geophysical Prospecting. *Pergamon Press, Oxford, UK. 517 pp.*

Kigam, J. K. (2001), "DIPRO for Windows Version 4.01". Copyright 1996-2001. *Heesong Geotek.*

Neil, A. and Ahmed, I. (2006). A generalized protocol for selecting appropriate geophysical techniques. *In Workshop on Application of Geophysics. Department of Geology and Geophysics, University of Missouri-Rolla, Rolla, Missouri, 65401. p. 19.*

Nigeria Geological Survey Agency (2006). Map of Ekiti State extracted from a Report on Geological Mapping of Ekiti State, Southwestern Nigeria.

Ofomola, M.O., Adiat, K.A., Olagunju, G.M. and Ako B.D. (2009). Integrated geophysical methods for post foundation studies, Obanla Staff Quarters of the Federal University of Technology, Akure Nigeria. *The Pacific Journal of Science and Technology. Vol.10, No. 2, pp. 93 – 110.*

Ogungbemi, O.S., Badmus, G.O., Ologe, O. and Idowu, K.A. (2013). Geoelectric and Electromagnetic Methods for Post Foundation Studies in a Typical Basement Terrain, *Journal of Emerging Trends in Engineering and Applied Sciences (JETEAS), 4(6): 863-868.*

Olorunfemi, M.O. and Meshida, E.A. (1987). Engineering Geophysics and its Application in Engineering site Investigation (Case study from Ile-Ife Area), The *Nigerian Engineer. Vol 22,No 2 pp 57-66.*

Omoyoloye, N.A., Oladapo M.I. and Adeoye, O.O. (2008). Engineering Geophysical Study of Adagbakuja New town Development, Southwestern Nigeria, *Medwell Online Journal of Earth Science. 2(2):55-63.*

Owoeye, A.O. (2000). The Effect of Location and Class Size on Academic Achievement of Secondary School Students in Ekiti State, Nigeria. *African Journal of Educational Planning and Policy Studies, 1(2): 153 – 161.*

Owoyemi, F.B. (1996). A Geological-Geophysical Investigation of Rain-Induced Erosional Features in Akure Metropolis. *Unpublished. M.Tech. Thesis, Federal University of Technology: Akure, Nigeria, pp. 11-18.*

Oyedele, K.F. and Okoh, C. (2011). Subsoil Investigation Using Integrated Methods at Lagos, Nigeria. *Journal of Geology and Mining Research, Vol. 3(7), pp169-179.*

Parasnis, D.S. (1975). Mining Geophysics, 2nd ed.(Elsevier Amsterdam). *Elsevier Scientific Publishing Co. pp 395.*

Parasnis, D.S. (1979). Principles of Applied Geophysics. *Third edition. Vol. 2A Tulsa: Society of Exploration Geophysicists, 271-283.*

Rahaman, M.A. (1988). Recent Advances in the Study of the Basement Complex of Nigeria. In: Precambrian Geology of Nigeria, *Geological Survey of Nigeria, Kaduna South. pp. 11-43.*

Reedman, J.H. (1979). Techniques in Mineral Exploration. *Applied Science Publisher Ltd. pp 1-24.*

Sharma, V.P. (1997). Environmental and Engineering Geophysics, *Published by Cambridge University Press, United Kingdom. pp. 40-45.*

Susan, E.P. (2004). The Role of Geophysics in 3-D Mapping Geological Survey of Canada, ON, *KIAOE8, Canada, pp 61-65.*

Telford, W.M. Geldart L.P. Sheriff R.E. (1990). Applied Geophysics. *2nd Edition, Cambridge University Press, Cambridge. pp 343-353*

Vander Velpen, B.P.A. (2004). WinRESIST *version 1.0* Resistivity Depth Sounding Interpretation Software. M.Sc. Research Project, ITC, Delft Netherland.

APPENDICES

Table 1a: Electromagnetic (VLF-EM) Field Readings for Traverse One in W-E Direction

Station No.	Real Comp. (%)	Imag. Comp.(%)	Filtered Real (%)	Filtered Imag. (%)
0	0.0	-3.9	-0.8	-1.6
1	-0.7	1.8	-1.2	-0.6
2	-0.6	-2.5	-1.9	0.2
3	-0.9	-0.6	-3.3	-1.0
4	-3.5	1.2	-1.1	-1.5
5	2.7	-1.7	-1.9	-2.3
6	-1.1	0.3	1.5	-0.7
7	2.8	1.1	2.9	0.2
8	0.3	-1.1	0.7	-1.6
9	1.1	4.5	0.2	-3.0
10	-1.5	9.0	1.0	-1.2
11	2.4	6.5	0.7	-2.4
12	-1.0	8.9	-3.3	0.2
13	-1.9	6.0	-2.3	1.2
14	-2.3	4.8	2.3	0.1
15	4.2	5.2	2.9	-0.7
16	-0.7	7.9	-0.1	-0.2
17	1.2	5.7	0.6	0.6
18	-0.9	6.1	-0.2	1.3
19	0.6	1.6	0.6	1.5

Table 1b: Electromagnetic (VLF-EM) Field Readings for Traverse Two in W-E Direction

Station No.	Real Comp (%)	Imag. Comp (%)	Filtered Real (%)	Filtered Imag. (%)
0	0.0	-0.2	0.1	0.9
1	0.4	-2.5	-0.2	1.1
2	-1.4	-4.9	2.5	-1.4
3	3.1	2.0	5.1	-2.7
4	2.5	2.7	3.2	-2.9
5	0.6	9.7	4.2	-1.0
6	3.7	4.6	2.5	1.0
7	0.2	6.1	-2.2	0.7
8	-2.6	0.0	0.5	0.1
9	1.9	10.4	3.6	1.7

10	1.6	-7.1	1.5	0.5
11	1.4	5.4	-1.4	-0.5
12	-3.2	14.2	-1.6	0.9
13	2.8	4.1	-5.8	4.0
14	-8.2	-3.7	-8.8	-0.3
15	-2.2	2.9	1.7	-4.8
16	-0.7	15.2	8.1	0.1
17	13.4	11.0	-2.2	9.4
18	17.4	-26.7	-0.1	-0.5
19	19.2	13.0	0.3	-0.6
20	-18.0	5.5	16.5	0.6
21	2.0	6.0	-4.0	-4.2
22	-9.3	14.8	-5.6	-0.5
23	2.9	10.4	0.1	2.3
24	-1.8	1.7	-6.2	-1.6
25	-5.0	18.0	-1.1	-0.1
26	2.6	4.3	2.0	-2.9
27	-0.6	6.5	-0.6	-0.6

Table 1c: Electromagnetic (VLF-EM) Field Readings for Traverse Three in W-E Direction

Station No.	Real Comp. (%)	Imag. Comp. (%)	Filtered Real (%)	Filtered Imag. (%)
0	0.0	8.8	-3.6	2.4
1	-1.2	2.3	-10.0	2.7
2	-10.9	-2.1	-3.3	-1.0
3	5.4	8.1	-4.0	-0.3
4	-1.9	2.3	-0.8	3.3
5	3.4	-5.5	3.6	0.1
6	0.6	1.5	-1.3	-1.0
7	-0.7	1.0	-4.7	1.5
8	-4.0	-3.4	-5.7	1.7
9	-2.3	-4.7	-4.8	1.5
10	-3.3	-7.5	-3.8	0.4
11	-1.5	-5.6	-0.2	-0.8
12	0.2	-3.8	2.3	0.2
13	2.4	-6.8	1.1	0.0
14	-0.7	-5.2	-0.4	-0.8
15	0.1	2.5	1.2	1.6

16	1.1	-10.0	-0.7	2.2
17	-0.7	-10.4	-4.0	0.2
18	-3.8	-10.3	-2.4	-0.6
19	0.8	-7.0	-0.6	-0.6
20	-2.0	-9.5	-0.6	-0.8
21	1.8	-4.7	0.7	-0.7
22	-2.4	-8.1	3.0	0.2
23	5.7	-4.7	2.5	0.5
24	-1.8	-11.7	-3.4	-10.2
25	-1.9	-3.8	0.9	-1.6
26	1.9	-5.9	1.9	-0.4

Table 1d: Electromagnetic (VLF-EM) Field Readings for Traverse Four in W-E Direction

Station No.	Real Comp. (%)	Imag. Comp (%)	Filtered Real (%)	Filtered Imag. (%)
0	0.0	-4.2	-4.5	2.5
1	-5.6	-14.2	-2.5	0.7
2	3.5	-4.5	-4.8	0.2
3	-7.2	-13.4	-9.4	0.5
4	-5.0	-10.0	2.7	-5.0
5	6.6	4.5	3.8	-1.8
6	-3.0	-5.1	3.2	0.4
7	7.1	0.2	3.9	-0.5
8	-1.3	-4.3	-5.2	1.4
9	-4.1	-2.6	-1.3	1.2
10	1.8	-8.0	0.6	1.7
11	-1.9	-7.6	0.1	0.5
12	3.1	-7.8	-1.9	1.6
13	-4.8	-12.3	-3.6	0.8
14	1.1	-10.4	-1.2	-0.3
15	-3.0	-10.5	-0.8	-0.1
16	1.1	-10.2	4.5	-0.3
17	3.4	-8.5	2.0	1.3
18	0.3	-14.9	-3.5	1.4
19	-2.9	-12.4	-4.4	-0.1
20	-3.5	-17.1	1.8	-3.8
21	3.5	-1.0	6.9	-6.5
22	3.2	2.5	6.6	-3.6
23	4.6	7.1	4.6	-2.6

Table 1e: Electromagnetic (VLF-EM) Field Readings for Traverse Five in N-S Direction

Station No.	Real Comp. (%)	Imag. Comp. (%)	Filtered Real (%)	Filtered Imag. (%)
0	0.0	19.2	4.7	-0.8
1	4.3	19.8	5.5	-1.3
2	2.8	24.1	1.1	0.6
3	-1.6	19.2	1.5	3.5
4	4.1	11.9	-1.3	4.2
5	-5.1	12.0	-4.1	0.3
6	0.4	15.4	-1.6	2.1
7	-4.1	5.4	2.7	0.5
8	5.7	10.3	6.1	-4.9
9	2.9	21.8	4.4	-0.7
10	-6.1	11.8	-5.1	0.5
11	-0.2	17.7	-1.6	0.1
12	-1.6	13.7	-4.6	4.1
13	-3.2	3.5	-1.6	1.4
14	0.0	10.3	3.2	0.4
15	2.7	5.4	2.0	0.8
16	1.2	4.7	-3.8	-4.3
17	-4.4	18.5	-4.4	-4.2

Table 1f: Electromagnetic (VLF-EM) Field Readings for Traverse Six in N-S Direction

Station No.	Real Comp. (%)	Imag. Comp. (%)	Filtered Real (%)	Filtered Imag. (%)
0	0.0	4.6		0.2
1	-0.1	2.2	-0.8	-1.7
2	-1.4	8.8	2.1	-3.8
3	2.3	13.4	5.4	-2.1
4	4.1	16.9	1.1	2.3
5	-1.9	4.0	-1.0	3.2
6	0.1	4.0	-0.3	-1.8
7	-0.7	10.6	-1.5	-3.0
8	-1.0	16.4	-0.9	0.1
9	0.4	10.5	-1.5	2.8
10	-3.0	3.6	2.6	-0.4
11	4.5	11.4	6.3	-2.3

12	2.7	13.9	0.1	-0.4
13	-0.3	9.9	-5,2	-1.1
14	-5.3	17.9	-3.7	0.8
15	-0.4	6.8	0.1	1.5
16	1.5	11.2	-5.1	2.4
17	-6.9	14.4	-2.8	-2.0
18	2.7	18.3	2.7	-1.8

Table 2a: Magnetic Field Reading for Traverse One in W-E Direction

Distance(m)	Mag1(nT)	Mag2(nT)	Average(nT)	Time(hr)	Time(Min)	Time(Sec)
0	33217.88	33231.75	33224.82	3	30	10
5	33226.74	33210.8	33218.77	3	30	42
10	33231.3	33227.76	33229.53	3	31	13
15	33234.62	33232.7	33233.66	3	31	41
20	33234.29	33234.09	33234.19	3	32	15
25	33232.89	33232.85	33232.87	3	32	49
30	33234.02	33233.39	33233.71	3	33	14
35	33234.74	33229.23	33229.91	3	33	35
40	33230.00	33229.82	33232.26	3	34	12
45	33232.02	33232.5	33233.43	3	34	38
50	33233.88	33232.97	33229.94	3	34	59
55	33231.4	33228.48	33229.59	3	35	20
60	33229.43	33229.74	33232.31	3	35	44
65	33232.83	33231.78	33230.74	3	36	5
70	33231.32	33230.16	33231.43	3	36	27
75	33230.96	33231.9	33227.79	3	37	0
80	33227.73	33227.85	33230.73	3	37	32
85	33231.05	33230.4	33229.32	3	37	55
90	33231.08	33227.55	33230.77	3	38	21
95	33230.67	33230.86	33230.77	3	38	49

Table 2b: Magnetic Field Reading for Traverse Two in W-E Direction

Distance(m)	MAG1(nT)	MAG2(nT)	AVERAGE(nT)	Time(hr)	Time(min)	Time(sec)
0	33242.91	33234.89	33238.9	3	41	24
5	33223.48	33222.22	33222.85	3	41	59
10	33230.13	33231	33230.57	3	42	25
15	33232.04	33232.26	33232.15	3	42	46
20	33244.82	33241.71	33243.27	3	43	7
25	33234.15	33234.61	33234.38	3	43	30
30	33232.55	33233.74	33233.15	3	43	52
35	33233.5	33235.22	33230.99	3	44	17
40	33232.83	33229.15	33234.32	3	44	47
45	33234.45	33234.19	33236.62	3	45	13
50	33236.55	33236.69	33234.44	3	45	36
55	33234.39	33234.48	33235.14	3	46	3
60	33235.99	33234.29	33234.7	3	46	20
65	33236.07	33233.33	33234.96	3	46	40
70	33235.39	33234.52	33235.06	3	46	59
75	33236.01	33234.1	33238.13	3	47	19
80	33237.9	33238.35	33237.99	3	47	39
85	33238.52	33237.45	33235.34	3	48	14

90	33236.33	33234.35	33235.34	3	48	37
95	33255.6	33244.85	33250.23	3	49	0
100	33237.01	33231.75	33234.38	3	49	27
105	33236.74	33234.43	33235.59	3	50	5
110	33235.19	33232.62	33233.91	3	51	3
115	33235.41	33232.47	33233.94	3	51	37
120	33231.44	33232.34	33231.89	3	52	5
125	33231.55	33231.29	33234.74	3	52	26
130	33234.32	33235.15	33232.91	3	52	50
135	33233.96	33231.85	33232.91	3	53	16

Table 2c: Magnetic Field Reading for Traverse Three in W-E Direction

Distance(m)	MAG1(nT)	MAG2(nT)	AVERAGE(nT)	Time(hr)	Time(min)	Time(sec)
0	33237.86	33239.3	33238.58	3	56	59
5	33252.51	33239.97	33246.24	3	57	28
10	33245.37	33246.2	33245.79	3	57	56
15	33238.06	33240.16	33239.11	3	58	13
20	33225.69	33228.67	33227.18	3	58	36
25	33233.76	33234.52	33234.14	3	59	10
30	33238.44	33238.94	33238.69	3	59	35
35	33236.4	33227.31	33231.54	3	0	1
40	33236.06	33227.01	33231.57	3	0	21
45	33236.05	33227.08	33238.58	3	0	45
50	33240	33237.15	33236.14	4	1	12
55	33236.49	33235.79	33236.92	4	1	35
60	33236.9	33236.93	33236.79	4	1	58
65	33236.73	33236.84	33235.75	4	2	16
70	33235.97	33235.52	33235.87	4	2	32
75	33235.87	33235.86	33234.6	4	3	2
80	33234.6	33234.6	33236.07	4	3	50
85	33235.98	33236.16	33246.11	4	4	20
90	33246.12	33246.09	33246.11	4	4	39
95	33240.35	33240.62	33240.49	4	5	5
100	33233.9	33235.68	33234.79	4	5	24
105	33237.04	33237.19	33237.12	4	5	47
110	33236.07	33236.12	33236.1	4	6	14
115	33235.62	33235.68	33235.65	4	6	37
120	33235.68	33235.33	33235.51	4	7	6
125	33236	33236.12	33235.81	4	7	38
130	33235.82	33235.79	33235.81	4	8	1

Table 2d: Magnetic Field Reading for Traverse Four in W-E Direction

Distance(m)	MAG1(nT)	MAG2(nT)	AVERAGE(nT)	Time(hr)	Time(min)	Time(sec)
0	33247.68	33247.68	33247.68	4	12	1
5	33244.83	33243.9	33244.37	4	12	51
10	33245.46	33243.58	33244.52	4	13	13
15	33242.31	33242.09	33242.2	4	13	33
20	33241.83	33241.9	33241.87	4	13	50
25	33239.98	33240.47	33240.23	4	14	13
30	33240.15	33240.1	33240.13	4	14	34
35	33239.45	33239.56	33239.51	4	14	50
40	33238.51	33238.95	33238.73	4	15	8
45	33239.03	33239.08	33239.06	4	15	23
50	33238.26	33238.09	33238.18	4	15	47
55	33244.66	33244.49	33244.58	4	17	15
60	33244.86	33244.64	33244.75	4	17	40
65	33243.71	33244.12	33243.92	4	18	17
70	33243.69	33243.68	33243.69	4	19	17
75	33241.64	33240.63	33241.14	4	19	30
80	33241.23	33242.15	33241.69	4	20	10
85	33241.89	33242.87	33242.38	4	20	35
90	33242.45	33243.17	33242.81	4	21	13
95	33241.6	33240.83	33241.22	4	21	45
100	33239.56	33238.42	33238.99	4	22	20
105	33234.17	33239.83	33237	4	22	45
110	33240.46	33240.44	33240.45	4	23	20
115	33231.89	33230.6	33231.25	4	23	56

Table 2e: Magnetic Field Reading for Traverse Five in N-S Direction

Distance(m)	MAG1(nT)	MAG2(nT)	AVERAGE(nT)	Time(hr)	Time(min)	Time(sec)
0	33225.25	33225.03	33225.14	4	30	30
10	33223.28	33222.84	33223.06	4	31	32
20	33194.35	33222.79	33208.57	4	32	25
30	33222.25	33222.48	33222.37	4	33	0
40	33223.07	33241.29	33232.18	4	33	32
50	33223.62	33223.03	33223.33	4	34	9
60	33223.48	33221.99	33222.74	4	34	46
70	33225.43	33225.69	33225.56	4	35	23
80	33224.4	33223.26	33223.83	4	36	54
90	33224.36	33223.98	33224.17	4	36	30
100	33224.86	33225.18	33225.02	4	37	7
110	33226.68	33227.16	33226.92	4	37	47
120	33244.86	33225.34	33235.1	4	38	13
130	33228.22	33226.43	33227.33	4	39	17

140	33230.79	33230.49	33230.64	4	39	49
150	33231.78	33231.06	33231.42	4	40	35
160	33232.63	33233.09	33232.86	4	41	18
170	33230.91	33230.93	33230.92	4	42	58

Table 2f: Magnetic Field Reading for Traverse Six in N-S Direction

Distance(m)	MAG1(nT)	MAG2(nT)	AVERAGE(nT)	Time(hr)	Time(min)	Time(sec)
0	33216.04	33215.86	33215.95	4	48	50
10	33212.21	33219.28	33215.75	4	49	30
20	33222.4	33225.46	33223.93	4	50	15
30	33222.4	33222.43	33222.42	4	50	49
40	33225.07	33241.29	33233.18	4	51	25
50	33225.62	33223.03	33224.33	4	51	50
60	33229.48	33221.99	33225.74	4	52	24
70	33233.43	33225.69	33229.56	4	53	58
80	33227.4	33223.26	33225.33	4	53	40
90	33226.36	33223.98	33225.17	4	54	14
100	33225.86	33225.18	33225.52	4	54	45
110	33227.68	33227.16	33227.42	4	55	15
120	33227.86	33227	33227.43	4	55	55
130	33227.22	33226.43	33226.83	4	56	25
140	33230.79	33230.49	33230.64	4	57	5
150	33231.78	33231.06	33231.42	4	57	35
160	33232.63	33233.09	33232.86	4	58	5
170	33230.49	33231.15	33230.82	4	58	35
180	33227.05	33226.78	33226.92	4	59	11

Table 3: VES Apparent Resistivity Data Obtained Within the Study Area

Electrode Position	AB/2 (m)	VES1 Ωm	VES 2 Ωm	VES 3 Ωm	VES 4 Ωm	VES 5 Ωm	VES 6 Ωm	VES 7 Ωm	VES 8 Ωm	VES 9 Ωm
1	1	14	170	54	187	147	277	261.	365	149
2	2	15	138	19	234	198	455	285	450	203
3	3	18	105	14	240	239	510	272	505	193
4	4	22	72	16	230	228	575	270	452	170
5	6	32	50	25	210	190	600	230	324	150
6	6	27	63	30	299	240	675	257	465	180
7	8	38	50	40	223	170	702	210	367	176
8	12	50	67	63	188	160	763	191	334	162
9	15	60	92	80	211	150	1106	193	321	207
10	15	65	92	90	196	158	899	153	329	205
11	25	79	143	137	313	209	640	167	501	344
12	32	120	193		376	274	621	214	594	370
13	40	151	252		482	300	671	273	817	419
14	40	120	261		449		559	262	704	431
15	65						750	432		
16										
Electrode Position	**VES10 Ωm**	**VES11 Ωm**	**VES12 Ωm**	**VES13 Ωm**	**VES14 Ωm**	**VES15 Ωm**	**VES16 Ωm**	**VES 17 Ωm**	**VES18 Ωm**	**VES 19 Ωm**
1	203	96	111	43	76	147	134	104	257	127
2	281	109	113	50	83	121	148	120	299	114
3	212	116	112	58	101	78	127	140	267	96
4	178	124	126	66	113	53	123	160	185	108
6	170	130	180	85	127	34	113	200	162	150
6	190	150	150	100	150	67	150	250	332	180
8	190	190	180	110	160	60	110	240	228	180
12	256	264	280	180	200	87	118	350	231	220
15	307	170	307	200	260	112	146	390	320	289
15	269	200	277	200	240	80	73	410	249	289
25	357	307	321	376	446	164	202	491	427	304
32	383	335	386	445	469	193	256	512	439	335
40	440	419	480	559	604	219	256	629	539	343
40	452	356	503	514	550	197	274	704	527	383
65						346	379			
100										

Table 4a: Dipole-Dipole Resistivity Data along Traverse 1in N-S Direction

Electrode Position	Geometric Factor (G)	Resistance R (ohm)	Apparent Resistivity(Ohm-m)
0 1 2 3	188.4956	0.3327	63
3 4	753.9822	0.1055	80
4 5	1884.9556	0.05234	99
5 6	3769.9112	0.04707	177
6 7	6597.3446	0.02992	197
1 2 3 4	188.4956	0.3814	72
4 5	753.9822	0.08866	67
5 6	1884.9556	0.07852	148
6 7	3769.9112	0.04413	166
7 8	6597.3446	0.01007	66
2 3 4 5	188.4956	0.2779	52
5 6	753.9822	0.1410	106
6 7	1884.9556	0.06421	121
7 8	3769.9112	0.06360	240
8 9	6597.3446	0.01907	126
3 4 5 6	188.4956	0.3966	75
6 7	753.9822	0.1308	99
7 8	1884.9556	0.07355	139
8 9	3769.9112	0.07314	275
9 10	6597.3446	0.04960	327
4 5 6 7	188.4956	0.4058	77
7 8	753.9822	0.1570	118
8 9	1884.9556	0.08349	157
9 10	3769.9112	0.06391	241
10 11	6597.3446	0.04829	319
5 6 7 8	188.4956	0.5003	94
8 9	753.9822	0.2130	161
9 10	1884.9556	0.1278	241
10 11	3769.9112	0.08684	327
11 12	6597.3446	0.05143	339
6 7 8 9	188.4956	0.5478	103
9 10	753.9822	0.1714	129
10 11	1884.9556	0.1034	195
11 12	3769.9112	0.05620	212
12 13	6597.3446	0.03885	256
7 8 9 10	188.4956	0.7324	138

10 11	753.9822	0.1957	148
11 12	1884.9556	0.08805	166
12 13	3769.9112	0.05184	195
13 14	6597.3446	0.04473	295
8 9 10 11	188.4956	0.7121	134
11 12	753.9822	0.1968	148
12 13	1884.9556	0.08947	169
13 14	3769.9112	0.02201	83
14 15	6597.3446	0.04646	307
9 10 11 12	188.4956	0.9424	178
12 13	753.9822	0.2059	156
13 14	1884.9556	0.1166	220
14 15	3769.9112	0.07000	264
15 16	6597.3446	0.03631	240
10 11 12 13	188.4956	0.7588	143
13 14	753.9822	0.2404	181
14 15	1884.9556	0.1034	195
15 16	3769.9112	0.04898	184
16 17	6597.3446	0.04098	270
11 12 13 14	188.4956	1.257	237
14 15	753.9822	0.3043	229
15 16	1884.9556	0.1095	206
16 17	3769.9112	0.5681	214
12 13 14 15	188.4956	1.562	294
15 16	753.9822	0.3885	293
16 17	1884.9556	0.1389	262
13 14 15 16	188.4956	1.197	226
16 17	753.9822	0.3408	257
14 15 16 17	188.4956	0.7902	149

Table 4b: Dipole-Dipole Resistivity Data along Traverse 2 in W-E Direction

Electrode Position	Geometric Factor (G)	Resistance R (ohm)	Apparent Resistivity(Ohm-m)
0 1 2 3	188.4956	2.363	223
3 4	753.9822	0.4149	157
4 5	1884.9556	0.2718	256
5 6	3769.9112	0.2029	383
6 7	6597.3446	0.3463	1142

1 2 3 4	188.4956	1.623	153
4 5	753.9822	0.4149	156
5 6	1884.9556	0.2211	208
6 7	3769.9112	0.1450	273
7 8	6597.3446	0.07172	258
2 3 4 5	188.4956	1.237	117
5 6	753.9822	0.4017	151
6 7	1884.9556	0.2079	196
7 8	3769.9112	0.08379	158
8 9	6597.3446	0.07179	237
3 4 5 6	188.4956	1.471	139
6 7	753.9822	0.4402	166
7 8	1884.9556	0.1684	159
8 9	3769.9112	0.1024	193
9 10	6597.3446	0.1024	338
4 5 6 7	188.4956	2.120	200
7 8	753.9822	0.4159	157
8 9	1884.9556	0.1998	188
9 10	3769.9112	0.1438	271
10 11	6597.3446	0.07710	254
5 6 7 8	188.4956	1.866	176
8 9	753.9822	0.4382	165
9 10	1884.9556	0.2668	252
10 11	3769.9112	0.1744	329
11 12	6597.3446	0.1815	599
6 7 8 9	188.4956	2.576	243
9 10	753.9822	1.146	432
10 11	1884.9556	0.7233	682
11 12	3769.9112	0.3834	723
12 13	6597.3446	0.06665	220
7 8 9 10	188.4956	2.363	223
10 11	753.9822	0.4686	177
11 12	1884.9556	0.1785	168
12 13	3769.9112	0.1065	201
13 14	6597.3446	0.07202	238
8 9 10 11	188.4956	3.033	286
11 12	753.9822	0.8633	325
12 13	1884.9556	0.5701	537

13 14	3769.9112	0.1886	356
14 15	6597.3446	0.1288	425
9 10 11 12	188.4956	2.576	243
12 13	753.9822	0.5042	190
13 14	1884.9556	0.4453	419
14 15	3769.9112	0.2282	430
15 16	6597.3446	0.2211	729
10 11 12 13	188.4956	3.611	340
13 14	753.9822	1.115	420
14 15	1884.9556	0.9231	870
15 16	3769.9112	0.1075	203
16 17	6597.3446	0.07172	237
11 12 13 14	188.4956	2.778	262
14 15	753.9822	1.014	382
15 16	1884.9556	0.5285	498
16 17	3769.9112	0.2394	451
17 18	6597.3446	0.1359	448
12 13 14 15	188.4956	16.91	1594
15 16	753.9822	9.871	3721
16 17	1884.9556	12.08	11385
17 18	3769.9112	0.1044	197
18 19	6597.3446	0.1349	445
13 14 15 16	188.4956	2.089	197
16 17	753.9822	0.4200	158
17 18	1884.9556	0.2100	198
18 19	3769.9112	0.1917	361
19 20	6597.3446	0.1531	505
14 15 16 17	188.4956	3.682	347
17 18	753.9822	1.197	451
18 19	1884.9556	1.328	1252
19 20	3769.9112	0.9516	1794
20 21	6597.3446	0.6787	2239
15 16 17 18	188.4956	2.485	234
18 19	753.9822	0.4210	159
19 20	1884.9556	0.5326	502
20 21	3769.9112	0.1623	306
21 22	6597.3446	0.1613	532
16 17 18 19	188.4956	2.049	193

19 20	753.9822	0.3378	127
20 21	1884.9556	0.1166	110
21 22	3769.9112	0.09826	185
22 23	6597.3446	0.1389	458
17 18 19 20	188.4956	3.013	284
20 21	753.9822	0.8765	330
21 22	1884.9556	0.2982	49
22 23	3769.9112	0.1410	266
23 24	6597.3446	0.1126	371
18 19 20 21	188.4956	3.286	310
21 22	753.9822	1.298	489
22 23	1884.9556	0.5326	1004
23 24	3769.9112	0.3875	730
19 20 21 22	188.4956	2.434	229
22 23	753.9822	0.5255	198
23 24	1884.9556	0.1582	149
20 21 22 23	188.4956	3.281	309
23 24	753.9822	0.9343	352
21 22 23 24	188.4956	3.256	307

Table 4c: Dipole-Dipole Resistivity Data along Traverse 3 in N-S Direction

Electrode Position	Geometric Factor (G)	Resistance R (ohm)	Apparent Resistivity(Ohm-m)
0 1 2 3	188.4956	0.1318	25
3 4	753.9822	0.03601	27
4 5	1884.9556	0.03550	67
5 6	3769.9112	0.06462	244
6 7	6597.3446	0.001846	12
1 2 3 4	188.4956	0.1846	35
4 5	753.9822	0.08268	62
5 6	1884.9556	0.02759	52
6 7	3769.9112	0.1602	604
7 8	6597.3446	0.05995	396
2 3 4 5	188.4956	0.6502	123
5 6	753.9822	0.05711	43
6 7	1884.9556	0.3642	687
7 8	3769.9112	0.1247	470
8 9	6597.3446	0.06066	400
3 4 5 6	188.4956	1.318	248
6 7	753.9822	0.1846	139
7 8	1884.9556	0.1815	342

8 9	3769.9112	0.08978	592
9 10	6597.3446	0.02637	174
4 5 6 7	188.4956	2.708	510
7 8	753.9822	1.044	787
8 9	1884.9556	0.4402	830
9 10	3769.9112	0.09201	339
10 11	6597.3446	0.06229	411
5 6 7 8	188.4956	3.449	650
8 9	753.9822	1.227	925
9 10	1884.9556	0.3070	579
10 11	3769.9112	0.1673	631
11 12	6597.3446	0.1268	84
6 7 8 9	188.4956	2.637	497
9 10	753.9822	0.4676	353
10 11	1884.9556	0.2201	415
11 12	3769.9112	0.1582	596
12 13	6597.3446	0.01410	843
7 8 9 10	188.4956	1.247	235
10 11	753.9822	0.4017	303
11 12	1884.9556	0.2607	491
12 13	3769.9112	0.1998	753
13 14	6597.3446	0.1278	843
8 9 10 11	188.4956	0.5630	106
11 12	753.9822	0.2972	224
12 13	1884.9556	0.2414	455
13 14	3769.9112	0.1481	977
14 15	6597.3446	0.07923	523
9 10 11 12	188.4956	0.5630	106
12 13	753.9822	0.2008	151
13 14	1884.9556	0.1034	195
14 15	3769.9112	0.05843	220
15 16	6597.3446	0.03936	260
10 11 12 13	188.4956	0.8116	153
13 14	753.9822	0.2211	167
14 15	1884.9556	0.1095	206
15 16	3769.9112	0.06188	233
11 12 13 14	188.4956	1.227	231
14 15	753.9822	0.3662	276
15 16	1884.9556	0.1592	600
12 13 14 15	188.4956	2.191	413
15 16	753.9822	0.5823	439
13 14 15 16	188.4956	2.018	380

Table 4d: Dipole-Dipole Resistivity Data along Traverse 4 in W-E Direction

Electrode Position	Geometric Factor (G)	Resistance R (ohm)	Apparent Resistivity(Ohm-m)
0 1 2 3	94.2478	0.8968	84
3 4	376.9911	0.6939	261
4 5	942.4778	0.2313	219
5 6	1884.9556	0.07963	150
6 7	3298.6723	0.06107	201
1 2 3 4	94.2478	0.3429	32
4 5	376.9911	0.08389	31
5 6	942.4778	0.04220	39
6 7	1884.9556	0.01228	23
7 8	3298.6723	0.008765	28
2 3 4 5	94.2478	0.3824	36
5 6	376.9911	0.1136	42
6 7	942.4778	0.03621	34
7 8	1884.9556	0.02039	38
8 9	3298.6723	0.01511	50
3 4 5 6	94.2478	0.5478	51
6 7	376.9911	0.1115	42
7 8	942.4778	0.06685	63
8 9	1884.9556	0.06472	122
9 10	3298.6723	0.04818	159
4 5 6 7	94.2478	0.2657	25
7 8	376.9911	0.06807	25
8 9	942.4778	0.04139	39
9 10	1884.9556	0.03408	64
10 11	3298.6723	0.02303	75
5 6 7 8	94.2478	0.6188	58
8 9	376.9911	0.2668	100
9 10	942.4778	0.2891	272
10 11	1884.9556	0.1957	368
11 12	3298.6723	0.07710	254
6 7 8 9	94.2478	0.4818	45
9 10	376.9911	0.1400	52
10 11	942.4778	0.07578	71
11 12	1884.9556	0.07537	142
12 13	3298.6723	0.1176	387
7 8 9 10	94.2478	1.095	103

10 11	376.9911	0.1186	45
11 12	942.4778	0.05600	53
12 13	1884.9556	0.05133	96
13 14	3298.6723	0.05579	184
8 9 10 11	94.2478	1.369	129
11 12	376.9911	0.2221	83
12 13	942.4778	0.03855	36
13 14	1884.9556	0.1146	216
14 15	3298.6723	0.03631	120
9 10 11 12	94.2478	2.992	282
12 13	376.9911	0.5914	223
13 14	942.4778	0.07963	75
14 15	1884.9556	0.04737	89
15 16	3298.6723	0.07811	258
10 11 12 13	94.2478	2.657	250
13 14	376.9911	0.5275	199
14 15	942.4778	0.1645	155
15 16	1884.9556	0.08511	160
16 17	3298.6723	0.05589	184
11 12 13 14	94.2478	3.347	315
14 15	376.9911	0.5508	208
15 16	942.4778	0.2515	237
16 17	1884.9556	0.1968	370
17 18	3298.6723	0.05660	186
12 13 14 15	94.2478	2.292	216
15 16	376.9911	0.2830	106
16 17	942.4778	0.08978	84
17 18	1884.9556	0.04646	87
18 19	3298.6723	0.05102	168
13 14 15 16	94.2478	2.495	235
16 17	376.9911	0.2840	107
17 18	942.4778	0.08978	84
18 19	1884.9556	0.1349	254
19 20	3298.6723	0.06472	213
14 15 16 17	94.2478	1.968	185
17 18	376.9911	0.2972	112
18 19	942.4778	0.2688	253
19 20	1884.9556	0. 2018	380
20 21	3298.6723	0.1308	431

15 16 17 18	94.2478	0.8876	83
18 19	376.9911	0.2201	82
19 20	942.4778	0.1237	116
20 21	1884.9556	0.04585	86
21 22	3298.6723	0.02018	67
16 17 18 19	94.2478	0.8268	78
19 20	376.9911	0.1805	68
20 21	942.4778	0.06239	58
21 22	1884.9556	0.03347	63
22 23	3298.6723	0.03814	126
17 18 19 20	94.2478	0.9850	93
20 21	376.9911	0.2617	99
21 22	942.4778	0.2140	202
22 23	1884.9556	0.1866	351
23 24	3298.6723	0.03354	110
18 19 20 21	94.2478	0.8562	80
21 22	376.9911	0.1988	75
22 23	942.4778	0.1521	143
23 24	1884.9556	0.1034	195
19 20 21 22	94.2478	0.4179	39
22 23	376.9911	0.07943	30
23 24	942.4778	0.07273	69
20 21 22 23	94.2478	0.7933	75
23 24	376.9911	0.1156	44
21 22 23 24	94.2478	0.8937	84

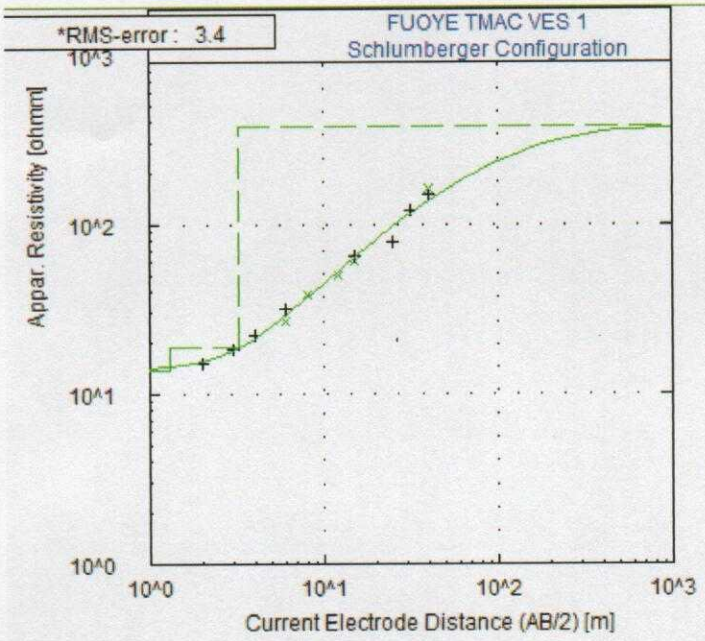

No	Res	Thick	Depth
1	13.6	1.3	1.3
2	18.7	2.0	3.3
3	372.7	-.-	-.-

* RMS on smoothed data

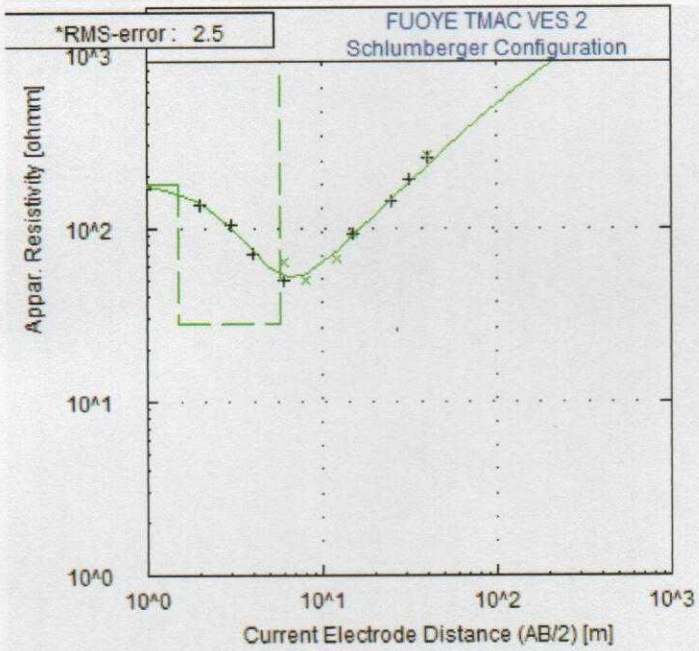

No	Res	Thick	Depth
1	179.3	1.5	1.5
2	28.0	4.2	5.7
3	2471.7	-.-	-.-

* RMS on smoothed data

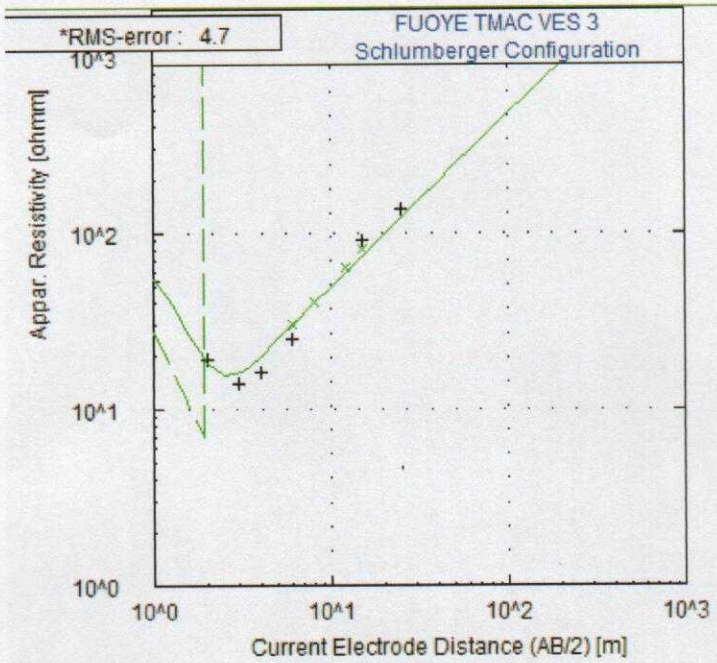

No	Res	Thick	Depth
1	103.9	0.5	0.5
2	6.9	1.4	1.9
3	10658.0	-.-	-.-

* RMS on smoothed data

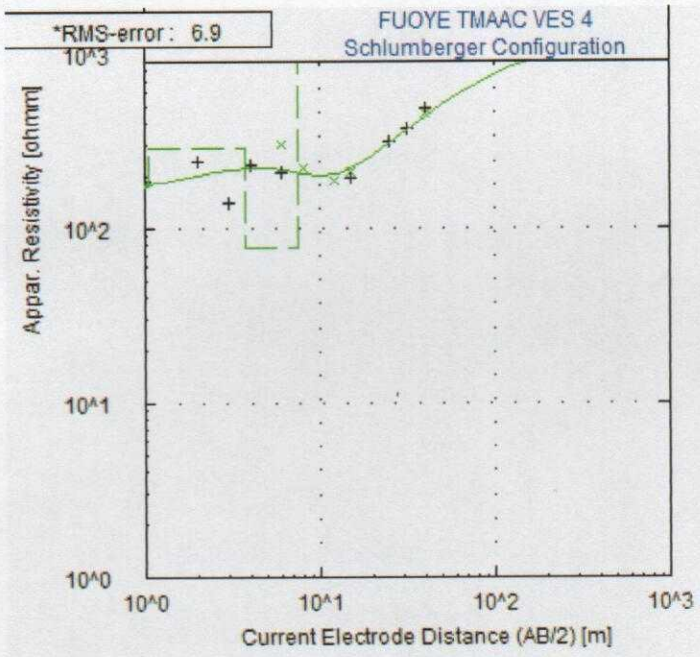

No	Res	Thick	Depth
1	172.2	1.0	1.0
2	288.2	2.7	3.8
3	77.1	3.8	7.5
4	1246.6	-.-	-.-

* RMS on smoothed data

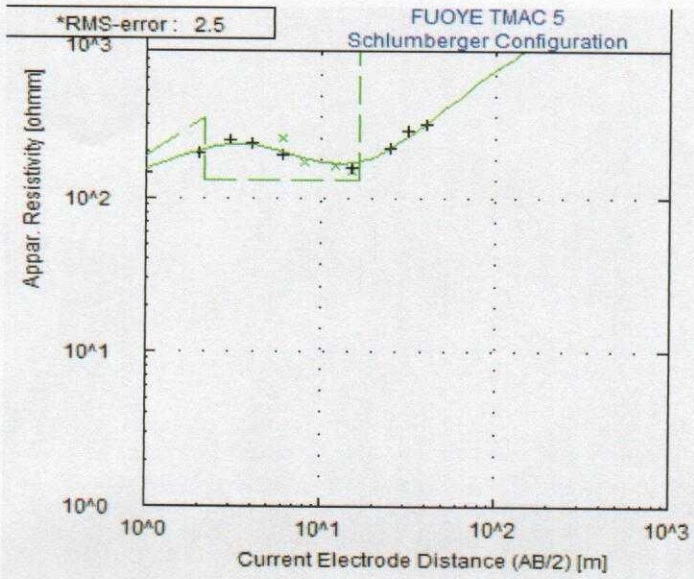

No	Res	Thick	Depth
1	121.9	0.6	0.6
2	330.9	1.6	2.2
3	130.3	14.5	16.6
4	3201.5	-.-	-.-

* RMS on smoothed data

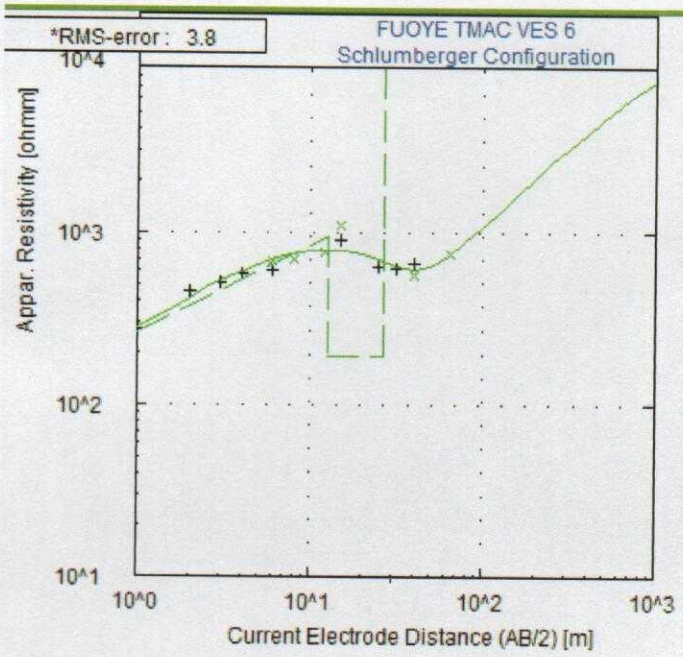

No	Res	Thick	Depth
1	216.8	0.7	0.7
2	955.0	12.1	12.8
3	190.9	13.6	26.4
4	19139.8	-.-	-.-

* RMS on smoothed data

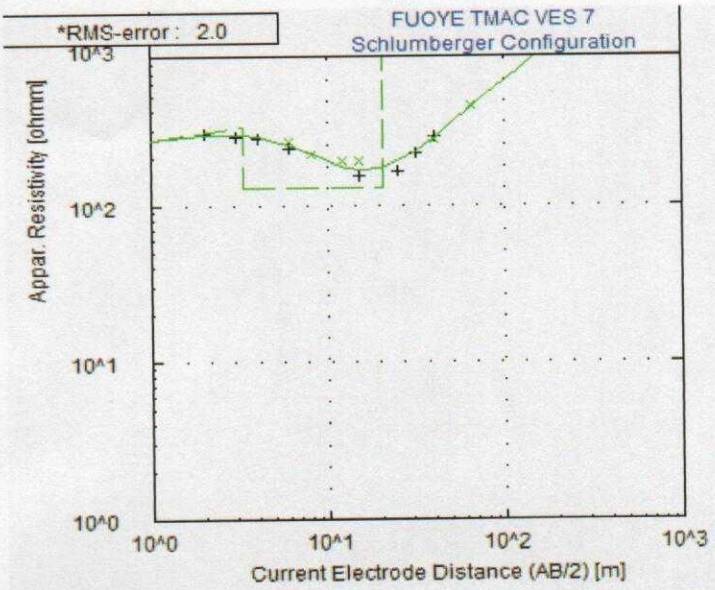

No	Res	Thick	Depth
1	255.0	0.8	0.8
2	318.8	2.5	3.3
3	130.0	17.5	20.8
4	6400.0	-.-	-.-

* RMS on smoothed data

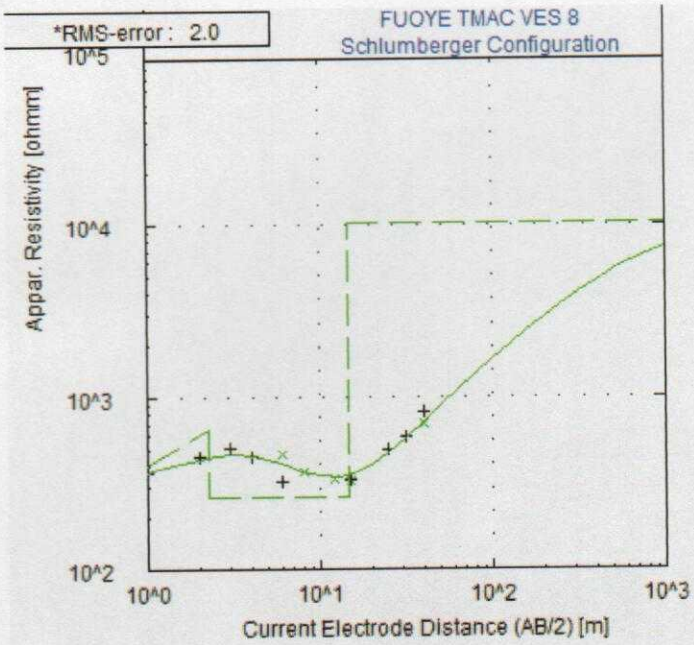

No	Res	Thick	Depth
1	330.2	0.7	0.7
2	653.0	1.5	2.2
3	260.7	12.4	14.7
4	10243.0	-.-	-.-

* RMS on smoothed data

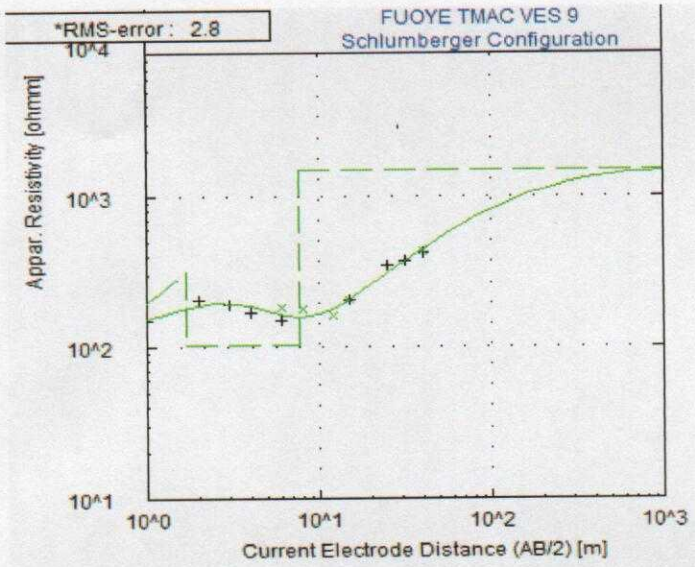

No	Res	Thick	Depth
1	122.4	0.6	0.6
2	313.6	1.1	1.7
3	103.6	6.0	7.7
4	1505.8	-.-	-.-

* RMS on smoothed data

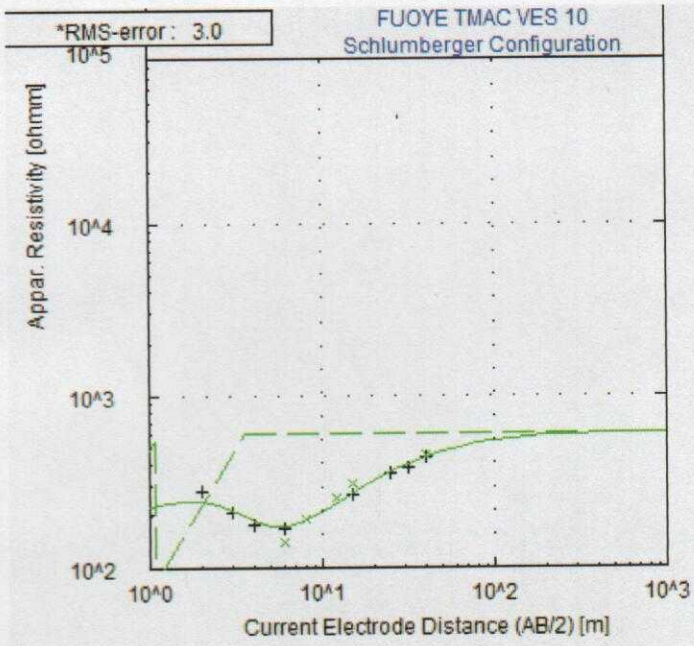

No	Res	Thick	Depth
1	173.6	0.5	0.5
2	543.6	0.6	1.1
3	81.9	2.5	3.6
4	602.3	-.-	-.-

* RMS on smoothed data

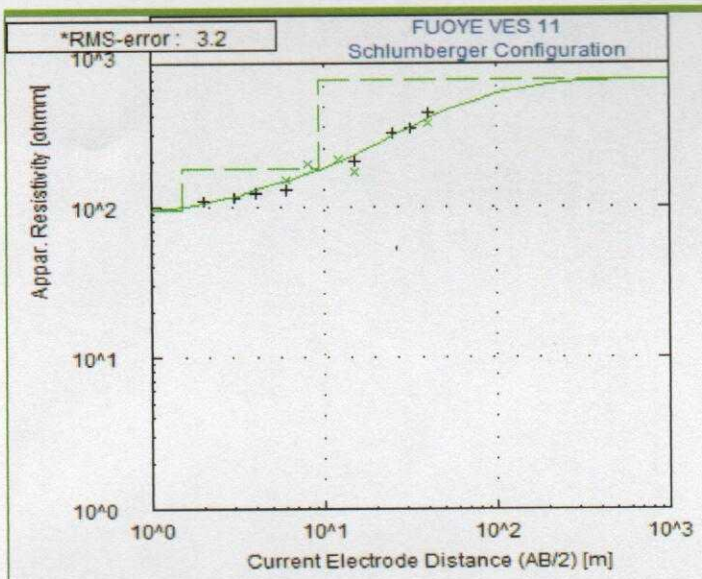

No	Res	Thick	Depth
1	94.5	1.5	1.5
2	177.7	7.7	9.2
3	705.0	-.-	-.-

* RMS on smoothed data

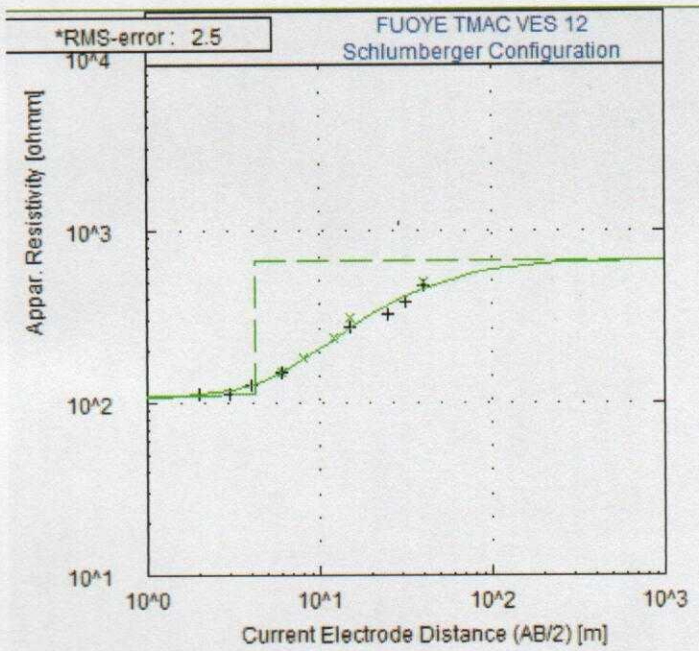

No	Res	Thick	Depth
1	108.3	1.0	1.0
2	113.6	3.3	4.2
3	660.4	-.-	-.-

* RMS on smoothed data

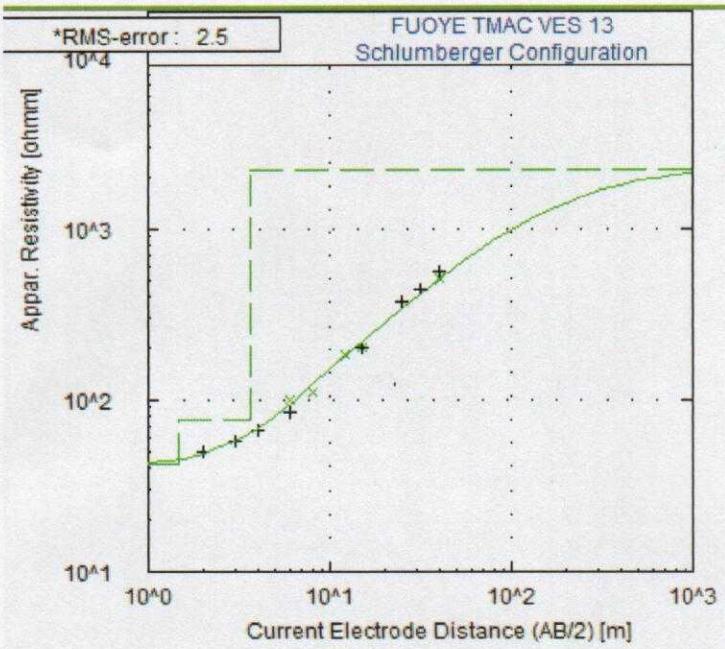

No	Res	Thick	Depth
1	42.0	1.5	1.5
2	77.6	2.2	3.7
3	2182.4	-.-	-.-

* RMS on smoothed data

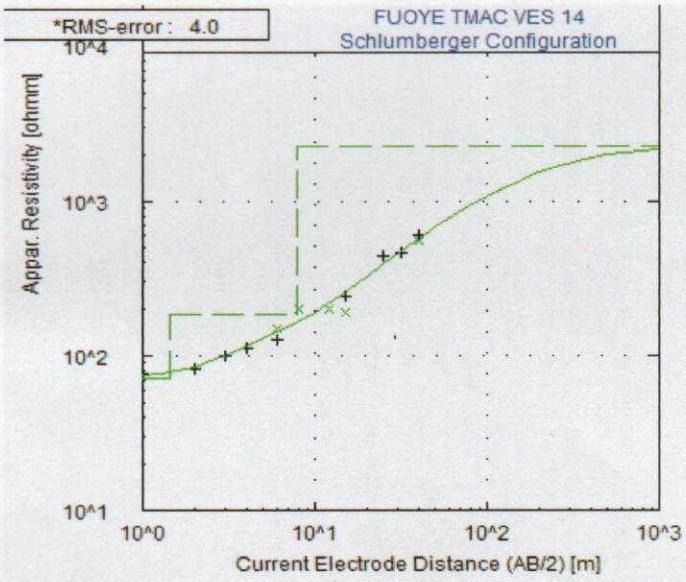

No	Res	Thick	Depth
1	72.0	1.4	1.4
2	186.0	6.5	8.0
3	2238.1	-.-	-.-

* RMS on smoothed data

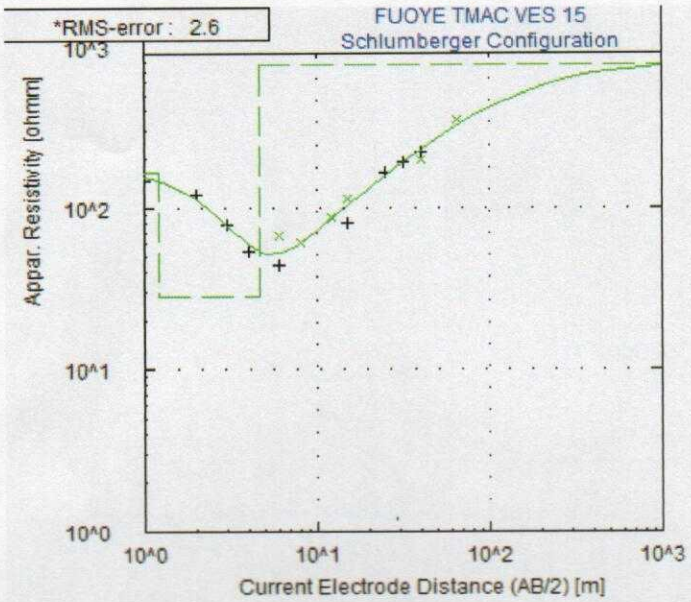

No	Res	Thick	Depth
1	163.9	1.2	1.2
2	27.8	3.4	4.6
3	761.4	-.-	-.-

* RMS on smoothed data

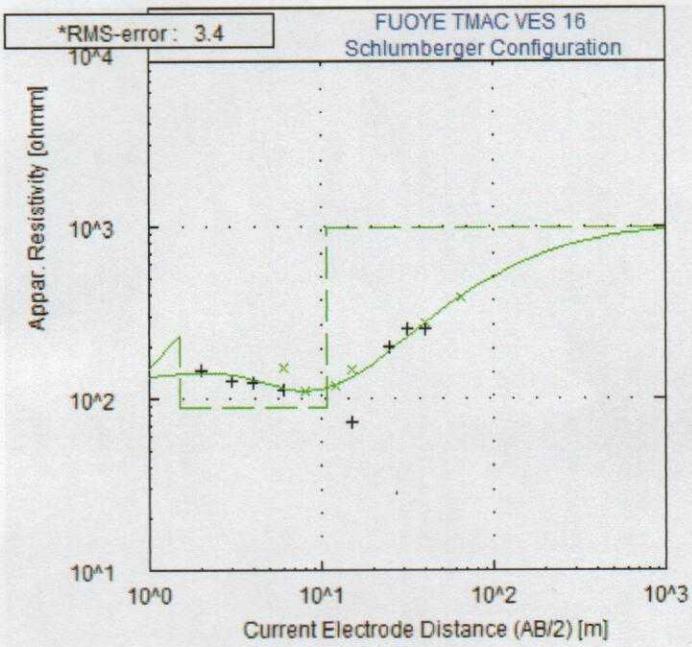

No	Res	Thick	Depth
1	126.9	0.8	0.8
2	229.1	0.6	1.5
3	89.3	9.1	10.6
4	980.3	-.-	-.-

* RMS on smoothed data

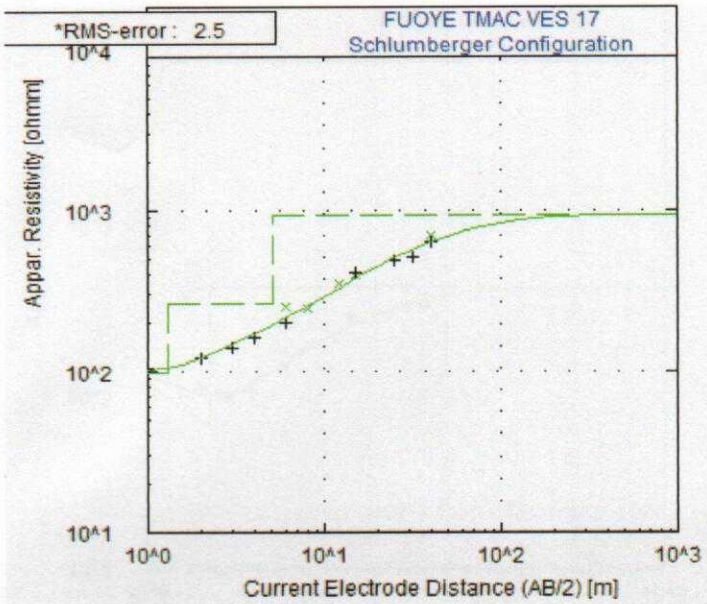

No	Res	Thick	Depth
1	96.8	1.3	1.3
2	263.6	3.8	5.1
3	937.2	-.-	-.-

* RMS on smoothed data

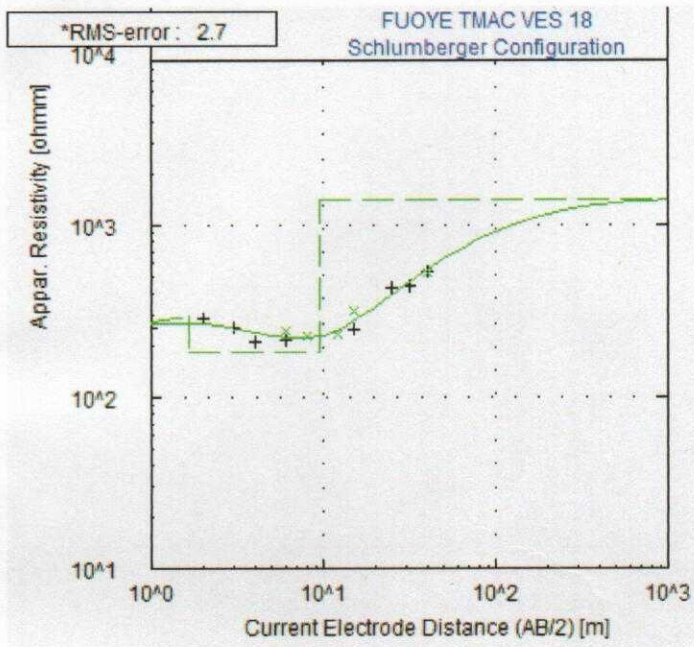

No	Res	Thick	Depth
1	257.4	0.5	0.5
2	296.6	1.1	1.7
3	180.2	7.9	9.5
4	1402.3	-.-	-.-

* RMS on smoothed data

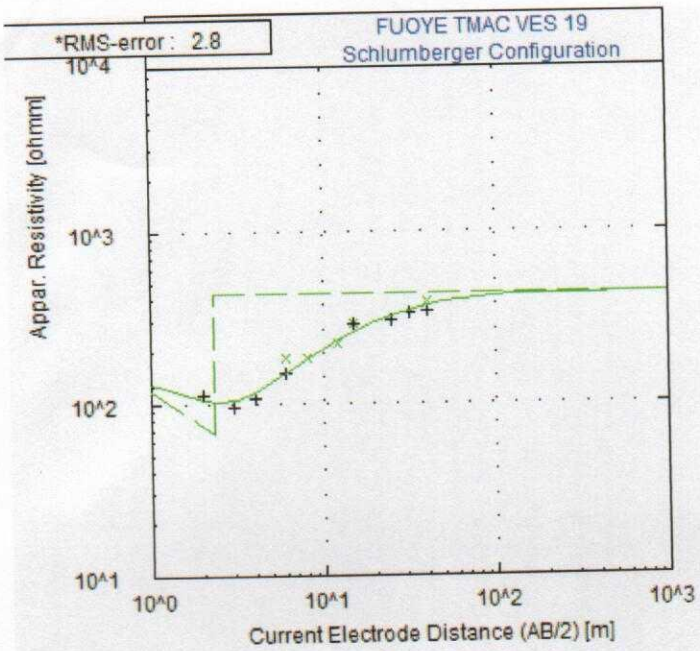

No	Res	Thick	Depth
1	147.6	0.7	0.7
2	66.1	1.6	2.3
3	427.9	-.-	-.-

* RMS on smoothed data